Personalized Drug Response Profiling for Patient-Derived CLL cells via Miniaturized Gene Expression and Drug Sensitivity Testing on Droplet Microarray

Zur Erlangung des akademischen Grades eines
DOKTORS DER NATURWISSENSCHAFTEN
(Dr. rer. nat.)

von der KIT-Fakultät für Chemie und Biowissenschaften
des Karlsruher Instituts für Technologie (KIT)

genehmigte

DISSERTATION

von

M. Sc. Razan El Khaled El Faraj

Eidesstattliche Erklärung

Hiermit versichere ich, dass ich die vorliegende Arbeit selbständig verfasst und keine anderen als die angegebenen Quellen und Hilfsmittel verwendet, sowie Literaturzitate kenntlich gemacht habe. Die Satzung des Karlsruher Instituts für Technologie (KIT) zur Sicherung guter wissenschaftlicher Praxis wurde beachtet. Die elektronische Version der Arbeit stimmt mit der schriftlichen überein und die Abgabe und Archivierung der Primärdaten gemäß Abs. A (6) der Regeln zur Sicherung guter wissenschaftlicher Praxis der KIT beim Institut ist gesichert.

Ort und Datum   Unterschrift

Table of Content

Acknowledgments

The completion of this dissertation marks a significant achievement in my academic journey, and I am deeply grateful to all those who have supported and guided me along the way.

First of all, I would like to express my deepest appreciation to my Ph.D. supervisor, Prof. Dr. Pavel Levkin (Institute of Biological and Chemical Systems - Functional Molecular Systems), for giving me the invaluable opportunity to join his research group. His continuous support, insightful feedback and expert guidance have been essential in shaping the direction and quality of my research. Throughout this journey, his encouragement and commitment to my academic and professional growth have been a constant source of motivation. I am deeply grateful for his mentorship, which has not only guided the successful completion of this dissertation but has also been a cornerstone of my overall academic development. His influence on my work and future career is immeasurable and I am sincerely grateful for his trust and belief in my potential.

I would like to express my deepest appreciation to my biology group leader and supervisor, Dr. Anna Popova. Her continuous support, both academically and personally, has enriched my journey to the fullest. Dr. Popova's kindness, friendliness and approachability provided a welcoming environment that made daily laboratory work a truly enjoyable experience. Her insightful guidance and encouragement were essential to the smooth progress of my project, and I am deeply grateful for the countless hours she dedicated to helping me overcome the challenges of my research. Her belief in me was a source of motivation and without her constant efforts and support this achievement would not have been possible. I am forever grateful for her mentorship and the profound impact she has had on my academic and personal development.

I am also deeply grateful to my Thesis Advisory Committee (TAC) members, Prof. Dr. Véronique Orian-Rousseau and Prof. Dr. Anne-Kristin Kaster, for their invaluable scientific guidance and advice. Their expertise and thoughtful insights have greatly enriched my work and I am deeply thankful for the time and effort they put into my research.I would like to express my sincere

gratitude to my collaborators, Prof. Dr. med. Sascha Dietrich and Dr. Vladimir Benes, for their continuous support and valuable contributions throughout our partnership. Their willingness to share their expertise and their commitment to our work have been instrumental in ensuring the smooth and productive progress of our collaborative projects.

To all the members of the Levkin lab and especially to all the members of the Biogroup, I would like to express my sincere appreciation. Being part of such a supportive, cooperative, and enthusiastic team made the lab environment not only enjoyable but also deeply inspiring. The group spirit we shared and the constant encouragement from each member was a major contributor to making my research journey both positive and productive. Your collective energy, fun and dedication were a constant source of motivation, and I am truly grateful to have worked alongside such remarkable colleagues.

Personally, I am deeply grateful to my brothers Wael and Abdallah for their unconditional encouragement. Having you both here in Germany has brought me immense comfort and made my tough times so much easier. I am truly grateful for the constant sensation of family and belonging you have given me throughout this journey.

Lastly, and most importantly, I would like to express my deepest gratitude to my parents, Mama and Baba, whose love and support have been the foundation of everything I have achieved. Even from miles away, your never-ending belief in me and your constant encouragement have given me the strength to carry on. Your faith in my abilities and your endless love have been my guiding light, carrying me through every achievement and challenge along this journey. Words cannot express the depth of my admiration for you for always standing by my side, offering your knowledge, support, comfort, and unconditional love. This thesis is as much yours as it is mine, a record of the sacrifices you've made and the limitless love you've given. From the bottom of my heart, I thank you for everything.

This dissertation is a reflection not only of my efforts, but also of the continued support, guidance and love of those who have stood by me throughout this journey. To everyone who has contributed to this achievement, I offer my deepest gratitude. Thank you all.

Abstract

High-throughput technology has changed the landscape of modern research in the biological, biochemical, and chemical sciences, enabling rapid screening of large numbers of compounds or genes with cells or proteins. These advances have enabled large-scale experiments generating large datasets critical to understanding complex biological systems and advancing drug discovery. The key benefits of these high-throughput methods are the ability to test thousands of samples simultaneously, the automation of workflows and the reduction of human error. However, these benefits also come with significant drawbacks, including the high cost of the equipment, consumables and reagents that are required. In addition, significant amounts of biological material, which can be both scarce and difficult to obtain, are often required for high-throughput experiments. The challenges posed by the complexity and volume of the data generated also require the use of sophisticated analytical tools and computational resources. To address these challenges, miniaturisation has emerged as a powerful strategy. By reducing the scale of reactions and the volume of samples, miniaturised platforms significantly reduce reagent costs while conserving valuable biological materials, making high-throughput experimentation more accessible and efficient. Scaling down also increases experimental throughput, allowing a greater number of conditions to be tested simultaneously, while reducing overall costs and resource requirements. The integration of miniaturisation into high-throughput systems is particularly important for the advancement of personalised medicine, where rapid and cost-effective testing is essential to identify promising therapeutic candidates tailored to the genetic, molecular and environmental profiles of individual patients. One important approach is Functional Precision Oncology, in which therapies are customised to the unique molecular and cellular characteristics of each patient's cancer. It involves testing the response of individual patients-derived cells to different drugs or combinations of treatments, allowing for more personalized and effective therapeutic strategy. It is particularly important in oncology, where treatment efficacy can vary widely between patients with the same type of cancer, due to the heterogeneity of tumours and their different genetic and phenotypic profiles. By maximising therapeutic efficacy while minimising side effects, precision oncology promises to improve patient outcomes. However, the realisation of functional precision oncology requires robust, high-

throughput screening tools capable of handling minute patient-derived samples and providing accurate, validated data.

The droplet microarray (DMA) platform is a promising solution that combines the strengths of high-throughput screening, miniaturisation, and parallelization in a single, versatile system. This platform has been shown in my work to perform drug sensitivity and response testing (DSRT), drug-induced gene expression analysis (DGEA) and other critical assays at the nanoliter scale. By significantly reducing sample and reagent requirements, the DMA platform improves the efficiency and cost-effectiveness of high-throughput experimentation while supporting the development of functional precision oncology strategies for clinical application. This combined approach has the potential to revolutionise functional precision oncology, enabling more accurate and individualised treatment plans tailored to the specific needs of each patient.

In my thesis, I focused on developing methods for functional precision oncology using a DMA chip on CLL (chronic lymphocytic leukemia) cells. I worked on optimizing workflows for cell culture conditions and enhancing the readout quality of information obtained after drug treatment. Since CLL cells, like most hematopoietic cells, do not proliferate in vitro and are prone to undergo spontaneous apoptosis in culture, overcoming these challenges was crucial.

In my first project, I focused on developing a novel methodology that integrates patient derived CLL cells into a hydrogel matrix on the DMA platform. This approach addresses the significant challenges associated with culturing CLL cells, which are prone to early apoptosis and exhibit poor viability under conventional in vitro conditions. Typically, CLL cells require co-culture with supportive stromal cells or the presence of soluble factors to enhance survival, mimicking the complex tumour microenvironment. Initial experiments in conventional media showed drastically low cell viability of CLL cells on DMA chip, highlighting the limitations of traditional culture methods. By incorporating a hydrogel matrix into the DMA platform, we were able to significantly improve CLL cell viability, achieving a remarkable 68% viability at 24 hours, a significant improvement over conventional method. The hydrogel matrix not only provided essential structural support, but also created a stable environment that enhanced cell survival over time, making it a valuable tool for DSRT of patient-derived CLL cells.

The second project introduces a novel miniaturised method for drug-induced differential gene expression analysis (DGEA) at the nanolitre scale, a critical tool for uncovering the molecular basis of cellular changes following drug treatment. This method is particularly valuable for high-throughput analysis of cancer cells derived from patient biopsies, where sample scarcity is a significant challenge. Using the DMA platform, this innovative approach enables parallel analysis of drug responses in patient-derived cells, effectively overcoming the limitations of traditional protocols. The method involves a series of steps including cell lysis for mRNA isolation, cDNA conversion and subsequent quantitative polymerase chain reaction (qPCR) analysis. This work demonstrates the potential of this approach for functional precision oncology, providing insights into individual tumour responses to cancer drugs. As a next step, I focused on the development and optimisation of the Seq-on-a-Chip protocol by introducing barcodes on the DMA platform for high-throughput global transcriptome analysis. This approach increases the efficiency and precision of RNA sequencing by miniaturising the sample preparation process and integrating barcoded oligo-dT primers with Unique Molecular Identifiers (UMIs). The integration of this method into the DMA platform allows for a reduction in reagent consumption and an increase in throughput, which is particularly beneficial in scenarios where patient sample availability is limited. Taken together, this project demonstrates the potential of the DMA platform as a comprehensive tool for DSRT, DGEA and global transcriptome analysis. Ongoing research and continued refinement of these methodologies is expected to transform functional precision oncology by enabling the development of precise, personalised treatment strategies unique to each patient's profile. Additionally, DGEA will provide deep, valuable understanding of the underlying mechanisms of drug response and reveal variations in how different patients respond to treatment. It will also highlight the mechanisms involved in drug resistance, enabling more accurate strategies for predicting patient-specific responses to therapies and ultimately improving clinical outcomes.

Zusammenfassung

Hochdurchsatztechnologien haben die moderne Forschung in den biologischen, biochemischen und chemischen Wissenschaften grundlegend verändert, indem sie ein schnelles Screening einer großen Anzahl von Verbindungen, Genen oder Zellen ermöglichen. Diese Fortschritte haben groß angelegte Experimente ermöglicht, die umfangreiche Datensätze generieren, die für das Verständnis komplexer biologischer Systeme und die Förderung der Arzneimittelentwicklung von entscheidender Bedeutung sind. Zu den wichtigsten Vorteilen dieser Hochdurchsatzmethoden gehören die Möglichkeit, Tausende von Proben gleichzeitig zu testen, die Automatisierung von Arbeitsabläufen und die Verringerung menschlicher Fehler. Diese Vorteile gehen jedoch auch mit erheblichen Nachteilen einher, darunter die hohen Kosten für die erforderliche Ausrüstung, Verbrauchsmaterialien und Reagenzien. Zudem sind für Hochdurchsatzexperimente oft beträchtliche Mengen an biologischem Material erforderlich, das sowohl knapp als auch schwer zu beschaffen sein kann. Die durch die Komplexität und das Volumen der generierten Daten verursachten Herausforderungen erfordern zudem den Einsatz hochentwickelter Analysetools und Rechenressourcen. Um diese Herausforderungen zu bewältigen, hat sich die Miniaturisierung als wirkungsvolle Strategie erwiesen. Durch die Verkleinerung des Maßstabs von Reaktionen und Probenvolumina reduzieren miniaturisierte Plattformen die Reagenzienkosten erheblich und sparen wertvolles biologisches Material, wodurch Hochdurchsatzexperimente zugänglicher und effizienter werden. Die Skalierung auf kleinere Dimensionen erhöht auch den experimentellen Durchsatz, sodass eine größere Anzahl von Bedingungen gleichzeitig getestet werden kann, während die Gesamtkosten und der Ressourcenbedarf sinken. Die Integration der Miniaturisierung in Hochdurchsatzsysteme ist besonders wichtig für den Fortschritt der personalisierten Medizin, bei der schnelle und kostengünstige Tests unerlässlich sind, um vielversprechende therapeutische Kandidaten zu identifizieren, die auf die genetischen, molekularen und umweltbedingten Profile einzelner Patienten abgestimmt sind. Ein wichtiger Ansatz ist die personalisierte Medizin, bei der Therapien auf die spezifischen Eigenschaften jedes Patienten zugeschnitten werden. Dieser Ansatz ist besonders in der Onkologie von Bedeutung, da die Wirksamkeit der Behandlung zwischen Patienten mit derselben Krebsart stark variieren kann. Durch die Maximierung der therapeutischen Wirksamkeit bei gleichzeitiger Minimierung von Nebenwirkungen verspricht

9

die personalisierte Medizin, die Behandlungsergebnisse zu verbessern. Die Verwirklichung der personalisierten Medizin erfordert jedoch robuste Hochdurchsatzwerkzeuge, die in der Lage sind, kleinste, patientenabgeleitete Proben zu verarbeiten und genaue, validierte Daten bereitzustellen.

Die Droplet Microarray (DMA)-Plattform stellt eine vielversprechende Lösung dar, die die Stärken von Hochdurchsatz-Screening, Miniaturisierung, Parallelisierung und Demultiplexierung in einem einzigen, vielseitigen System vereint. Es wurde gezeigt, dass diese Plattform Medikamentensensitivitäts- und Reaktionstests (*Drug sensitivity and resistance testing* = DSRT), medikamenteninduzierte Genexpressionsanalysen (DGEA) und andere wichtige Assays im Nanoliterbereich durchführen kann. Durch die erhebliche Reduzierung der Proben- und Reagenzienbedarf verbessert die DMA-Plattform die Effizienz und Kosteneffizienz von Hochdurchsatzexperimenten und unterstützt gleichzeitig die Entwicklung personalisierter Strategien für die klinische Anwendung in der Onkologie. Dieser kombinierte Ansatz hat das Potenzial, die funktionelle Präzisionsmedizin zu revolutionieren, indem genauere und individualisierte Behandlungspläne ermöglicht werden, die auf die spezifischen Bedürfnisse jedes Patienten abgestimmt sind.

Das erste Projekt stellt eine neuartige Methodik vor, bei der patientenabgeleitete chronisch lymphatische Leukämiezellen (CLL) in eine Hydrogelmatrix auf der DMA-Plattform integriert werden. Dieser Ansatz zielt darauf ab, die erheblichen Herausforderungen bei der Kultivierung von CLL-Zellen zu bewältigen, die zu früher Apoptose neigen und unter konventionellen In-vitro-Bedingungen eine geringe Überlebensfähigkeit aufweisen. Typischerweise erfordern CLL-Zellen eine Co-Kultur mit unterstützenden Stromazellen oder das Vorhandensein löslicher Faktoren, um das Überleben zu fördern und die komplexe Tumormikroumgebung nachzuahmen. Erste Experimente in herkömmlichen Medien zeigten eine drastisch niedrige Zellviabilität, was die Einschränkungen traditioneller Kulturmethoden verdeutlicht. Durch die Integration der Hydrogelmatrix in die DMA-Plattform konnten wir die Viabilität von CLL-Zellen erheblich verbessern und nach 24 Stunden eine bemerkenswerte Überlebensrate von 68 % erreichen, eine signifikante Verbesserung gegenüber herkömmlichen Methoden. Die Hydrogelmatrix bot nicht nur die notwendige strukturelle Unterstützung, sondern schuf auch eine stabile Umgebung, die das Überleben der Zellen über

die Zeit hinweg förderte, was sie zu einem wertvollen Werkzeug für das DSRT von patientenabgeleiteten CLL-Zellen macht.

Das zweite Projekt stellt eine neuartige miniaturisierte Methode für die medikamenteninduzierte differentielle Genexpressionsanalyse (DGEA) im Nanoliterbereich vor, ein wichtiges Instrument zur Aufdeckung der molekularen Grundlage zellulärer Veränderungen nach einer medikamentösen Behandlung. Diese Methode ist besonders wertvoll für die Hochdurchsatzanalyse von Krebszellen, die aus Patientenbiopsien stammen, da hier die Knappheit der Proben eine erhebliche Herausforderung darstellt. Mithilfe der DMA-Plattform ermöglicht dieser innovative Ansatz eine parallele Analyse der Arzneimittelreaktionen in patientenabgeleiteten Zellen und überwindet effektiv die Einschränkungen traditioneller Protokolle. Die Methode umfasst eine Reihe von Schritten, darunter Zelllyse zur Isolierung von mRNA, cDNA-Konversion und anschließende quantitative Polymerase-Kettenreaktion (qPCR)-Analyse. Diese Arbeit demonstriert das Potenzial dieses Ansatzes für die funktionelle Präzisionsonkologie, indem sie Einblicke in die individuellen Tumorreaktionen auf Krebsmedikamente bietet.

Das dritte Projekt konzentriert sich auf die Entwicklung und Optimierung eines Seq-on-a-Chip-Protokolls unter Verwendung der DMA-Plattform für die Hochdurchsatzanalyse des globalen Transkriptoms. Dieser Ansatz erhöht die Effizienz und Präzision der RNA-Sequenzierung durch die Miniaturisierung des Probenvorbereitungsprozesses und die Integration von barcodierten Oligo-dT-Primeren mit Unique Molecular Identifiers (UMIs). Die Studie zeigt, dass die DMA-Plattform vergleichbare und in einigen Aspekten sogar überlegene Leistungen gegenüber herkömmlichen PCR-Röhrchenmethoden erbringt, insbesondere bei der Erfassung und genauen Erfassung komplexer transkriptomischer Profile. Die Integration dieser Methode in die DMA-Plattform ermöglicht eine Reduzierung des Reagenzienverbrauchs und eine Steigerung des Durchsatzes, was insbesondere in Szenarien von Vorteil ist, in denen die Verfügbarkeit von Patientenproben begrenzt ist. Zusammengefasst demonstrieren diese Projekte das Potenzial der DMA-Plattform als umfassendes Werkzeug für DSRT, DGEA und globale Transkriptomanalysen. Es wird erwartet, dass die laufende Forschung und die kontinuierliche Verfeinerung dieser Methodologien die funktionelle Präzisionsonkologie transformieren werden, indem sie die Entwicklung präziser, personalisierter

Behandlungsstrategien ermöglicht, die auf das Profil jedes einzelnen Patienten zugeschnitten sind.

List of figures

List of tables

List of abbreviations

1. **5-mC -** 5-Methylcytosine

2. **ACTB -** β-Actin

3. **ALL -** Acute Lymphocytic Leukemia

4. **AML -** Acute Myeloid Leukemia

5. **ANDeS -** Automated Nanoliter Droplet Selection and Collection Device

6. **BHM -** Barcoded Hydrogel Microspheres

7. **BTK -** Bruton's Tyrosine Kinase

8. **CAR T-cell -** Chimeric Antigen Receptor T-cell

9. **Calcein AM -** Calcein Acetoxymethyl Ester

10. **CBC -** Complete Blood Count

11. **CEL-Seq -** Cell Expression Sequencing

12. **cDNA -** Complementary DNA

13. **CNVs -** Copy Number Variants

14. **CLL -** Chronic Lymphocytic Leukemia

15. **CML -** Chronic Myeloid Leukemia

16. **CT -** Computed Tomography

17. **DCM –** Dichloromethane

18. **DGEA -** Differential Gene Expression Analysis

19. **DMA -** Droplet Microarray

20. **DMF -** Dimethylformamide

21. **DMSO -** Dimethyl Sulfoxide

22. **DSRT -** Drug Sensitivity and Resistance Testing

23. dPCR - Digital PCR

24. dscDNA – double stranded cDNA

25. ECM - Extracellular Matrix

26. ESTs - Expressed Sequence Tags

27. FACS - Fluorescence-Activated Cell Sorting

28. FGF - Fibroblast Growth Factor

29. FPO - Functional personalized oncology

30. FISH - Fluorescence In Situ Hybridization

31. FDA - Food and Drug Administration

32. g - Gravitational force (used in centrifugation)

33. *GAPDH* - Glyceraldehyde-3-Phosphate Dehydrogenase

34. GBL - Gamma-Butyrolactone

35. GFP - Green Fluorescent Protein

36. hr – Hour

37. lncRNAs - Long Non-Coding RNAs

38. HL - Hodgkin's Lymphoma

39. HPV - Human Papillomavirus

40. HTS - High-Throughput Screening

41. K. pneumoniae - Klebsiella pneumoniae

42. MRD - Minimal Residual Disease

43. MRI - Magnetic Resonance Imaging

44. MRSA - Methicillin-Resistant Staphylococcus aureus

45. miRNAs – MicroRNAs

46. MMPs - Matrix Metalloproteinases

47. MM - Multiple Myeloma

48. MDS - Myelodysplastic Syndrome

49. MTP - Microtiter Plate

50. ml - Milliliter

51. mm² - Square millimeter

52. mm³ - Cubic millimeter

53. mRNA - Messenger RNA

54. N - Number of cells (used in cell concentration calculation)

55. NMP - N-Methyl-2-pyrrolidone

56. NGS - Next-Generation Sequencing

57. NHL - Non-Hodgkin's Lymphoma

58. OHA - Oligonucleotide Hydrogel Array

59. PBS - Phosphate-Buffered Saline

60. PET - Positron Emission Tomography

61. PI3K/Akt - Phosphoinositide 3-Kinase/Protein Kinase B

62. PFDT - 1H,1H,2H,2H-Perfluorodecanethiol

63. PROTAC - PROteolysis TArgeting Chimeras

64. PCR - Polymerase Chain Reaction

65. qPCR - Quantitative Polymerase Chain Reaction

66. qRT-PCR - Quantitative Real-Time PCR

67. rRNA - Ribosomal RNA

68. RLT - RNA Later Lysis Buffer

69. RNA-seq - RNA Sequencing

70. RT-PCR - Reverse Transcription Polymerase Chain Reaction

71. scRNA-seq - Single-Cell RNA Sequencing

72. ScmRNA - Single-Cell Messenger RNA

73. SAGE - Serial Analysis of Gene Expression

74. SNPs - Single Nucleotide Polymorphisms

75. siRNAs - Small Interfering RNAs

76. smRNA - Small RNA

77. SMRT - Single Molecule Real-Time

78. sscDNA - Single-Stranded Complementary DNA

79. **THF -** Tetrahydrofuran

80. **TKIs -** Tyrosine Kinase Inhibitors

81. **UMI -** Unique Molecular Identifier

82. UV – Ultraviolet

83. VEGF - Vascular Endothelial Growth Factor

84. WCA - Water Contact Angle

85. µL - Microliter

Chapter 1. Introduction

1.1 Cancer

Cancer arises from the abnormal growth of any type of cell in the body, and there are over a hundred different types of cancer, each with its own behaviour and response to treatment. [4-6] Tumours, which arise from abnormal cell growth, can be either benign or malignant. A key aspect of cancer pathology is distinguishing benign from malignant. Benign tumours remain confined to the original site of the tumour and do not invade the surrounding normal tissue or spread to other parts of the body. In contrast, malignant tumours have the ability to invade surrounding tissues and spread throughout the body via the circulatory or lymphatic systems, a process known as metastasis.[7, 8] Only malignant tumours are classified as cancers, and it is their invasive and metastatic properties that make them particularly dangerous. While benign tumours can often be removed surgically, the ability of malignant tumours to spread to distant sites often renders local therapy unsuccessful.[8]

Tumours are classified according to the type of cell from which they originate, both benign and malignant. Most types of cancer fall into one of three main groups: carcinomas, sarcomas, and leukaemia's or lymphomas.[9] Carcinomas, which account for about 90% of human cancers, are malignancies of epithelial cells.[10] Sarcomas, which are rare in humans, are solid tumours that develop in connective tissues such as muscle, bone, cartilage and fibrous tissue.[11] Leukaemia and lymphomas, which account for about 8% of human malignancies, arise from blood-forming cells and cells of the immune system, respectively. [12] Tumours are further classified according to the tissue from which they originate (e.g., lung cancer or breast cancer) and the type of cells that are involved. For example, fibrosarcoma arises from fibroblasts, while erythroid leukaemia arises from precursors of red blood cells (erythrocytes). [6, 10] (Figure 1)

Cancer is the second most common cause of death in Europe.[6, 13] It was estimated that around 323,545 men and 282,260 women were diagnosed with cancer in 2023 in Germany, with the most common types of cancer being breast cancer, prostate cancer, colorectal cancer, and lung cancer.[14] Across Europe, an estimated 4,878,513 new cancer cases were diagnosed in 2023, with 2,211,362 cancer-related deaths. Globally, the number of new cancer cases was projected to exceed 20 million in 2023, highlighting the growing global burden of

the disease.[15] Approximately 37% of these diagnosed cancers are estimated to have been preventable. The four most common cancers - breast, prostate, lung and colorectal - account for more than half of all cancers. Lung cancer, which is the most deadly, is responsible for almost 30% of all deaths due to cancer.[6]
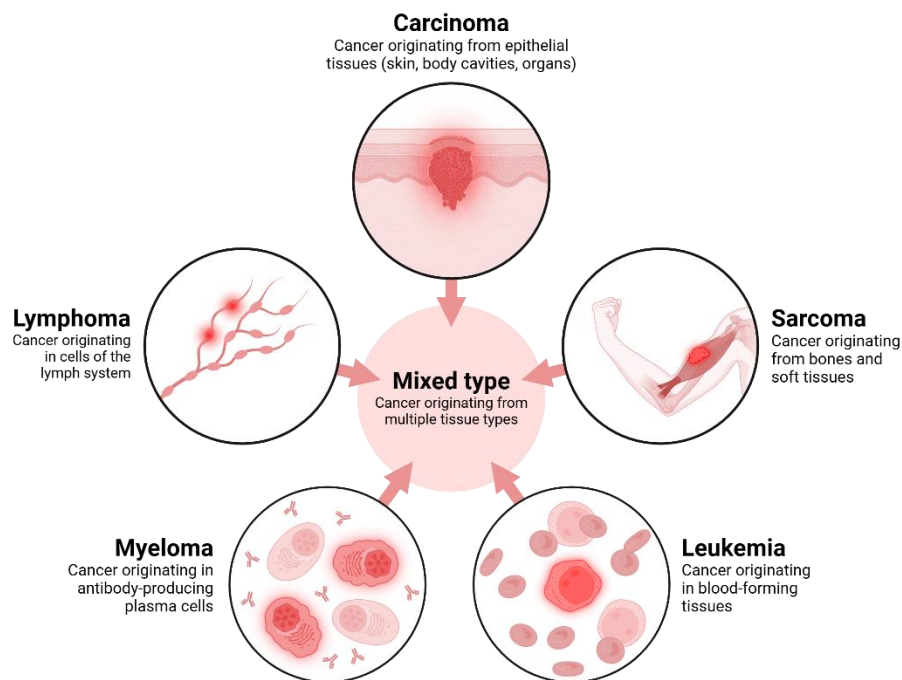
Figure 1. Overview of Cancer Classifications by Histological Type

This figure illustrates the different histological classifications of cancer, detailing the specific characteristics and categorizations of various cancer types, including carcinoma, lymphoma, sarcoma, myeloma, and leukemia. Image sourced from: National Cancer Institute. Cancer Classification | SEER Training. Cancer.gov. Published 2019. Cancer Classification.[16]

1.1.1 Cancer development and properties of cancer cells

At the cellular level, the development of cancer is seen as a multi-step process involving mutation and selection for cells with progressively increasing capacities for proliferation, survival, invasion and metastasis.[7, 17] The initial phase of cancer development, known as tumour initiation, is believed to arise from a genetic mutation within a single cell. This genetic alteration disrupts the normal regulatory mechanisms that control cell growth and division, leading to uncontrolled cell proliferation. During this process, the affected cell gains the ability to divide more rapidly and avoid the normal apoptotic signals that would normally lead to its destruction. This uncontrolled proliferation marks the beginning of tumour formation as the

single mutated cell and its progeny continue to grow and accumulate further genetic changes, setting the stage for subsequent stages of cancer progression.[18, 19] This uncontrolled proliferation drives the expansion of a population of clonally derived tumour cells, all of which originate from the initial mutated cell. This is driven by mutations in genes that regulate the cell cycle, such as oncogenes and tumor suppressor genes, allowing cells to divide continuously without the usual regulatory checks. Additionally, cancer cells often evade apoptosis, the process of programmed cell death, which further contributes to their unchecked growth.[20] As the tumour develops, additional genetic mutations occur within this growing population of cells. Some of these mutations confer selective advantages to certain cells, such as accelerated growth rates, enhanced survival mechanisms or improved ability to invade and metastasise. This evolutionary process is known as clonal selection. It allows cells with advantageous mutations to outcompete others, leading to their dominance within the tumour. Cancer cells also demonstrate impaired differentiation. While normal cells undergo maturation to perform specific functions, cancer cells frequently remain in an undifferentiated state. This failure to differentiate properly enables them to maintain a high proliferative capacity. For example, in leukemias, cancerous cells are arrested at early stages of development, preventing their maturation into functional blood cells and enabling continuous proliferation.

Clonal selection is a dynamic and ongoing process throughout tumour progression. The accumulation of mutations leads to increasingly aggressive and malignant cell populations as the tumour evolves. These highly adapted cells exhibit characteristics such as resistance to apoptosis, an enhanced ability to evade the immune system, and an increased potential to invade surrounding tissues and form secondary tumours (metastases) in distant organs. As a result, the tumour becomes more heterogeneous, with subpopulations of cells that have different genetic profiles and phenotypic characteristics, contributing to the complexity and difficulty of treatment of advanced cancers.[18, 19, 21]

Carcinogens play an important role in the development of cancer, which is a complex, multi-step process influenced by many factors, and have been identified through experimental animal studies and epidemiological analysis of human cancer incidence. Several agents have been shown to induce cancer in animals and humans, including radiation, chemicals, and

viruses. Radiation and many chemical carcinogens, such as those found in tobacco smoke and aflatoxin, act by damaging DNA and inducing mutations, thus acting as initiating agents in the development of cancer.[22] Smoking, a major source of carcinogenic chemicals such as benzo(a)pyrene, is responsible for nearly one-third of all cancer deaths worldwide and is the leading cause of lung cancer. The harmful chemicals in tobacco smoke induce DNA damage and mutations that are the initiators of cancer development.[23] In addition to initiators, other carcinogens, known as tumour promoters, play a crucial role in cancer progression. They stimulate cell proliferation. For example, phorbol esters activate protein kinase C, which promotes cell division, while hormones such as oestrogen can increase the risk of endometrial and breast cancer by stimulating the proliferation of hormone-sensitive cells.[24] In addition, certain viruses are major contributors to cancer incidence, causing 10 to 20% of cancer cases worldwide. For example, hepatitis B and C viruses are associated with liver cancer, and human papillomavirus (HPV) is associated with cervical cancer. These oncogenic viruses provide valuable insights into the molecular mechanisms of carcinogenesis, in addition to directly inducing cellular transformation and tumour formation. By integrating their genetic material into the host genome, these viruses can disrupt normal cell regulatory pathways. This leads to uncontrolled cell growth and cancer. The study of these viral mechanisms has advanced our understanding of cancer biology and is a key factor in the development of vaccines and targeted therapies.[10, 25, 26]

Two key properties of cancer cells are essential for their ability to invade surrounding tissues and spread to distant sites: secreting proteases and promoting angiogenesis. Cancer cells produce and secrete a variety of proteases, such as matrix metalloproteinases (MMPs) and collagenases, which play a crucial role in the degradation of the extracellular matrix (ECM). The ECM is a complex network of proteins and carbohydrates that provides structural support to tissues and organs. By degrading components of the ECM, such as collagen and fibronectin, cancer cells disrupt the structural integrity of the surrounding tissue. This degradation of the ECM facilitates the invasion of cancer cells into adjacent tissues by creating a more accessible pathway through which they can penetrate the basement membrane and spread to neighbouring areas.[27]

Cancer cells also stimulate angiogenesis, the formation of new blood vessels from existing ones. Tumours need a constant supply of oxygen and nutrients to grow beyond a certain size.[18, 19, 28] To meet this need, cancer cells release growth factors such as vascular endothelial growth factor (VEGF) and fibroblast growth factor (FGF). These growth factors induce endothelial cells to proliferate and form new capillaries, effectively creating a network of blood vessels within the tumour. This new vascular network not only supports the growing tumour by supplying essential nutrients and oxygen, but also provides routes for tumour cells to enter the bloodstream. When cancer cells invade these newly formed blood vessels, they can circulate through the bloodstream and form secondary tumours in distant organs by metastasis.[29] Cancer cells often have abnormal differentiation patterns in comparison to normal cells. Fully differentiated cells typically reach a mature state where they either stop dividing or divide infrequently. However, cancer cells often remain blocked in early stages of differentiation. This failure to mature properly allows cancer cells to continue to proliferate uncontrollably. For example, in leukaemia, leukemic cells are arrested at early stages of blood cell development, preventing them from maturing into functional blood cells and allowing them to proliferate indefinitely.[30-32]

Apoptosis, or programmed cell death, is a crucial process for eliminating damaged or unwanted cells and ensuring normal cell turnover. This process is essential for maintaining cellular homeostasis and differentiation. However, many cancer cells develop mechanisms to evade apoptosis, which contributes to their prolonged survival. Cancer cells often acquire mutations or alterations in signalling pathways that allow them to bypass the normal apoptotic signals triggered by DNA damage or other cellular stressors. These apoptosis evasion mechanisms allow tumour cells to survive despite severe genetic damage and prolonged exposure to potentially lethal treatments.[33] Cancer cells can evade apoptosis through several strategies: they can alter the expression of apoptotic regulatory proteins, such as Bcl-2 family members, or activate anti-apoptotic signalling pathways, such as the Phosphoinositide 3-Kinase/Protein Kinase B (PI3K/Akt) pathway.[34, 35] In addition, cancer cells often exhibit the ability to survive in the absence of external growth factors that are normally essential for cellular maintenance and proliferation. This is achieved by upregulating intrinsic survival signals and altering cellular metabolism. The resistance to apoptosis not only allows cancer cells to endure DNA damage but also contributes to their resilience against

conventional treatments like radiation and chemotherapy. These therapies rely on inducing apoptosis in cancer cells, but the ability of cancer cells to avoid programmed cell death limits their effectiveness and promotes treatment resistance. Consequently, the combination of continuous proliferation and enhanced survival significantly contributes to the persistent growth and aggressive nature of tumours.[18, 19, 36]

Understanding these mechanisms of differentiation failure and apoptotic evasion is crucial for developing more effective cancer therapies. Researchers are actively exploring ways to target these pathways to restore normal apoptotic processes and improve treatment outcomes for cancer patients.

1.1.2 Chronic Lymphocytic Leukemia (CLL) and other blood cancers

Blood cancers, also known as haematological cancers, start in the bone marrow and include leukaemia, lymphoma and myeloma. These cancers are the result of the uncontrolled growth of abnormal blood cells and the disruption of the normal function of healthy blood cells. Chronic lymphocytic leukaemia (CLL) is a slowly progressing type of leukaemia that originates in the B-lymphocytes in the bone marrow.[37] It is predominantly characterised by genetic mutations and chromosomal abnormalities such as deletions of chromosomes 13q, 11q and 17p, trisomy 12 and mutations in genes such as TP53, NOTCH1, SF3B1 and ATM. These genetic changes result in the build-up of malfunctioning mature B-lymphocytes in the blood, bone marrow and lymphatic tissue.[38-40] CLL is a disease of the elderly, with a median age at diagnosis of about 70 years. Risk factors include a family history of blood cancer and prolonged exposure to certain chemicals, such as pesticides and herbicides. CLL often progresses slowly. Many patients remain asymptomatic for years. When symptoms develop, they may include fatigue, swollen lymph nodes, frequent infections, unexplained weight loss, night sweats, anaemia and splenomegaly (enlarged spleen). Diagnosis typically involves blood tests that show an increase in the number of B-lymphocytes, flow cytometry to identify characteristic markers on the surface of cells, bone marrow biopsy, and genetic testing to detect chromosomal changes and mutations.[37, 41] Treatment strategies vary depending on the stage of the disease and the patient's overall health. Early-stage CLL often only requires

active surveillance or "watchful waiting" with regular monitoring. Advanced-stage CLL may be treated with various therapies, including chemotherapy, targeted therapies, such as BTK inhibitors ibrutinib and acalabrutinib, BCL-2 inhibitor venetoclax, PI3K inhibitor idelalisib, anti-CD20 monoclonal antibodies rituximab and obinutuzumab, and anti-CD52 monoclonal antibody alemtuzumab, as well as combinatorial therapies, and stem cell transplantation.[39, 40, 42] Ongoing research in CLL is focused on understanding its molecular mechanisms in order to develop more effective treatments and personalised medicine approaches, with current studies aiming to identify novel genetic targets, improve existing therapies and explore the role of the immune system in controlling CLL, thereby improving prognosis and quality of life for patients.

Other types of blood cancer include acute lymphoblastic leukaemia (ALL), which is a fast-growing cancer that arises from immature lymphocytes in the bone marrow and is characterised by genetic mutations and chromosomal abnormalities such as presence of Philadelphia chromosome and expression of BCR-ABL fusion gene.[43] In contrast, acute myeloid leukaemia (AML) is an aggressive cancer of the myeloid cells, often involving genetic mutations such as FLT3, NPM1 and DNMT3A.[44] Chronic myeloid leukaemia (CML) is also characterised by the presence of BCR-ABL fusion gene causing an uncontrolled proliferation of myeloid cells.[45] Lymphomas originate in the lymphatic system and include Hodgkin lymphoma (HL), characterized by the uncontrolled proliferation of Reed-Sternberg cells, and non-Hodgkin lymphoma (NHL), which encompasses several subtypes.[46, 47] Finally, multiple myeloma (MM) is a cancer of the plasma cells that causes anaemia, bone pain and susceptibility to infection.[48]

Accurate diagnosis and ongoing research into innovative therapies are essential for effective treatment and improved patient outcomes in all types of blood cancer. (Figure 2)
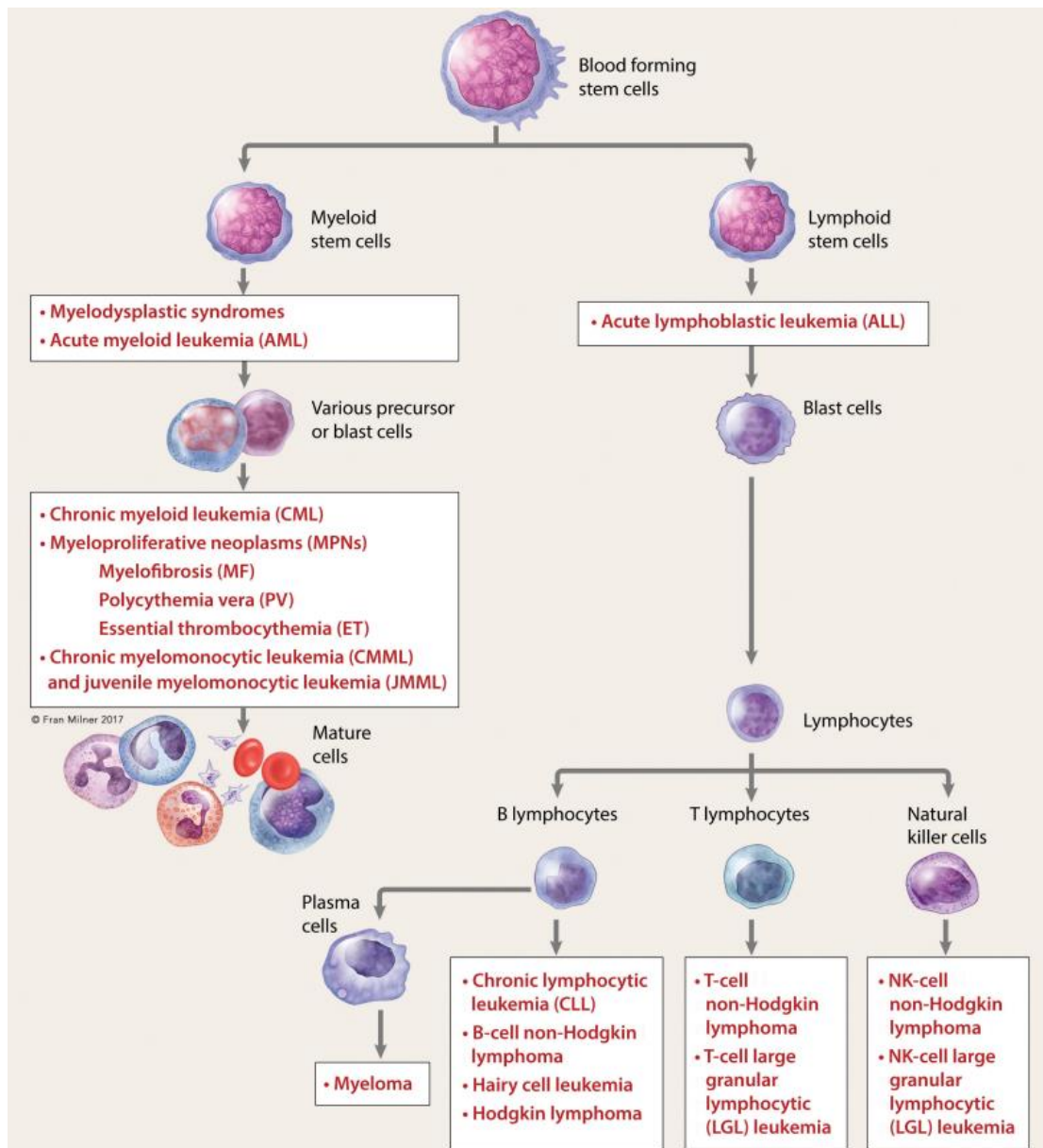
Figure 2. Blood Cancer Family Tree and Subtypes

This figure illustrates the hierarchical relationships and classifications of blood cancers, including leukemia, lymphoma, and myeloma, along with their respective subtypes. Leukemia is further divided into Acute Lymphocytic Leukemia (ALL), Acute Myeloid Leukemia (AML), Chronic Lymphocytic Leukemia (CLL), and Chronic Myeloid Leukemia (CML). Lymphoma includes Hodgkin Lymphoma and Non-Hodgkin Lymphoma. Myeloma is represented by Multiple Myeloma. This visualization aids in understanding the complex structure and specific categories within blood cancers. Image sourced from The Leukemia & Lymphoma Society website. [49]

1.1.3 Advances in blood cancer diagnosis and emerging therapies

Diagnosing blood cancers such as leukaemia, lymphoma and multiple myeloma requires a comprehensive approach. The diagnostic process includes a medical history, physical examination, blood tests CBC (Complete Blood Count) and peripheral blood smear, bone marrow aspiration and biopsy for the detection and identification of malignant cells.[50] In recent years, the survival rates for these diseases have improved significantly due to advancements in immunotherapy. In 2023, in the European Union (EU), leukemia affects approximately 50,000 people annually, with a slight male predominance. Lymphoma cases are around 85,000 annually, with a balanced gender distribution. Multiple myeloma affects about 35,000 people each year in the EU, with a higher incidence in men compared to women. In Germany specifically, leukemia affects around 20,000 people annually, lymphoma around 30,000, and multiple myeloma about 10,000.[14, 51] Survival rates have improved considerably over recent decades due to advancements in treatment. In Germany, the five-year survival rate for leukemia has increased from approximately 40% in the 1970s to about 60% in 2023. For lymphoma, the survival rate has improved from about 50% in the early 1970s to approximately 70% in 2023. Multiple myeloma's five-year survival rate has increased from around 25% in the 1960s to over 55% in 2023.[14, 52] To detect specific genetic mutations and chromosomal abnormalities, flow cytometry, cytogenetic analysis (karyotyping and FISH) and molecular techniques such as polymerase chain reaction (PCR) and next-generation sequencing (NGS) are used.[44, 53-55] The spread of the disease is assessed using imaging techniques such as Computed tomography (CT), Magnetic Resonance Imaging (MRI) and Positron Emission Tomography (PET) scans. For lymphoma, a lymph node biopsy may be carried out. These diagnostic procedures are essential in determining the type, stage and extent of haematological malignancies, and in guiding treatment plans. For example, the diagnosis of CLL involves a detailed patient history, physical examination, CBC, peripheral blood smear, bone marrow aspiration, flow cytometry, cytogenetic analysis, molecular testing and imaging studies to accurately classify and stage the disease. This information is used to determine prognosis and guide therapy. Recent advances in targeted therapies, immunotherapies and novel modalities have significantly improved patient outcomes in the treatment of blood cancers. Targeted therapies, such as imatinib (Gleevec) for chronic myeloid leukaemia (CML)[56, 57] and blinatumomab (Blincyto) for acute lymphoblastic

leukaemia (ALL),[58] selectively inhibit cancer cell survival pathways. Imatinib targets the BCR-ABL tyrosine kinase, which is responsible for the proliferation of CML cells, while blinatumomab is a bispecific T-cell engager that targets CD19 on leukemia cells and CD3 on T-cells, promoting the destruction of ALL cells.[48] Immunotherapies harness the immune system to fight cancer, including CAR T-cell therapy. This approach has shown success in treating certain leukaemia and lymphomas. For example, CAR T-cell therapies targeting the CD19 antigent, such as tisagenlecleucel (Kymriah)[59] and axicabtagene ciloleucel (Yescarta),[60] have been particularly effective. Tisagenlecleucel is used for the treatment of relapsed or refractory B-cell ALL , while axicabtagene ciloleucel is used for large B-cell lymphoma.[59-62] These therapies involve modifying a patient's T-cells to express a chimeric antigen receptor (CAR) that specifically targets CD19 on the surface of cancer cells, leading to their destruction. Cell-based therapies, as well as monoclonal antibodies and proteasome inhibitors, have expanded the range of treatment options for diseases such as non-Hodgkin's lymphoma and multiple myeloma. New treatment modalities are being driven by genetic and molecular understanding. These include small molecule inhibitors, epigenetic modifiers and immune checkpoint inhibitors. Future directions will focus on genomic profiling, personalised medicine, combination therapies and advances in the engineering of CAR T cells to improve outcomes and broaden the applicability of treatments.[63]

The evolving landscape of blood cancer treatment aims to address challenges like treatment resistance and toxicity, offering personalized, effective therapies to enhance patient prognosis and quality of life. Personalized medicine, which tailors' treatment to the unique genetic and molecular profile of each patient's cancer, is increasingly recognized as crucial for optimizing therapeutic outcomes and minimizing adverse effects, underscoring its importance in the fight against cancer.

1.2 Personalized medicine

Personalized medicine, also known as precision medicine, is an innovative approach to patient care that aims to individualize medical treatment to each patient's unique characteristics. By taking into account genetic, environmental and lifestyle factors, personalized medicine aims

to optimize therapeutic efficacy and minimize adverse effects. In the context of blood cancers, personalized medicine has transformed treatment approaches by enabling highly specific and targeted interventions. By analyzing detailed genetic and molecular profiles of individual patients, this approach enables the development of tailored therapies that improve efficacy, reduce side effects and improve overall patient outcomes.[55, 64, 65]

1.2.1 Personalized medicine and the human genome

The integration of genomic data into medical decision-making is transforming the field of personalized medicine. By using the information derived from genome sequencing - including RNA profiles, protein expression patterns and metabolite levels - clinicians are now able to improve health assessments by customizing them to individual genetic profiles. This approach enables healthcare professionals to predict the risk of disease, to identify genetic carriers, to make precise diagnoses and to formulate accurate prognoses. As a result, personalized medicine makes it easier to create tailored care plans, which can adapt at any stage of the disease. [44, 66]

Within the continuum from health to disease, genomic applications are revolutionizing personalized healthcare at several key points. DNA-based assessments can quantify and predict an individual's susceptibility to various diseases.[67] These insights remain consistent throughout a person's lifetime. In addition, advanced techniques such as transcriptional profiling, protein expression analysis and metabolite measurements, combined with advanced imaging technologies, provide precise methods for screening individuals at high risk of developing disease, even in its earliest, subclinical stages.[68] This comprehensive genomic information supports definitive diagnoses and enables molecular classifications that predict disease outcomes. In addition, pharmacogenomics - the study of how genetic variations affect drug response - is demonstrating the practical application of genomic information in refining personalized treatment strategies. By understanding genetic differences in drug efficacy and toxicity, healthcare providers can optimize medication plans, minimize adverse effects, and improve therapeutic outcomes. Overall, the integration of genomic data into medical practice represents a significant leap forward in tailoring healthcare to each individual's unique genetic makeup.[4, 55, 68] (Figure 3)

Personalization of Medicine
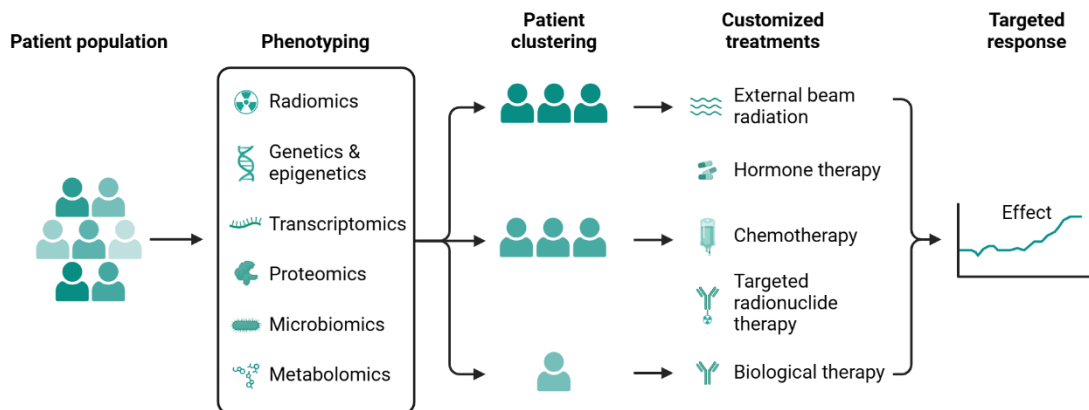
Figure 3. Personalized Medicine and Targeted Therapy

This figure illustrates the concept of personalized medicine, highlighting the process of phenotyping patients to customize treatments tailored to individual characteristics. By analyzing genetic, phenotypic, and environmental factors, personalized medicine enables the development of targeted therapies that are more effective and have fewer side effects compared to traditional treatments. This approach represents a significant advancement in precision healthcare, aiming to improve patient outcomes through individualized treatment plans. Image customized using BioRender

1.2.2 The genome toolbox: pathways to precision medicine

1.2.2.a Genomics

Genomics is the comprehensive study of an organism's entire genetic make-up, or genome. It focuses on the analysis of genome structure, function, evolution, and mapping to understand how genes and their interactions affect health, disease, and development.[18, 55, 69] Genetic variation within the human genome is manifested by several different types of changes. Single nucleotide polymorphisms (SNPs) are the most common type of variation and involve changes in a single nucleotide base pair that can influence an individual's susceptibility to disease and response to treatment. Insertions and deletions (indels) involve the addition or loss of small segments of DNA that can potentially disrupt the function of a gene or create new variants of the gene. Copy number variants (CNVs) are differences in the number of copies of specific DNA regions that affect the dosage of genes and contribute to diseases such as cancer and neurological disorders. Structural changes, including chromosomal rearrangements and large deletions or duplications, affect the organization and function of chromosomes.[38, 70] Repeat variations, which involve altering repeated DNA sequences, are associated with genetic disorders such as Huntington's Disease. Advances in NGS technology

have transformed genomics by enabling high-throughput sequencing, significantly reducing the cost of genome sequencing to around $10,000, with predictions of a future reduction to around $1,000. This cost reduction may soon make whole-genome sequencing a standard tool in medical testing, enabling personalized approaches to understanding and managing individual health risks.[71, 72]

1.2.2.b Advances and applications of next-generation sequencing (NGS)

The sequencing of the first human genome was a monumental achievement, requiring 20 years of international collaboration and approximately $3 billion in funding. Launched in 1990 and completed in 2003, the Human Genome Project involved contributions from thousands of scientists in several countries and laid the foundation for advances in genomics and personalized medicine.[73] Meanwhile, modern technologies have dramatically reduced the cost of sequencing a human genome at 30-fold coverage to around $1000 [74]. This dramatic reduction is due to rapid advances in sequencing technologies,[75] which greatly improve throughput over traditional Sanger sequencing[76]. Since 2005, a variety of high-throughput sequencing technologies have emerged,[77, 78] but the technology from Illumina has become the dominant player in the market.[79] This method, a variant of sequencing-by-synthesis using cyclic reversible termination[80, 81], involves preparing DNA samples by adding immobilizing adapters to fragmented DNA to allow attachment to flow cells.[82]Early versions of this technology used random attachment, but more recent iterations have used patterned nano-well flow-cells to increase the density of the template.[83] After annealing, the DNA templates are amplified in place using 'bridging amplification', producing clusters of thousands of clonal copies.[82] Sequencing-by-synthesis then proceeds by simultaneously adding all four nucleotide bases, each modified with a unique fluorophore and cleavable chain terminator, ensuring only one base is incorporated. The fluorescence emitted by each clonal cluster is recorded, and after each cycle the fluorophore and chain terminator are cleaved, allowing the next sequencing cycle to proceed. Based on the fluorescence data,[75] base calling is performed after a predetermined number of cycles. Initially limited to 26 bases per read,[75]advances have increased read lengths to 600 bases (300 bases paired-end) on some

Illumina machines.[84, 85] Despite these improvements, common sequencing errors include substitutions due to incorrect base incorporation, with errors becoming more common towards the end of reads due to phasing issues where some clonal molecules fail to cleave fluorophores or incorporate bases properly.[75]

In contrast to clonal amplification-based short-read technologies, two major single-molecule real-time sequencing technologies are advancing rapidly. Pacific Biosciences (PacBio) uses a method that detects DNA synthesis from a single, fixed polymerase enzyme using fluorescently labelled nucleotides.[86] This technique, known as Single Molecule Real-Time (SMRT) sequencing, offers long read lengths and high accuracy, making it suitable for applications such as de novo genome assembly and isoform sequencing. Oxford Nanopore Technologies, on the other hand, uses a different approach that does not rely on sequencing by synthesis. Their method is based on membrane proteins that form nanopores that are immobilized SMRTon an array.[87] When a DNA molecule passes through a nanopore, the unique molecular structure of each nucleotide causes changes in the ion current that are detected and interpreted.[88] This technology is promising, although significant challenges remain in signal interpretation. It can directly detect base modifications such as 5-methylcytosine (5-mC).[89] It can also perform direct RNA sequencing without the need for prior cDNA synthesis.[90] Today, Illumina sequencers dominate the market for generating large amounts of high-quality data at the lowest cost per base. This makes them the preferred choice for many applications, including RNA sequencing studies.

Table 1: Comparison of Sequencing Platforms

This table provides a comprehensive comparison of various sequencing platforms used in RNA sequencing and their applications in cancer diagnosis and targeted therapy. Key features include the company, platform name, sequencing mechanism, maximum read length, highest throughput, run time, and error rate. The comparison offers insights into the strengths and limitations of each platform, aiding in the selection of the most appropriate technology for different genomic sequencing needs. This table content is adopted from the source "RNA Sequencing and its Applications in Cancer Diagnosis and Targeted Therapy."[91]

Company	Platform	Sequencing Mechanism	Current Model	Maximum Read Length (bp)	Highest Throughput	Turnaround Time	Error Rate (%)
Roche	454	Synthesis reaction + pyrophosphate release, chemiluminescence detection	GS FLX+	1000	700Mb	23 hours	1
			GS Junior	400	35Mb	10 hours	1
Illumina	Solexa	Synthesis reaction + colorimetric label detection	HiSeqX	150	1.8Tb	3 days	0.4
			HiSeq 2500	150	180Gb	40 hours	0.4
			NextSeq500	150	39Gb	26 hours	0.4
			MiSeq (MiSeqDx)	300	15Gb	8.5 hours	0.4
Life Technology	SOLiD	Ligation reaction + colorimetric label detection	5500xl W	50	320Gb	6 days	0.1
	Ion Torrent	Synthesis reaction + proton release and PH sensing	PGM	400	2Gb	3 hours	1
			Proton	400	10Gb	4 hours	1
Oxford Nanopore	Nanopore	None reaction, single molecule electronics-based sensing	GridION	100,000	185Mb	6 hours	4
			MinION	100,000	28G/10node 1 day	N/A	4
Pacific Biosciences	PacBio	Synthesis reaction + single molecule real-time (SMRT) colorimetric label detection	PacBio RS II	30,000	350Mb	10 hours	15

1.2.3 Differential gene expression

Gene expression is a crucial biological process responsible for converting the genetic information encoded in DNA into functional molecules including proteins and RNA. This process leads to the production of the necessary components for cellular function and regulation by ensuring that the instructions embedded in DNA are accurately interpreted and executed. DNA, or deoxyribonucleic acid, is a vital biomolecule. It contains the complete genetic blueprint of an organism. It is the hereditary material that is passed from one generation to the next. It ensures the continuity of genetic information and the preservation of species-specific traits. The role of DNA is fundamental to the maintenance of life, as it controls the synthesis of proteins and RNA, which are essential for countless biological activities and processes.[92] The central dogma of molecular biology, which was first formulated by Francis Crick in 1958, describes the directional flow of genetic information within a biological system. This flow involves several key processes: replicating DNA, transcribing DNA into transient messenger RNA (mRNA), and translating mRNA into amino

acid sequences by ribosomes, ultimately leading to protein synthesis (Figure 4). This process involves highly sophisticated regulatory mechanisms rather than a simple linear pathway. These mechanisms precisely control the timing, location and amount of gene product production. Through various regulatory processes, cells ensure that each gene is expressed at the right time, in the right place and in the right amount to maintain proper cellular function and respond to internal and external signals.[93] In multicellular organisms, the wide variety of cell types and their specialized functions are made possible by differential gene expression. Although each cell with a nucleus contains the entire sequence of DNA, known as the genome, which includes all the genes and non-coding regions, only a specific subset of these genes is expressed in each cell type. This selective gene expression results in the production of a unique set of proteins, known as the proteome. The proteome determines the identity and function of the cell. A critical role in shaping the proteome and thus defining the characteristics of the cell is played by the specific patterns of transcription, the process by which DNA is copied into mRNA. Importantly, transcriptional control is not a simple on/off switch. Instead, the levels of mRNA produced can vary widely and often correlate with the abundance of the corresponding proteins. This sophisticated regulation allows cells to fine-tune protein production in response to developmental cues and environmental signals, ensuring that each cell type effectively fulfils its designated role within the organism.[94, 95]

The regulation of gene expression levels is achieved through several key mechanisms: chromatin state, DNA methylation, transcription factors and enhancers. Chromatin state involves the packaging of DNA into complex nucleoprotein structures. The degree of chromatin condensation affects gene accessibility and transcriptional activity.[96] DNA methylation, specifically the addition of methyl groups to cytosine residues to form 5-mC , serves as an important epigenetic mark that generally results in the silencing of genes and plays a critical role in development and cellular differentiation.[97] Transcription factors, which are proteins with sequence-specific binding properties, bind to the promoter regions of genes to initiate and modulate transcription, acting either as activators or repressors of gene expression.[98] Enhancers, which are regulatory DNA sequences located at variable distances from the transcription start site, contain binding sites for transcription factors and significantly increase transcription when they are brought into close proximity to promoter regions by DNA looping. Together, these mechanisms ensure that genes are expressed at

appropriate levels, in specific cell types and at precise times, which is essential for normal development, cellular differentiation and maintenance of cellular function. Together, these mechanisms allow precise control of gene expression patterns leading to specific cellular functions, phenotypes, and development. Understanding transcriptional regulation is crucial for understanding biological processes such as development and the link between transcriptional mis-regulation and various diseases, including cancer.[98] As our knowledge of gene expression mechanisms expands, new avenues for therapeutic intervention and advances in biotechnology will emerge.
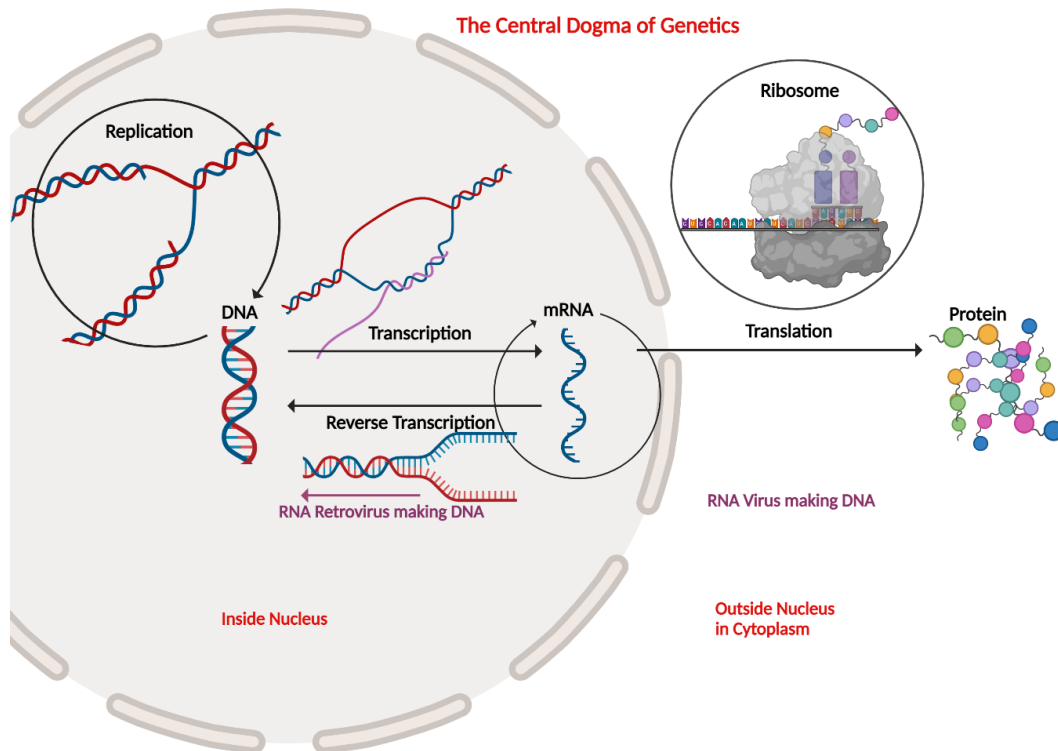
Figure 4. The Central Dogma of Molecular Biology

This figure illustrates the central dogma of molecular biology. It describes the flow of genetic information within a biological system. The process starts with DNA replication, followed by the transcription of DNA into messenger RNA (mRNA), and ends with the translation of mRNA into proteins. This basic concept emphasizes the directional transfer of genetic information: DNA → RNA → Protein, highlighting the critical roles of replication, transcription, and translation in expressing genes and synthesizing proteins. The image is adopted from exploringnature.org and created using Biorender.[99]

1.2.4 mRNA quantification methods: historical perspectives and cutting-edge technologies

There is a natural interest in the quantification of mRNA transcripts. This is because gene expression levels play a crucial role in the regulation of cellular functions and developmental processes in cells, tissues, and organisms. The history of mRNA quantification dates back to 1977 with the development of "Northern blots",[100] a technique in which RNA molecules separated by electrophoresis are transferred to paper membranes and detected by means of radioactively labelled probes. This method laid the foundation for subsequent advances in mRNA analysis. Fluorescence in situ hybridization (FISH) improved the spatial resolution of gene expression studies by using fluorescently labelled DNA probes to quantify mRNA directly in tissue samples, a technique introduced by Pachmann in 1987.[101] Another powerful tool for mRNA quantification was the advent of polymerase chain reaction (PCR) in 1986.[102] By reverse transcribing mRNA into complementary DNA (cDNA) and amplifying it by PCR, researchers could obtain quantitative data by incorporating fluorescent dyes and measuring the signals emitted after each amplification cycle, a method known as quantitative PCR (qPCR). [102, 103] However, these methods were limited to the quantification of specific mRNAs and lacked the ability to provide a comprehensive, genome-wide view of the transcriptome.

To overcome these limitations, techniques such as the sequencing of cloned cDNA, expressed sequence tags (ESTs),[104, 105] have been developed to survey the transcriptome, although they do not provide quantitative information. The first techniques that provided global gene expression data with quantitative information are serial analysis of gene expression (SAGE) DNA microarrays revolutionized mRNA quantification by immobilizing synthetic DNA oligonucleotide probes on a surface. Initially, the oligonucleotides were synthesized and dotted onto the surface in a dense pattern, but this later evolved into direct synthesis directly on the surface.[106] These probes, designed to be complementary to cDNA, allowed fluorescently labelled cDNA to hybridize to the complementary oligonucleotides, producing a fluorescent signal where hybridization occurred. The intensity of this signal was proportional to the amount of hybridized cDNA, allowing precise quantification of gene expression. Microarrays gained popularity due to their relative ease of use, cost effectiveness and high-quality data output. The journey of mRNA quantification has evolved from Northern blots to

advanced techniques such as qPCR, FISH, SAGE and microarrays, each contributing to our understanding of gene expression with varying degrees of specificity and comprehensiveness. These developments have paved the way for more detailed and accurate profiling of the transcriptome, providing invaluable insights into the molecular mechanisms governing cellular and developmental processes.

Quantitative real-time PCR (qRT-PCR) remains a key tool in molecular biology due to its exceptional sensitivity and specificity. In this method, mRNA is first converted into cDNA and then amplified by quantitative PCR. Gene expression level can be precisely quantified by measuring the fluorescence emitted during each amplification cycle in real time. RNA sequencing (RNA-seq) has helped revolutionize transcriptome analysis by sequencing cDNA fragments to provide a comprehensive view of gene expression. This technique allows the detection of novel transcripts and splice variants, providing insights that were previously unattainable. Digital PCR (dPCR) further enhances mRNA quantification by dividing the PCR reaction into multiple droplets or wells, with each partition ideally contain a single molecule of the target nucleic acid, which is then amplified independently. The number of positive partitions is then counted for absolute quantification, providing highly accurate mRNA measurements. Each of these methods has unique advantages, and the choice between them depends on factors such as sensitivity, throughput and the nature of the samples being studied. qRT-PCR is favored for its high sensitivity and specificity, but it requires prior knowledge of the target genes and its typically limited to quantifying a set number of genes, making it ideal for detecting known, low-abundance transcripts. In contrast, RNA-seq is exceptional in its ability to provide a comprehensive view of the transcriptome without a need for prior knowledge of the genes involved beforehand, allowing for the discovery of novel transcripts and explore splice variants. dPCR excels in absolute quantification, critical for applications requiring precise measurement of gene expression. Improvements in micro-arraying technology have also broadened its applications. Enhancements such as increased probe density and improved fluorescence detection have enabled the detection of genes with low expression levels.[107] Despite these advances, microarrays still have one major limitation: they can only detect known cDNA sequences because the oligonucleotide probes have to be designed in advance. This limitation means that microarrays are best suited to model organisms with well-characterized transcriptomes, such as mice and humans, and are

less effective for discovering new genes or splice variants. These limitations have been overcome with the advent of RNA-seq. RNA-seq uses next-generation sequencing technologies to analyze large amounts of cDNA fragments. This provides a comprehensive and unbiased view of global gene expression in a sample.[108] This breakthrough technology allows researchers to explore the entire transcriptome, discover new genes and investigate complex gene expression patterns with unprecedented detail and accuracy. In brief, while qRT-PCR, RNA-seq and dPCR each offer distinct advantages, RNA-seq stands out for its ability to provide a thorough and comprehensive analysis of gene expression. This makes it a critical tool in modern molecular biology and genomics. (Figure 5)
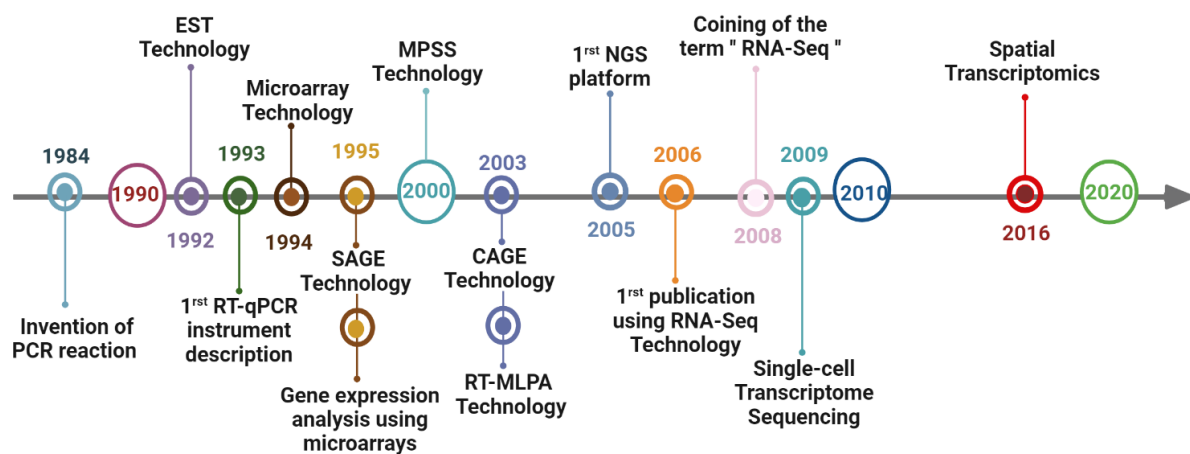
Figure 5. Timeline of Key Advances in Gene Expression Technologies

In 1984, Kary Mullis invented Polymerase Chain Reaction (PCR). By 1993, Real-Time qPCR (RT-qPCR) was developed by Higuchi et al., enabling real-time detection and quantification of mRNA expression. Between 1992 and 2003, various technologies like Expressed Sequence Tags (EST), Serial Analysis of Gene Expression (SAGE), Massively Parallel Signature Sequencing (MPSS), Cap Analysis of Gene Expression (CAGE), and Reverse-transcriptase Multiplex Ligation-dependent Probe Amplification (RT-MLPA) were introduced to analyze multiple genes simultaneously. In 1994, Affymetrix commercialized microarray technology, allowing the measurement of gene expression for hundreds or thousands of genes (Schena et al.). The early 2000s saw the development of Next Generation Sequencing (NGS), revolutionizing genomics and transcriptomics (Mardis). The first publication using RNA-Seq technology appeared in 2006 (Bainbridge et al.), and by 2008, the term RNA-Seq became commonly used (Lister et al.; Mortazavi et al.). In 2009, RNA-Seq was applied to single-cell technology for the first time (Tang et al.). In 2016, spatial transcriptomics emerged, providing new advancements in transcriptomics research (Ståhl et al.). Adapted from Martínez-Pérez, A., Estévez, O., & González-Fernández, Á. (2022).[109] Contribution and Future of High-Throughput Transcriptomics in Battling Tuberculosis. https://doi.org/10.3389/fmicb.2022.835620. This image is adopted and reproduced with permission using Biorender.

1.2.5 Transcriptomics and RNA-sequencing

Transcriptomics is the comprehensive study of RNA expression levels across the entire genome under specific conditions or in a specific cell. The field focuses on understanding a

wide range of RNA molecules, from mRNA to various types of non-coding RNAs. This field focuses on understanding the patterns and levels of RNA expression, including messenger RNA (mRNA) and various types of noncoding RNAs, to gain insights into gene function and regulation. With this, it can classify diseases, predict future disease states, and elucidate the biological mechanisms underlying these conditions through statistical analysis and clustering of co-expressed genes. Transcriptomics includes several critical aspects that collectively deepen our understanding of gene function and regulation. One of the main focuses of transcriptomics is RNA expression profiling. This involves measuring the expression levels of all RNA molecules in a cell, tissue or organism at a given time. This allows researchers to determine which genes are active and to what extent, providing valuable insights into gene activity and cellular function. Another important aspect of transcriptomics is the study of gene regulation. This involves understanding how gene expression is controlled in different biological contexts, including development, disease and environmental changes. By studying gene regulation, scientists can uncover the mechanisms that dictate when and how genes are turned on or off, and how these processes contribute to normal physiology and pathological conditions. In addition to focusing on protein-coding RNAs, transcriptomics is also investigating the role of various non-coding RNAs in gene regulation and cellular processes. These include microRNAs (miRNAs), small interfering RNAs (siRNAs) and long non-coding RNAs (lncRNAs). Non-coding RNAs play a critical role in regulating gene expression at multiple levels, including transcriptional and post-transcriptional regulation, thereby influencing a wide range of biological processes and disease states.

RNA sequencing (RNA-seq) is a key technology in transcriptomics, enabling the detailed and comprehensive analysis of RNA expression levels across the entire transcriptome, and has become the most widely used method for analyzing global gene expression, overcoming the limitations of previous transcriptomic approaches. It was first introduced by several groups in 2008.[67, 110, 111]RNA-seq involves the simultaneous sequencing of a large number of cDNA fragments derived from mRNA samples using high-throughput DNA sequencing technologies. This method provides comprehensive profiling that provides both quantitative and qualitative data on gene expression without the need for pre-designed probes or selection, overcoming the limitations of microarrays in detecting RNA splicing patterns and discovering previously unannotated genes.[108, 112-114]

Despite the existence of numerous library preparation methods for RNA sequencing,[115] the general workflow can be summarized in a few key steps. Library preparation refers to the process of converting RNA or DNA into a format suitable for sequencing, which includes adding specific adapters and barcodes for efficient analysis. First, RNA is extracted from the sample of interest. Since more than 80% of a cell's RNA content is uninformative ribosomal RNA (rRNA), protocols typically include steps to deplete rRNA or enrich for mRNA, such as the selection of polyadenylated RNA species (poly-A+ mRNA).[116] Next, the mRNA is reverse transcribed into cDNA. Because the length of most mRNA molecules in eukaryotic cells exceeds the sequencing read length, and clustering of DNA molecules on the sequencer's flow cell is inefficient for molecules larger than ~1 kb, transcripts must be fragmented before analysis. This fragmentation can be done at the RNA level using heat or chemical fragmentation (RNA hydrolysis)[108, 117] or at the cDNA level using sonication[118] or enzymatic processes.[119, 120] During library preparation, sequencing adapters are ligated to the fragmented cDNA molecules. These adapters serve two purposes: one adapter is necessary to bind the sequencing line, and the other contains sample-specific DNA barcodes, allowing for multiplexing. Multiplexing refers to the process of pooling multiple samples in a single sequencing run, made possible by the addition of unique barcodes to each sample. This ensures that sequences from different samples can be identified and separated during data analysis.[121, 122] After adapter ligation, the final sequencing libraries are typically amplified using library PCR [123] before being loaded onto high-throughput sequencing machines at specific concentrations .[114] On Illumina platforms, this massively parallel sequencing process typically generates millions of reads per sample, with sequencing costs generally the only limiting factor.[124, 125] For RNA-seq data analysis, the first stage is to demultiplex the generated reads based on the sample-specific multiplexing barcodes used.[126] The reads, typically 50–100 base pairs (bp) in length, are then aligned to the reference genome of the organism under study to identify their genomic locations. This alignment process is computationally intensive, especially since most transcripts are composed of multiple exons interspersed with long intronic sequences in the reference genome.[127] Splice-aware alignment software has been developed to accurately map short reads across both known and novel splice junctions.[128] Once aligned, reads can be quantified either at a per-base level across the gene body sequence or as gene/isoform-level counts to estimate expression

levels. Quality control checkpoints are essential throughout the analysis to ensure high quality, reliable results.[125] The quality of raw reads should be thoroughly evaluated by examining several key metrics. First, the base calling quality score distribution provides information about the accuracy of the sequencing process at each position in the read, indicating how confident the sequencing platform is about each nucleotide call. Next, k-mer analysis involves identifying overrepresented short nucleotide sequences (k-mers), which can signal contamination, adapter sequences, or biases in the library preparation. Finally, the GC content distribution should be assessed to ensure it matches the expected genome-wide GC content for the organism under study, as deviations may indicate biases in sequencing or amplification that could affect downstream analyses.

Tools such as RSeQC[124] and Picard can be used to monitor the quality of the mapping step. Typically, in human and mouse experiments, more than 60-80% of the reads should align to the reference genome. Additional quality metrics such as GC bias, uniformity of read distribution, and sequence duplication level also provide insight into data quality.[129] It is essential that replicate gene expression values show high correlation, especially for technical replicates, during the quantification phase. For biological replicates, acceptable correlation factors depend on the variance and heterogeneity of the biological system under study.[125] (Figure 6)

RNA Sequencing
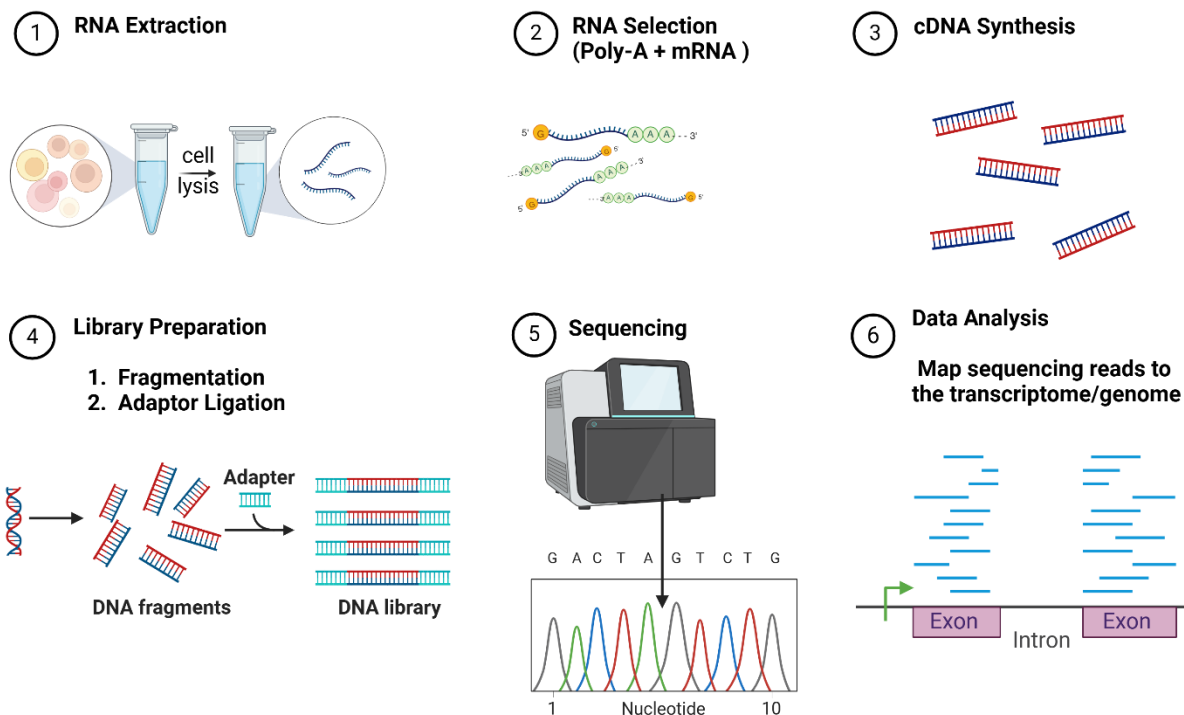
Figure 6. Schematic of the RNA Sequencing Process

(1.) RNA is first extracted from a variety of biological samples, such as tissues or cells. The extracted RNA (2.) is then reverse transcribed into complementary DNA (cDNA), (3.) which is subsequently fragmented to an appropriate size for sequencing. (4.) After fragmentation, sequencing adapters are ligated to the cDNA fragments. (4.) These adapters include two key components: one adapter enables the attachment of cDNA to the sequencing flow cell, while the other contains unique sample-specific barcodes that allow for multiplexing, i.e., the simultaneous sequencing of multiple samples in a single run. (5.) Finally, high-throughput sequencing is performed to analyze the prepared cDNA libraries, providing detailed information on gene expression profiles. (6.) Image generated using BioRender.

1.2.6 Transcriptomic profiling and biomarker identification in Chronic Lymphocytic Leukemia (CLL)

Transcriptomic profiling, using advanced RNA sequencing technologies, plays a crucial role in the personalized medicine in the treatment of CLL. This enables comprehensive analysis of the CLL transcriptome, allowing the identification of specific gene expression patterns, RNA splicing events, and molecular markers that drive disease progression and influence treatment response.[130] Transcriptomic profiling of CLL has uncovered critical alterations in gene expression involved in key cellular pathways, such as dysregulation of genes involved in the B-cell receptor signaling pathway, apoptosis, and cell cycle regulation. These

43

transcriptomic aberrations have important prognostic and therapeutic implications. For example, overexpression of certain oncogenes or altered splicing of tumor suppressor genes can be associated with poor prognosis and resistance to conventional chemotherapy, prompting clinicians to consider alternative treatment strategies, including targeted therapies and novel agents like Bruton's tyrosine kinase (BTK) inhibitors. As an example, one prominent finding is the overexpression of genes such as MYC, a well-known oncogene associated with aggressive disease progression in CLL.[131] Similarly, BCL2, a key regulator of apoptosis, is frequently overexpressed, contributing to the survival of malignant cells and resistance to chemotherapy.[132] Mutations in SF3B1, a gene involved in RNA splicing, have also been identified in a subset of CLL patients, leading to aberrant splicing events that influence disease outcome.[131, 133] These transcriptomic alterations have significant prognostic and therapeutic implications.

The identification of these dysregulated genes has led to the development of targeted therapies. For instance, BTK inhibitors, such as ibrutinib and acalabrutinib, are designed to target the BTK protein, a critical component of the B-cell receptor signaling pathway that is often dysregulated in CLL.[134] BTK inhibitors have shown remarkable efficacy in clinical trials, especially in patients with poor prognostic markers such as TP53 mutations or del(17p).[135] These findings have highlighted the importance of transcriptomic profiling in identifying actionable targets and tailoring treatment to the molecular characteristics of a patient's cancer.[136]

In addition to identifying therapeutic targets, transcriptomic profiling facilitates the detection of minimal residual disease (MRD), providing insights into the effectiveness of therapy and early signs of relapse. For example, RNA-seq can detect low-level expression changes in genes like LEF1, a marker of MRD, providing early warnings of potential relapse.[137] This allows timely adjustments to treatment plans to maintain remission and improve long-term outcomes. Monitoring MRD is critical for assessing treatment efficacy and making timely adjustments to therapeutic strategies to maintain remission and improve long-term outcomes.[138]

Overall, transcriptomic profiling using RNA-seq is a powerful tool in the precision medicine approach to CLL, enabling a deeper understanding of the disease's molecular landscape and guiding the development of more effective, individualized treatment plans.

1.2.7 Single-cell RNA sequencing

Traditional RNA sequencing methods typically require substantial amounts (100-1000 ng) of total RNA as an input, which can be restrictive when analyzing samples with only a few cells. This limitation poses a significant challenge to the study of cellular heterogeneity and to the understanding of the distinct transcriptional landscapes within complex tissues or rare cell populations. Single-cell RNA sequencing (scRNA-seq) overcomes these challenges by enabling the analysis of gene expression at the level of individual cells. This technique allows researchers to simultaneously capture the transcriptomes of thousands to millions of individual cells.[139] scRNA-seq involves the isolation of individual cells, followed by reverse transcription of RNA into cDNA, amplification of the cDNA, and subsequent sequencing.

Key advantages of scRNA-seq include resolution of cellular heterogeneity, discovery of rare cell types and trajectory analysis. By examining individual cells, scRNA-seq can identify distinct cell types, states and lineages within a heterogeneous population. This provides insight into cellular diversity and function. This method can detect rare cell populations that may be missed by bulk RNA sequencing, leading to discoveries in developmental biology, cancer and immunology.[140] For example, scRNA-seq allows the exploration of global gene expression variability within cell types[141] or between different cell groups. [142, 143] This increased resolution allowed researchers to discover previously unknown subpopulations in various conditions and biological samples, such as the immune system [144], liver [145] and pancreas. [144, 146, 147] In addition, scRNA-seq has helped reveal novel dynamics and heterogeneity in embryonic[148] , blood[149, 150] and brain [151] developmental processes. Furthermore, scRNA-seq is crucial for investigating heterogeneity in disease states. This is particularly relevant for understanding cancer evolution.[152-154] scRNA-seq data can be used to identify developmental trajectories and cellular differentiation pathways, helping to understand dynamic biological processes.

scRNA-seq workflow typically involves single-cell isolation using techniques such as fluorescence-activated cell sorting (FACS), microfluidic platforms or droplet-based methods like the 10x Genomics system. A critical step in the process is the barcoding of single-cell RNA molecules, where unique molecular identifiers (UMIs) are added to the RNA captured from each individual cell. This allows the RNA from different cells to be tracked through the sequencing and analysis process. After barcoding, the captured RNA is reverse transcribed into cDNA within each individual cell followed by cDNA amplification and library preparation. High-throughput sequencing is then performed on platforms such as Illumina, and extensive data analysis using computational methods for quality control, normalization, clustering and differential expression analysis. By providing unprecedented insights into the molecular mechanisms underlying health and disease, scRNA-seq has revolutionized our understanding of complex biological systems.[155]

Whole transcriptome amplification methodshave been developed to overcome the limitation of low RNA input quantities, which is a common challenge in ScRNA-seq and other low-input studies.[156] Traditional RNA sequencing methods require substantial amounts of RNA (100–1000 ng), but scRNA-seq often works with only picograms of RNA per cell, making RNA amplification necessary to obtain sufficient material for sequencing. The majority of current low-input protocols use exponential PCR amplification [157], linear in vitro transcription,[158] or multiple displacement amplification.[159] With the advent of RNA-seq, these technologies were soon adapted to single cell transcriptome sequencing.[160] These revolutionary technologies have subsequently changed our understanding of biology.[161-163] These platforms are particularly advantageous in applications requiring the isolation and analysis of rare cell populations, which is often challenging with traditional bulk analysis methods.[164, 165]

Despite the clear advantages and promising opportunities provided by single-cell RNA sequencing, both the experimental techniques and computational analyses have yet to reach their optimal forms. To generate and interpret data accurately, it is essential to comprehend the properties, capabilities, and limitations of scRNA-seq technologies.

1.2.8 Advanced technologies for Single-cell RNA sequencing

New technologies have emerged to overcome the limitations of traditional methods and provide comprehensive workflows for capturing and analyzing gene expression profiles at the single-cell level. By integrating advanced microfluidic and molecular biology techniques, it is now possible to acquire high-quality data from single cells with improved sensitivity and accuracy. These advances are driving major breakthroughs in fields such as cancer biology, developmental biology, and immunology. They are also enriching our understanding of cellular heterogeneity and gene regulation.

Recent reviews highlight the significant progress in microfluidics-based single-cell analysis, detailing how these technologies facilitate high-throughput, high-resolution data acquisition.[166, 167] For instance, in droplet microfluidic platforms, individual cells are isolated within tiny droplets that are surrounded by an oil phase. These droplets act as miniature reaction chambers where various steps of single-cell analysis—such as cell lysis, reverse transcription, and amplification—can be carried out in a highly controlled manner.[168] The encapsulation of single cells in individual droplets ensures that each cell's content remains separate, preventing cross-contamination and allowing for precise gene expression profiling at the single-cell level.

This method is particularly beneficial for studying rare cell populations, as it enables the analysis of individual cells in a high-throughput format, which would be difficult to achieve using traditional bulk sequencing methods. Droplet-based platforms also offer the flexibility to scale up the analysis to thousands or even millions of cells, providing a comprehensive view of cellular heterogeneity.[169]

In addition to enhancing sensitivity and accuracy, these advanced techniques provide a more detailed view of the cellular landscape, aiding in the identification of distinct cellular subpopulations and their roles in various biological processes. This is crucial for understanding complex diseases like cancer, where heterogeneity among tumor cells can significantly impact treatment outcomes.[170]

Several methods are available to capture cells for RNA sequencing. Dedicated microfluidic chips can capture and process 96 or 800 cells in the Fluidigm C1. (Figure 7 A) [171, 172]

Another application of microfluidic technology is the use of microdroplets, where cells are encapsulated in nanoliter droplets in a water-in-oil emulsion. This droplet capture method is suitable for the unbiased, high-throughput capture of a large number of single cells, regardless of their size.(Figure 7 B)[173-175] However, a major challenge with droplet-based methods is that damaged cells can release RNA, which can cause background noise and loss of sequencing coverage.

Among the most widely used droplet-based platforms is 10x Genomics Chromium. This platform combines microfluidics with molecular barcoding to capture and analyze thousands of individual cells in parallel. In the 10x Genomics system, individual cells are encapsulated within oil droplets along with gel beads that are coated with barcoded oligonucleotides. Each cell's mRNA is reverse-transcribed into cDNA within the droplet, where it is tagged with a unique molecular identifier (UMI) and a cell-specific barcode. After droplet breakage, the barcoded cDNA is amplified, allowing for subsequent library preparation and sequencing. The high scalability, accuracy, and speed of 10x Genomics technology have made it a dominant platform in the field of single-cell RNA sequencing, enabling comprehensive profiling of cellular heterogeneity and identification of rare cell types.[173, 175, 176]

In many experiments it is desirable to pre-select certain cell types. Fluorescence-activated cell sorting (FACS) is often used for this purpose, where single cells can be sorted directly into individual wells of 96- or 384-well plates.[142, 177-179] These plates typically contain lysis buffer to lyse cells and release RNA. In additionally, with compatible FACS machines, 'index sorting' can be performed, where fluorescence data for each cell is linked to its well position, providing additional information. (Figure 7 C)[180] A relatively new approach is to deposit cells in microfabricated nano-wells by restricting dilution, offering high output without requiring microfluidic dropping devices.(Figure 7 D)[181-183] Streets et al. have developed a method for sequencing single cell messenger RNA (ScmRNA) using a microfluidic valve-based technique in which single cells are captured, lysed, and reverse transcribed from mRNA to cDNA. The resulting single-stranded cDNA (sscDNA) is transferred to conventional PCR tubes to amplify and purify, facilitating subsequent sequencing.[184] By using droplet microfluidics, Klein et al. have developed inDrop RNA sequencing, a technique that is capable of indexing thousands of individual cells. In the inDrop platform, cells are encapsulated in droplets that contain lysis buffer, reverse transcription reagents, and barcoded oligonucleotide primers.

Within each droplet, during the synthesis of cDNA, the mRNA released from the lysed cell is barcoded. After barcoding, material from all cells is combined by breaking the droplets. The cDNA library is sequenced using established methods.[168] Microwell-based platforms are also being used in various fields, including cell culture, image analysis and single-cell RNA sequencing, as demonstrated by S. Bose et al. In this context, the microfluidic device captures single-cell lysates in microwells. The mRNA molecules released from the lysed cells hybridize to oligo(dT) primers on the glass surface, forming single-cell mRNA prints. On-chip reverse transcription then converts the mRNA prints to cDNA, which is stained for fluorescence imaging, allowing to visualize gene expression patterns at the single cell level.[185] Gierahn et al. used sub-nanoliter wells to capture cells and barcode them using poly(dT) mRNA capture beads for subsequent on- and off-chip procedures, including reverse transcription, cDNA amplification, library preparation and paired-end sequencing.[182]

To analyze differential gene expression at the single-cell level within a given cellular state, these methods play a crucial role. Cells or pre-existing mRNA are introduced into these platforms from external sources, such as cells extracted from different tissues, or subjected to drug treatments using different platforms such as multi-well plates. However, none of these platforms integrates both drug treatment and sample preparation.

The DMA platform utilized in the current study offers a significant advantage by seamlessly combining drug treatment and sample preparation for differential gene expression analysis within a single system. On the DMA platform, cells can be treated with drugs and observed under the microscope for phenotypic changes such as changes in morphology and viability. Following phenotypic assessment, the platform is used to prepare and synthesizing dscDNA to be used for downstream applications and to perform DGEA. Within an individual droplet on DMA, the platform allows for cell lysis, RNA extraction, and conversion of mRNA to cDNA, enabling molecular analysis such as gene expression profiling. By combining these steps—phenotypic observation and subsequent gene expression analysis—the platform provides comprehensive insights into cellular responses to drug treatments. This makes the DMA platform an invaluable tool for advanced single-cell analysis, offering both phenotypic data and detailed molecular information from the same set of cells.
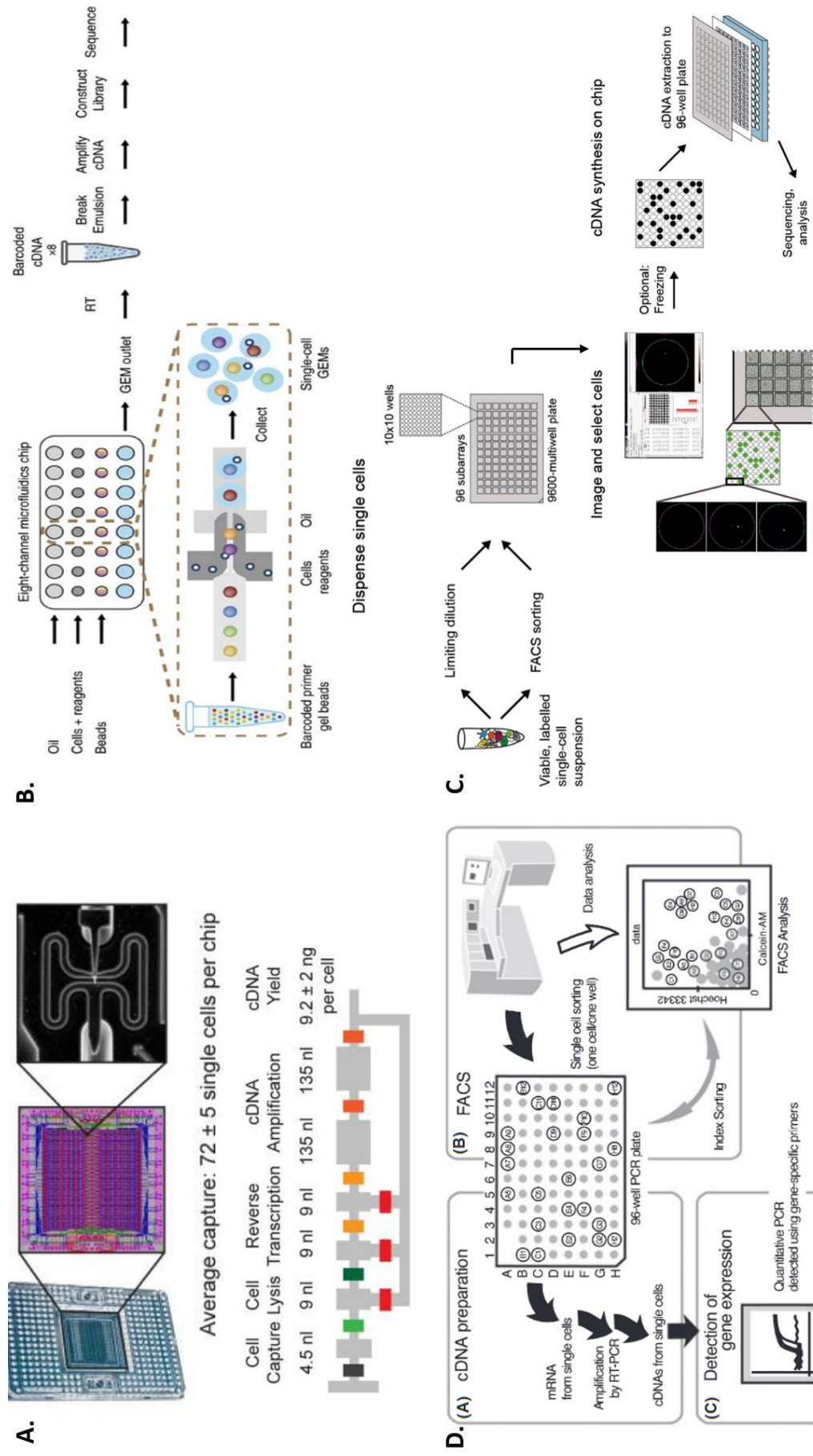
Figure 7. Advanced Technologies for Single-Cell RNA Sequencing

This figure illustrates key single-cell RNA sequencing (scRNA-seq) technologies, including droplet-based microfluidics for high-throughput cell capture and barcoding, microplate-based methods for precise processing, and spatial transcriptomics for combining spatial and transcriptomic data. (A.) The C1 Single-Cell Auto Prep System captures single cells and quantifies mRNA levels by using a microfluidic integrated fluidic circuit (IFC).[170] (B.) The scRNA-seq workflow on the GemCode platform involves combining cells and reagents with gel beads in a microfluidic chip to form GEMs, where RT occurs, followed by pooling, amplification, and library construction. Gel beads with barcoded oligonucleotides prime RT of polyadenylated RNAs, and the finished library molecules are sequenced.[174] (C.) Single-cell gene profiling of planarian stem cells using fluorescent activated cell sorting (FACS) and its "index sorting" function for stem cell research.[179] (D.) The figure provides an overview of the STRT-seq-2i workflow and shows the distribution of molecule and gene counts for cortex data.[182]

1.3 The Droplet Microarray (DMA) platform

1.3.1 Manufacturing

At this point, I would like to introduce what our group is specialized in, focusing on conducting experiments within nanoliter droplets on a droplet microarray (DMA) platform. This technology represents an advanced lab-on-chip approach that enables researchers to manipulate and analyze very few quantities, such as cells and reagents, in nanoliter droplets formed on a specially coated surface. This surface features patterns that are designed to hold nanoliter droplets in defined areas, allowing higher throughput and miniaturization in nanoliter volumes, which was developed in the Levkin group at KIT in 2011.[186-188]

To fabricate the three different types of DMA slides, the following surfaces are created: Poly(2-hydroxyethyl methacrylate-co-ethylene dimethacrylate) (HEMA-EDMA),[189] dendrimer surfaces,[190] and nanoparticle surfaces. The DMA technology utilizes thiol-yne and thiol-ene click chemistry, which are rapid and versatile reactions that allow for precise control over the patterning process. This enables to engineer surfaces with distinct hydrophilic and superhydrophobic properties.[187] The water contact angle (WCA) serves as a measure of the angle formed when a water droplet interacts with a solid surface, indicating the wettability of that surface. A superhydrophobic surface features a WCA exceeding 150°, demonstrating significant resistance to water.[191] Conversely, a surface with a WCA of less than 10° indicates superhydrophilicity, where water droplets spread extensively across the surface.[192] By manipulating these properties during the fabrication of DMA slides, researchers can tailor surfaces for specific applications in various experimental setups.

To develop the HEMA-EDMA surface, a porous alkyne polymer layer is generated through the modification of glass with HEMA-EDMA. In this process, a glass slide coated with nano-porous HEMA-co-EDMA copolymer, esterified with 4-pentynoic acid, and modified by photolithography to create an array of hydrophilic spots on a superhydrophobic background.[189, 193] To activate the surface, standard microscopy glass slides (25 mm x 75 mm) are treated with aqueous solutions of 1 M NaOH and 1 M HCl for one hour each, cleaving terminal silyl ethers to expose reactive hydroxyl groups. After washing with water and ethanol, the slides are coated with a solution of 3-(trimethoxysilyl)propyl methacrylate in ethanol and covered with another activated glass slide. This forms covalent silane bonds with the surface

hydroxyl groups.[194] Subsequently, the slides are washed with ethanol, leaving a surface with methacryl groups. A polymerization mixture containing HEMA, EDMA, porogens and a photo initiator is applied and covered with a fluorinated glass slide. The slides are treated with 1H,1H,2H,2H-perfluorooctyl trichlorosilane in the gas phase. The sandwiched slides are irradiated with Ultraviolet (UV)-light at 254 nm to induce polymerization. The methacrylate groups firmly anchor the polymer coating to the glass slide. The fluorinated glass slide is then removed, and the smooth top layer of polymer is peeled off with a piece of adhesive tape to expose the nanoporous structure. The resulting polymer layer has a static water contact angle (WCA) of 6°,[195] is approximately 12 μm thick,[196] and is hydrophilic due to the hydroxyl groups of HEMA. It should be noted that WCA measurements on porous hydrophilic surfaces differ from those on non-porous surfaces. This is because capillary forces first fill the pores with water, causing the droplet to stand on the liquid-filled surface. The next step is the Steglich esterification of the hydroxyl groups with 4-pentynoic acid by immersion of the entire slide in the reaction solution.[197] This introduces alkyne groups to the polymer surface. The polymer surface becomes hydrophobic and non-wettable with a static water contact angle (WCA) of 115°.[198] The difference between wettable and non-wettable surfaces is evident as the polymer coating appears opaque when dry and transparent when wet. The final manufacturing step involves a UV-induced thiol-yne click reaction with 1H,1H,2H,2H-perfluorodecanethiol (PFDT) and cysteaminium chloride or beta-mercaptoethanol. A solution of PFDT is spread over the surface. Areas that are to remain hydrophilic are covered with a photomask. UV irradiation at 254 nm causes the PFDT to bind covalently to the 4-pentynoic acid, forming a thioether. After washing, a solution of the hydrophilic thiol is applied, and the slide is covered with a non-patterned quartz glass and irradiated again. This photolithographic process precisely controls the spatial attachment of the different thiols, resulting in a significant difference in wettability: Areas modified with PFDT are non-wettable with a static WCA of 170° (advancing contact angle: 173°, receding contact angle: 164°), whereas areas modified with cysteaminium chloride are wettable with a static WCA of 4°.[198] The inherent material properties and the covalent bonding of each layer and modification are responsible for the mechanical and chemical stability of DMA.[199] As a result, the DMA is resistant to all common solvents such as Dichloromethane (DCM), Dimethyl Sulfoxide (DMSO), Dimethylformamide (DMF), Gamma-Butyrolactone (GBL), N-Methyl-2-pyrrolidone (NMP),

Tetrahydrofuran (THF), toluene, pyridine, methanol, ethanol, acetone, isopropanol, acetic acid and water, even when fully immersed for days at a time. It can withstand slightly alkaline or acidic conditions and temperatures of up to 70°C. After such treatments, the DMA can be dried with an air gun without losing parts of the coating or pattern, which is particularly important for multi-step experiments involving multiple wash steps or different reactions. It is important to note that this protocol is not intended for biological work and represents a previous method used in the development of DMA technology.

For the nanoparticle surface, the glass surface is salinized with vinyltrimethoxysilane. Whereas in the case of the dendrimer surface, glass slides are salinized using triethoxyvinylsilane, followed by modification with 1-thioglycerol and esterification with 4-pentenoic acid to achieve the dendrimer structure. Subsequently, the surfaces are modified by photomasking under UV light with 1H,1H,2H,2H-perfluorodecanethiol (PFDT) and cysteamine hydrochloride, resulting in superhydrophobic and superhydrophilic surfaces, respectively.

1.3.2 Applications

The DMA has been employed across various fields, including biology, chemistry, and materials science. The array consists of hydrophilic spots surrounded by superhydrophobic boundaries, which facilitate discontinuous de-wetting. This configuration allows water droplets to form discrete nano- and microliter-sized droplets, depending on the size of the spot. These droplets function as individual nano- and micro- reservoirs that can be addressed either manually through pipetting or automatically via dispensing.

The working volumes of the spots vary significantly depending on their size. Round spots with diameter of 900 μm (Cat.No 203) can having a working volume ranging from 50 to 150 nanoliters. This is particularly useful for applications requiring very small sample sizes, enabling the conservation of valuable reagents. Larger spots, with diameters of 3 mm, can manage volumes between 5 to 10 microliters (Cat. No 201). This size is often employed in applications needing larger sample volumes while still maintaining high precision. Others having smaller spots, with a side length of 500 μm, have working volumes between 20 to 40

nanoliters, which are all ideal for ultra-high-throughput experiments where space and sample conservation are paramount. The miniaturization afforded by DMAs represents a significant advancement over traditional methods. One such traditional format is the 1536-well plate, which has been a staple in high-throughput screening but comes with limitations. Each well in a 1536-well plate typically holds about 10 microliters, suitable for many applications but not optimal for reducing reagent usage and increasing throughput. In contrast, DMAs allow for miniaturization from microliter (μL) to nanoliter (nL) volumes, representing an order of magnitude improvement in reagent efficiency. The physical dimensions of a 1536-well plate, approximately 128 x 86 mm, limit the number of plates that can be processed simultaneously and require substantial space and resources. The miniaturization of spot sizes and working volumes on DMAs enables high-throughput experimentation, crucial for modern scientific research and industrial processes. High-throughput experimentation allows for increased sample processing, as smaller spot sizes and volumes mean more samples can be processed in parallel, significantly speeding up experimental workflows. The ability to work with nanoliter volumes drastically reduces the amount of reagents required, lowering costs and enabling the use of expensive or scarce materials. Smaller, precisely controlled volumes can improve the accuracy and reliability of experimental results by reducing variability and improving the consistency of conditions across samples.

The first step was the validation of the substrate's biocompatibility in a number of biological systems. HEK 293 cells were reverse-transfected with mCherry and Green Fluorescent Protein (GFP) plasmids on the chip, cultured for two days, and then analyzed via fluorescence microscopy.[189] This validation paved the way for high-throughput screening applications, first demonstrated in 2015 using a sandwich approach. A chemical library was printed onto a glass slide with an automated liquid dispenser and then dried. This arrayed library was then sandwiched on a DMA containing cells in droplets, allowing each individual volume to be treated with a specific compound. Results were obtained through either direct live imaging or live staining with Calcein AM after 24 hours of incubation. For live staining, two methods were utilized: Calcein AM was either printed on a new glass slide, dried, and applied to the cell drops, or the entire DMA was submerged in the staining fluid. Fluorescence microscopy was employed for final analysis. This workflow was subsequently refined for suspension cells and

simplified with the introduction of a "sandwiching device" to assist in aligning the two slides.[1, 200]

In the following years, the range of biological applications expanded significantly.[201] The DMA platform was adapted for more advanced applications; for instance, by inverting the droplet microarray in a slide holder, embryoid bodies formed in the "hanging droplets" were screened for toxicity and embryoid body formation using a 774-drug library approved by the Food and Drug Administration (FDA). This demonstrated that the DMA is not only suitable for 2D cell culture but also supports 3D cell culture, while preserving the arrayed format and separate, miniaturized droplets essential for high-throughput screening. One goal of 3D cell culture is to screen complex tissue models or organoids to more accurately mimic whole living systems, which is both cost-effective and efficient compared to using animals. Miniaturization has been particularly advantageous for rare materials, such as patient-derived cancer cells, enabling personalized medicine. Given the limited number of cells available from biopsies, this approach has been crucial for testing various drugs and drug combinations. High-throughput screening of pluripotent mouse embryonic stem cells has been successfully performed using the DMA platform, thanks to its favorable surface chemistry and structure. Spontaneous differentiation was inhibited during 72 hours of culture.[202] Additionally, it has been demonstrated that zebrafish larvae can be cultured on the DMA and screened for toxicity in high throughput.[203] Another study validated a high-throughput screening (HTS) workflow using DMA to identify antimicrobial compounds. It demonstrated that low-volume dispensers can generate droplets with defined bacterial counts and that a simple colorimetric read-out method allows rapid and quantitative analysis. The HTS system screened 2826 compounds against Klebsiella pneumoniae (K. pneumoniae) and 2060 against Methicillin-Resistant Staphylococcus aureus (MRSA). Six novel candidates with activity against multi-drug resistant bacteria were successfully identified.[204] On the same DMA platform, we have developed a droplet merging method for the high-throughput generation of spatially organized 2D monolayer cells and 3D spheroids within individual sub-microliter droplets. This automated technique allows the creation of cell microenvironments by merging droplets, enabling paracrine signaling interactions between 2D and 3D cell colonies without direct physical contact. The system was used to demonstrate the propagation of Wnt signaling between Wnt-3a-producing spheroids and reporter cells in both 2D and 3D formats. This approach can

replicate complex in vivo cellular architectures in vitro and, when combined with biomaterials such as hydrogels, is suitable for high-throughput screening of biological processes such as cancer invasion, cell signaling and embryonic development that require complicated coculture models.[205] In vitro cell-based experiments are crucial for fundamental biological research. While microscopy-based readouts are commonly used to detect cellular changes in response to stimuli, gene expression analysis is essential for understanding the underlying molecular mechanisms. However, variability between experiments, particularly with different readout methods, can be a challenge. To address this, platforms that integrate cell screening with both morphological and gene expression analysis are needed. The DMA platform facilitates cell screening in hundreds of nanoliter droplets. This study introduces a "Cells-to-cDNA on Chip" method that enables on-chip mRNA isolation from live cells and conversion to cDNA within individual 200 nL droplets. This method is effective for generating cDNA from varying cell numbers, including single cells per droplet. It represents the first miniaturized on-chip approach that combines cell screening, phenotypic assessment via microscopy, and mRNA to cDNA conversion for gene expression analysis using real-time PCR on an open DMA platform. This novel approach paves the way for a wide range of applications to explore molecular dynamics in cultured cells.[2]

In addition to its biological applications, the droplet microarray (DMA) has also had applications in the field of material research. The hydrophilic spots on the DMA acted as 2-dimensional molds for an alginate solution, which formed hydrogel particles when a $CaCl_2$ solution was applied to them.[3] By adjusting the positions of the two slides, the adhesion of the formed hydrogel particles could be controlled, allowing them to either remain on the DMA or be detached by immersion in a medium. Magnetic particles and live cells could be incorporated into the alginate solution prior to curing, maintaining high viability over 7 days compared to traditional 2D cell cultures. Integrating high-throughput techniques into materials research allowed screening of responsive hydrogels in nanoliter compartments.[206] Pre-polymerization mixtures were printed on DMA with varying amounts of crosslinker, then polymerized using 365 nm UV light. The hydrogel particles degraded due to its inherent stability upon exposure to 254 nm UV light.

Performing chemical reactions in a miniaturized, parallelized format that allows immediate biological screening of the resulting products is another application of the DMA, aligning with the ChemBio concept, which integrates chemistry and biology for rapid and efficient analysis. This approach facilitates the rapid assessment of the biological activity of synthesized compounds, streamlining the process of identifying potential therapeutic agents. This combination of synthesis and screening on the same chip accelerates drug discovery while reducing the use of materials such as chemicals, solvents and biologicals. For example, a library of 25 lipidoids was synthesized on-chip, converted into lipoplexes and screened for transfection efficiency, highlighting the ease of compound handling and modification in this arrayed format.[207] Although on-chip extraction via sandwiching has been demonstrated as a potential purification step, there remains a need for more versatile options, particularly to accommodate multi-step reactions for complex chemistries. The solid phase synthesis approach facilitated the simultaneous removal of impurities and excess starting material by washing the DMA with solvents such as acetone or ethanol.[198] The nano-porous HEMA-co-EDMA polymer used in the hydrophilic moieties served as the solid phase and was modified with a photolysis linker. This modification allowed stable attachment of the starting material via photo-linker and release of the product by 365 nm UV irradiation for less than 20 minutes, without the need for additional additives such as acids. The platform was shown to be effective for tripeptide synthesis and did not affect the viability of HEK293T cells under UV cleavage conditions.[198] Additionally, a one-pot combinatorial synthesis approach using the Ugi 4-component reaction on the DMA platform enabled the production of 132 PROTAC-like molecules in nanoliter droplets with minimal material usage, integrating on-chip synthesis, purification, UV-controlled release, and cell-based screening to further accelerate drug development and reduce costs.[208] Another approach using DMA has been the development of a cost-effective method for the preparation of cell-compatible hydrogel arrays (OHA) for sequence-selective solid-phase extraction of oligonucleotides. This method offers high reproducibility and sufficient capacity for a wide range of applications. The OHA platform supports 320 parallel independent experiments and allows for miniaturized, selective purification and controlled release of nucleic acids. This makes it adaptable to various applications in transcriptomics and other assays.[209] (Figure 8)
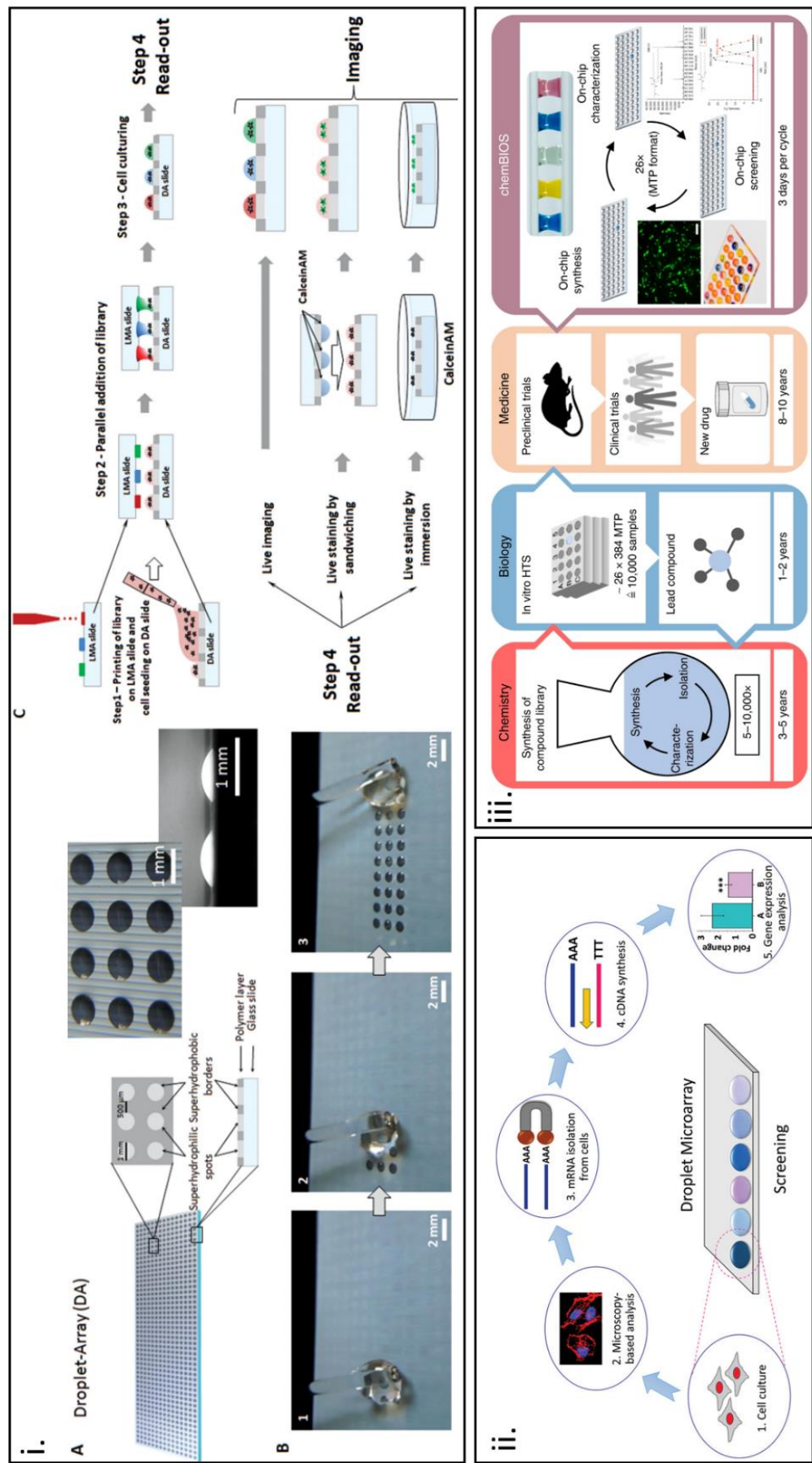
Figure 8. Applications of Droplet Microarray Technology

This figure illustrates the diverse applications of droplet microarray technology across various fields. (i) (A.) Schematic illustration of a DA slide (left) alongside images showing droplets formed on a superhydrophobic-superhydrophilic pattern. (B) The effect of discontinuous dewetting with water on a DMA featuring 900 μm round spots. (C) The procedure for parallel cell screening on the DMA using the sandwiching technique. A chemical library was printed on a glass slide, dried, and then used to sandwich a DMA containing cells, allowing the different volumes to be treated with specific compounds. After incubation, cells can be analyzed either through live imaging or following staining with CalceinAM. Staining can be achieved either by sandwiching the cells with the staining solution or by immersion. Image adapted with permission.[1] (ii.) Schematic of the "Cells-to-cDNA on Chip" method. 1 = Culturing and screening cells in micro/nanoliter droplets on a DMA, 2 = Performing phenotypic analysis of cells using microscopy techniques, 3 = Lysing cells and isolating mRNA with poly-T magnetic beads, 4 = Converting mRNA to cDNA within the same droplet, 5 = Collecting cDNA for subsequent qualitative and quantitative gene expression analysis.[2] (iii.) Schematic illustrating the drug discovery process. Traditional drug discovery is often inefficient due to the rigid separation between chemistry (synthesis) and biology (assays). ChemBIOS integrates miniaturized, solution-based chemical synthesis in a microarray format with characterization and biological screening. This approach streamlines all early-stage drug discovery steps, reducing the timeline from years to just a few days.[3]

58

1.4 Objective

The aim of my thesis is to advance the application of the DMA platform for personalized drug response profiling in CLL research, focusing on drug sensitivity and resistance testing (DSRT) and miniaturized gene expression analysis. The first project involves screening of CLL cells from different patients for their drug response using a pre-printed library of 33 drugs on the DMA platform conducting DSRT. The selected 33-drug library consists of FDA-approved chemotherapeutic and targeted agents commonly used in clinics and hospitals for the treatment of CLL patients. The drug response was assessed across a range of concentrations to predict the patient-specific variability. For the first time, culture conditions for CLL cells on DMA were successfully optimized using dextran-polyethylene glycol (PEG) hydrogels, which significantly improved cell viability compared to traditional medium conditions. The total volume per droplet for drug testing was reduced to 300 nL, making the protocol efficient and resource-saving. This optimization provides a robust method for high throughput drug screening, providing insight into patient-specific drug responses, which is crucial for the development of personalized medicine strategies. The experimental work related to DSRT in plates versus DMA platform was performed in collaboration with Düsseldorf university, with specific data obtained by Berit. Data generated by Annika, Tobias and Vicky for optimizing CLL culture conditions, as well as conducting comprehensive analysis of DSRT in patient-derived CLL cells, was done under my supervision.

In the second project, a protocol for differential gene expression analysis using CLL patient-derived cells was developed and optimized. This involved optimizing the cell lysis process to accommodate cell lines and patient-derived cells, ensuring effective mRNA extraction. The quality of the generated cDNA was then checked to ensure its suitability for subsequent gene expression analysis via bioanalyzer, PCR and qPCR, providing a reliable method for studying gene expression variations in CLL patients. qPCR was used to assess the expression of SYK and GADD45b genes, which were found to be upregulated following treatment with doxorubicin on CLL patient cells. This method, tested as a proof of concept, supports the identification of patient-specific genetic profiles, and furthers the goal of personalized treatment approaches. As the next step, the same protocol was used to test sample preparation for sequencing. Barcoded oligonucleotide primers were employed per spot on the DMA platform, allowing for accurate sample detection during sequencing. This approach aimed to validate the DMA

platform for future applications in nanoliter sample preparation, significantly reducing the costs associated with sample preparation reagents, drugs, and sequencing.

The DMA platform is a suitable tool for personalized medicine due to its multiple advantages, including miniaturization, parallelization, and high-throughput capabilities. It accelerates the research process and reduces resource consumption by efficiently handling small sample volumes and performing multiple tests simultaneously. By optimizing these protocols and validating the DMA platform for these applications, my thesis aims to increase the utility of DMA in CLL research, providing a comprehensive, efficient, and cost-effective tool for drug screening and gene expression studies, ultimately contributing to advancing personalized medicine.

Chapter 2. Experimental Section

Materials and Methods

2.1. Materials

2.1.1 Chemicals

Table 2. List of Drugs Used and Their Concentrations

Drug	Drug Number	Target	C5 (mM)	C4 (mM)	C3 (mM)	C2 (mM)	C1 (mM)
PRT062607	1	SYK	1	0.2	0.04	0.008	0.0016
MIK665	2	MCL	1	0.2	0.04	0.008	0.0016
Birinapant	3	IAP	0.25	0.05	0.01	0.002	0.0004
Ganetespib	4	HSP	0.2	0.04	0.008	0.0016	0.00032
Vorinostat	5	HDAC	1	0.2	0.04	0.008	0.0016
Ceritinib	6	ALK	1.5	0.3	0.06	0.012	0.0024
Ibrutinib	7	BTK	0.1	0.02	0.004	0.0008	0.00016
Lenalidomide	8	IKFZ1/3	0.5	0.1	0.02	0.004	0.0008
Venetoclax	9	BCL2	0.04	0.008	0.0016	0.000 32	6.4×10^{-5}
Carfilzomib	10	Proteasome	0.02	0.004	0.000 8	0.000 16	3.2×10^{-5}
Idelalisib	11	PI3K	0.2	0.04	0.008	0.0016	0.00032
Navitoclax	12	BCL2	0.2	0.04	0.008	0.0016	0.00032
Acalabrutinib	13	BTK	0.5	0.1	0.02	0.004	0.0008
Doxorubicine	14	Topoisomerase II	0.5	0.1	0.02	0.004	0.0008
I-BET-762	15	BRD	1	0.2	0.04	0.008	0.0016
Fludarabine	16	Antimetabolite	1	0.2	0.04	0.008	0.0016
Everolimus	17	mTOR	0.2	0.04	0.008	0.0016	0.00032
Ruxolitinib	18	JAK	1.5	0.3	0.06	0.012	0.0024
Dexamethasone	19	Glucocorticoid receptor	0.1	0.02	0.004	0.0008	0.00016
Quizartinib	20	FLT3	0.5	0.1	0.02	0.004	0.0008
UMI-77	21	MCL1	3	1.5	0.3	0.06	0.012
SCH772984	22	ERK	0.5	0.1	0.02	0.004	0.0008
Melphalan	23	Chemotherapeutic	1.25	0.25	0.05	0.01	0.002
Nutlin-3a	24	MDM2/p53	2	0.4	0.08	0.016	0.0032
Selinexor	25	XPO1	0.5	0.1	0.02	0.004	0.0008
Etoposide	26	Topoisomerase II	2	0.4	0.08	0.016	0.0032
Azacytidine (Vidaza)	27	Antimetabolite	2	0.4	0.08	0.016	0.0032
Palbociclib	28	CDK	1.5	0.3	0.06	0.012	0.0024
Alpelisib	29	PI3K	1	0.2	0.04	0.008	0.0016
Cytarabine	30	Antimetabolite	2	0.4	0.08	0.016	0.0032
Dasatinib	31	TKI	0.1	0.02	0.004	0.0008	0.00016
Vemurafenib	32	BRAF	1.5	0.3	0.06	0.012	0.0024
Bendamustin	33	Crosslinking	1.5	0.3	0.06	0.012	0.0024
Dimethyl sulfoxide (DMSO)					CAS: 67-68-5		

2.1.2 Media, buffers, and solutions

Table 3: List of Used Media, Buffers, and Solutions

Name	Company	Catalog number
RPMI 1640 + L-Glutamine	Thermo Fisher Scientific (Germany)	21875-034
Penicillin-streptomycin (Pen/Strep)	Thermo Fisher Scientific (Germany)	15140-122
Fetal Bovine Serum (FBS)	Thermo Fisher Scientific (Germany)	10270-106
Humanserum (HS)	Sigma-Aldrich	H6914
Dulbecco's phosphate-buffered saline (DPBS)	Thermo Fisher Scientific (Germany)	14190144

2.1.3 Cell stains and dyes

Table 4: List of Cell Dyes and Stains

Name	Company	Catalog number
Trypan Blue Solution, 0,4 %	Thermo Fisher Scientific (Germany)	15250-061
Hoechst	Thermo Fisher Scientific (Germany)	H3570
Calcein AM	Thermo Fisher Scientific (Germany)	C3099
Propidium iodide	Thermo Fisher Scientific (Germany)	P3566
CellTiter-Glo® Luminescent Cell Viability Assay	Promega	G755A
SYBR™ Safe DNA gel stain	Invitrogen (Germany)	S33102

2.1.4 Cells

Table 5. List of Involved Cells and Cell Lines

Name	Company	Medium
SU-DHL-4 (human diffuse large B-cell lymphoma)	ATCC CRL-2957 (US) / CRL-2957 ™	RPMI-1640 + 10% heat inactivated FBS + 1 % Pen/strep
S2 Drosophila cell line		Drosophila Medium + 10% heat inactivated FBS + 1% Pen/strep
CLL- Patient derived cells	German Cancer Research Centre in Heidelberg, Germany	RPMI-1640 + 10% HS + 1 % Pen/strep

2.1.5 Kits and reagents

Table 6. List of Kits

Name	Company	Catalog Number
Maxima H minus reverse transcriptase	Thermo Fisher Scientific (Germany)	13233159
Invitrogen™ Ambion™ RNase inhibitors, cloned, 40 U/µl	Thermo Fisher Scientific (Germany)	10177094
Exonuclease I	VWR International GmbH (Germany)	EN0581
Ampure XP beads	Beckman Coulter (Germany)	A63880
Nuclease-free water (NFW)	Life Technologies GmbH (Germany)	E476-500ML
1 kb DNA ladder	New England Biolabs GmbH (Germany)	N3200S
Low molecular weight DNA ladder	New England Biolabs GmbH (Germany)	N3233S
Taq PCR Master Mix Kit	Qiagen GmbH (Germany)	201443
Gotaq qPCR Master Mix	Promega GmbH (Germany)	A6001
3-D Life Dextran-PEG Hydrogel SG	Cellendes GmbH (Germany)	G92-1
RNase Zap Decontamination solution	Thermo Fisher Scientific (Germany)	AM9780
Triton-X-100	Alfa Aesar (USA)	A16046.AE

2.1.6 Primers

Table 7. List of Primers and their Sequences Used

Primer	Sequence	Company
Glyceraldehyde-3-phosphate dehydrogenase (*GAPDH)*- Forward	CTC TGC TCC TCC TGT TCG AC	
Glyceraldehyde-3-phosphate dehydrogenase (*GAPDH*)- Reverse	CCC AAT ACG ACC AAA TCC GT	
ACTB (*β-actin*) – Forward	GACCCAGATCATGTTTGAGACC	
ACTB (*β-actin*) – Reverse	TAACAACGCATCTCATATTTGGAA	Integrated DNA Technologies (IDT) (Belgium)
Spleen-associated tyrosine kinase (*SYK*) – Forward	GGT CCT CAC CAA AGT TCT CTG	
Spleen-associated tyrosine kinase (*SYK*) – Reverse	CCA GGT AAT CTT CTG CCT CCT	

DNA damage inducible beta (*GADD45β*) – Forward	GCC AGG ATC GCC TCA CAG TG	
DNA damage inducible beta (*GADD45β*) – Reverse	GGA TTT GCA GGG CGA TGT CA	

2.1.7 Barcoded oligo-dT

Table 8. List of Barcoded Oligo-dT

No.	Barcoded Primers	Primer sequence (5' to 3')
B1	E3V6NEXT1	/5Biosg/ACACTCTTTCCCTACACGACGCTCTTCCGATCT**AAAACT**NNNNNNNNNNTTTTTTTTTTTTTTTTTTTTTTTTTTTTTTTTTVN
B2	E3V6NEXT2	/5Biosg/ACACTCTTTCCCTACACGACGCTCTTCCGATCT**AAAATC**NNNNNNNNNNTTTTTTTTTTTTTTTTTTTTTTTTTTTTTTTTTVN
B3	E3V6NEXT3	/5Biosg/ACACTCTTTCCCTACACGACGCTCTTCCGATCT**AAACAT**NNNNNNNNNNTTTTTTTTTTTTTTTTTTTTTTTTTTTTTTTTTVN
B4	E3V6NEXT4	/5Biosg/ACACTCTTTCCCTACACGACGCTCTTCCGATCT**AAACTA**NNNNNNNNNNTTTTTTTTTTTTTTTTTTTTTTTTTTTTTTTTTVN
B5	E3V6NEXT5	/5Biosg/ACACTCTTTCCCTACACGACGCTCTTCCGATCT**AAAGTT**NNNNNNNNNNTTTTTTTTTTTTTTTTTTTTTTTTTTTTTTTTTVN
B6	E3V6NEXT6	/5Biosg/ACACTCTTTCCCTACACGACGCTCTTCCGATCT**AAATAC**NNNNNNNNNNTTTTTTTTTTTTTTTTTTTTTTTTTTTTTTTTTVN
B7	E3V6NEXT7	/5Biosg/ACACTCTTTCCCTACACGACGCTCTTCCGATCT**AAATCA**NNNNNNNNNNTTTTTTTTTTTTTTTTTTTTTTTTTTTTTTTTTVN
B8	E3V6NEXT8	/5Biosg/ACACTCTTTCCCTACACGACGCTCTTCCGATCT**AAATGT**NNNNNNNNNNTTTTTTTTTTTTTTTTTTTTTTTTTTTTTTTTTVN
B9	E3V6NEXT9	/5Biosg/ACACTCTTTCCCTACACGACGCTCTTCCGATCT**AAATTG**NNNNNNNNNNTTTTTTTTTTTTTTTTTTTTTTTTTTTTTTTTTVN
B10	E3V6NEXT10	/5Biosg/ACACTCTTTCCCTACACGACGCTCTTCCGATCT**AACAAT**NNNNNNNNNNTTTTTTTTTTTTTTTTTTTTTTTTTTTTTTTTTVN
B11	E3V6NEXT11	/5Biosg/ACACTCTTTCCCTACACGACGCTCTTCCGATCT**AACATA**NNNNNNNNNNTTTTTTTTTTTTTTTTTTTTTTTTTTTTTTTTTVN
B12	E3V6NEXT12	/5Biosg/ACACTCTTTCCCTACACGACGCTCTTCCGATCT**AACTAA**NNNNNNNNNNTTTTTTTTTTTTTTTTTTTTTTTTTTTTTTTTTVN
B13	E3V6NEXT13	/5Biosg/ACACTCTTTCCCTACACGACGCTCTTCCGATCT**AAGATT**NNNNNNNNNNTTTTTTTTTTTTTTTTTTTTTTTTTTTTTTTTTVN
B14	E3V6NEXT14	/5Biosg/ACACTCTTTCCCTACACGACGCTCTTCCGATCT**AAGTAT**NNNNNNNNNNTTTTTTTTTTTTTTTTTTTTTTTTTTTTTTTTTVN
B15	E3V6NEXT15	/5Biosg/ACACTCTTTCCCTACACGACGCTCTTCCGATCT**AAGTTA**NNNNNNNNNNTTTTTTTTTTTTTTTTTTTTTTTTTTTTTTTTTVN
B16	E3V6NEXT16	/5Biosg/ACACTCTTTCCCTACACGACGCTCTTCCGATCT**ATGGGG**NNNNNNNNNNTTTTTTTTTTTTTTTTTTTTTTTTTTTTTTTTTTVN
B17	E3V6NEXT17	/5Biosg/ACACTCTTTCCCTACACGACGCTCTTCCGATCT**CATCTT**NNNNNNNNNNTTTTTTTTTTTTTTTTTTTTTTTTTTTTTTTTTVN
B18	E3V6NEXT18	/5Biosg/ACACTCTTTCCCTACACGACGCTCTTCCGATCT**CCGTAA**NNNNNNNNNNTTTTTTTTTTTTTTTTTTTTTTTTTTTTTTTTTVN
B19	E3V6NEXT19	/5Biosg/ACACTCTTTCCCTACACGACGCTCTTCCGATCT**ACCTTC**NNNNNNNNNNTTTTTTTTTTTTTTTTTTTTTTTTTTTTTTTTTVN
B20	E3V6NEXT20	/5Biosg/ACACTCTTTCCCTACACGACGCTCTTCCGATCT**GGAAGG**NNNNNNNNNNTTTTTTTTTTTTTTTTTTTTTTTTTTTTTTTTTTVN
B21	E3V6NEXT21	/5Biosg/ACACTCTTTCCCTACACGACGCTCTTCCGATCT**TTCGCT**NNNNNNNNNNTTTTTTTTTTTTTTTTTTTTTTTTTTTTTTTTTVN
B22	E3V6NEXT22	/5Biosg/ACACTCTTTCCCTACACGACGCTCTTCCGATCT**TGTCCA**NNNNNNNNNNTTTTTTTTTTTTTTTTTTTTTTTTTTTTTTTTTVN

2.1.8 Reagent and reaction mix preparation

Table 9: Lysis Buffer Reaction Mix

Reagent	Volume
NEB HF Phusion buffer (5x)	0.2 µL
Nuclease free water	75 µL
Proteinase K (20 mg/mL)	5.5 µL

Table 10: Reverse Transcription Reaction Mix (RT)

Reagent	Volume
Polyethylene glycol 40% solution (v/v)	2 µL
Nuclease free water	2 µL
5X Maxima H RT buffer	4 µL
10 mM dNTPs	0.8 µL
E5V6NEXT (100 µM)	0.4 µL
RNaseOut	0.5 µL
Maxima H reverse transcriptase	0.5 µL

Table 11: Exonuclease Treatment Mix

Reagent	Volume
10X Exonuclease I buffer	2 µL
Exonuclease I (20U/µL)	1 µL

Table 12: cDNA Amplification Mix

Reagent	For 1 Reaction
Terra Direct buffer (2x)	25 µL
SINGV6 primer (10 µM)	1 µL
Terra polymerase (1.25 U/µL)	1 µL
Nuclease free water	3 µL

Table 13: Cells in Hydrogel Reagents Mix

3-D Life Dextran- PEG Hydrogel SG Kit (Cellendes) catalogue number: G92-1

Reagents	Volumes for 100 μL gel (μL)
Water	35.3
10x CB, pH 7.2	8
SG Dextran (30 mmol/L SH reactive groups)	6.7
Cell sus*pension*	40
PEG-Link (20 mmol/L SH groups)	10
Total	100

Table 14: PCR Sample Preparation

Using Kit: Qiagen Taq PCR mix

All reagents are thawed on ice.

Reagent mix	Per reaction (uL)
Taq PCR Mix.	10
Forward Primer (10 uM)	1
Reverse Primer (10 uM)	1
cDNA	2
NFW	6
Total	20

2.1.9 Equipment

Table 15. List of Equipment Used

Name	Company
CO2 Incubator CB260	Binder GmbH (Tuttlingen, Germany)
Heraeus Labofuge 400R centrifuge	Thermo fisher scientific (USA)
I-Dot noncontact dispenser	Dispendex GmbH (Stuttgart, Germany)
Keyence fluorescence Microscope BZ-X810	Keyence
Leica TCS SPE confocal laser scanning microscope	Leica Microsystem CMS GmbH (Mannheim, Germany)
Nanodrop 2000	Thermofisher scientific (USA)
Olympus IX81 inverted motorized microscope	Olympus (Tokyo, Japan)
Leica Thunder 3D imager	Leica (USA)
sciFLEXARRAYER S11 dispenser	Scienion AG (Berlin, Germany)
StepOnePlus Real-Time PCR system	Thermo fisher scientific (USA)
Life Technologies Countess II cell counter	Thermo fisher scientific (USA)
Thoma cell counting chamber	Faust Lab Science

2.1.10 Consumables

Table 16. List of Consumables

Name	Company	Catalog Number
Corning thermowell GOLD PCR tubes	Conring (New York, USA)	3475
DMA Slides	Aquarray GmbH (Eggenstein-Leopolshafen, Germany)	Cat. Nos. G-np-102
Parafilm roll	Fischer Scientific GmbH	
Metal in situ adapter	Antylia Scientific, Cole-Parmer GmbH	
3D printed PCR chamber lid	Creabis GmbH	
Neodymium block magnet	Supermagnete Webcraft GmbH (Germany)	
CELLSTAR Cell culture dishes	Greiner Bio-one International GmbH	664160
CELLSTAR cell culture flasks	Greiner Bio-one International GmbH	690160, 658170
40 µm filter	Greiner Bio-One GmbH (Germany)	
384-well microtiter plates	Axygen Scientific GmbH (Germany)	4008796
Eppendorf Conical Tubes	Eppendorf AG (Hamburg, Germany)	0030125,150
qPCR seal	4titude (Surrey, UK)	4ti-0560

2.2 Cell culture

SU-DHL-4 cells were cultured in RPMI 1640 medium supplemented with 10% heat inactivated FBS and 1% P/S. Cell culture was maintained in a standard cell culture incubator at 37°C with 5% CO_2. All experiments were performed with approximately 95% cell viability. Patient-derived CLL cells were obtained from the University of Heidelberg and stored in liquid nitrogen. To thaw CLL cells, the vial containing frozen cells was placed in a 37 °C water bath for 2-3 minutes to ensure rapid thawing of cells. The cell suspension was then immediately transferred to RPMI 1640 medium containing 10% heat-inactivated FBS and 1% P/S. After centrifugation at 400g for 5 minutes, the cell pellet was resuspended in the same cell culture medium and then filtered through a 40 µm strainer. The filtered CLL cells in medium were again centrifuged at 400g for 5 minutes. Finally, the resulting cell pellet was resuspended in

RPMI 1640 medium supplemented with 10% heat-inactivated HS and 1% P/S. The cells were then printed on DMA slides at the desired concentrations.

2.3 Cell counting procedure

To determine cell density and viability of a cell culture using trypan blue, mix 10µl of cell culture with 10µl trypan blue. Then, 10 µl of this mixture is pipetted into a Thoma cell counting chamber. The Thoma-chamber has four large squares, each measuring 1 mm², and each of these large squares is further divided into 16 smaller squares. The height under the coverslip is 0.1 mm, so the volume of a large square is calculated as follows: 1 x 1 x 0,1 = 0,1 mm3 = 10-4 ml. After counting N, N cells in a large square, the cell concentration is N x 10-4 cells per ml. After counting N cells in all four large squares, the cell concentration is cells $\frac{N}{4}\times$ 10-4 per ml.

Since the cell suspension was diluted 1:2 with trypan blue before counting, the final cell concentration is calculated as $\frac{N}{4}\times$ 2 x 10-4 cells per ml. (Figure 9)
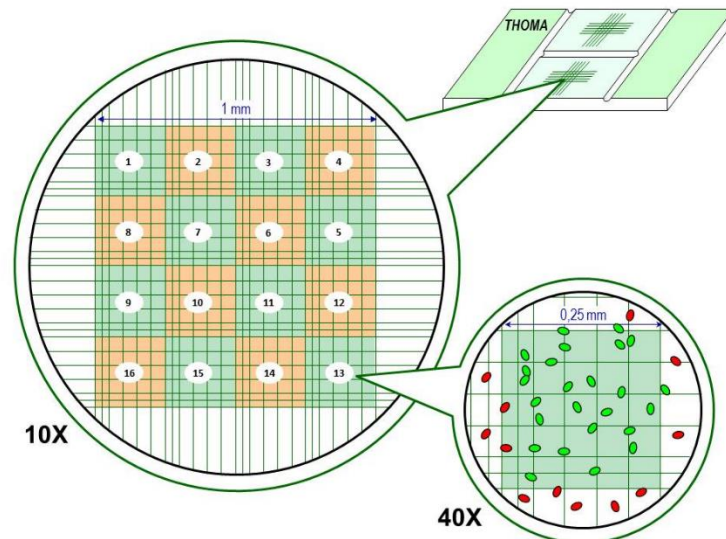

Figure 9. Illustration of the Usage of a Thoma Cell Counting Chamber

Demonstration of the structure of the chamber with its large and small squares, shown at 10x and 40x magnification for cell counting. Adapted from http://insilico.ehu.eus/counting_chamber/thoma.php.

2.4 Cell culture on DMA

For culturing cells on DMA chips in liquid media, cells were first counted, diluted to the desired cell density (to obtain a specific number of cells per spot) and dispensed onto a sterile 672-spot DMA slide using an I-DOT ONE automated dispenser. The DMA slide was sterilized with 100% ethanol and dried under a sterile bench for 10 minutes. A humidified Petri dish (10 cm) was prepared to maintain humidity and prevent droplet evaporation on the DMA slide. This humidified Petri dish was prepared by placing a tissue pad in the lid, wetting it with 6 ml PBS and adding 2 ml PBS inside the Petri dish. The humidified Petri dish was prepared in advance and placed in a cell culture incubator to equilibrate the humidity. After dispensing, the DMA chip containing cells was immediately placed in the humidified Petri dish and placed in a standard cell culture incubator. For the culture of CLL cells on DMA chips in hydrogels, we used Cellendes 3-D Life Dextran PEG Hydrogel SG Kit. The hydrogel mixture was prepared according to the manufacturer's instructions (Table 13). The cell density in the cell suspension added to the mixture was adjusted according to the desired number of cells per spot. The hydrogel mixture was then immediately dispensed onto DMA slides at a volume of 150 nL hydrogel per spot. The DMA slide was then transferred to a humidified Petri dish and placed in a cell culture incubator to allow the gel to solidify for at least 45 minutes. After solidification, a total of 150 nL of cell culture medium (RPMI-1640 medium supplemented with 10% heat-inactivated HS and 1% P/S) was added to the established hydrogel pads and returned to the humidified Petri dish and cell culture incubator for culture.

2.5 Drug screening library

In order to conduct drug screening, we utilized the sciFLEXARRAYER S11 to deposit 2 nL of drugs at 5 distinct concentrations in a randomized fashion onto a DMA chip. The specific drugs and their concentrations can be referenced in Table 2. Following drug deposition, we subjected the DMA slide to drying conditions for 48 hours within a chamber containing silica gel until complete dryness was achieved. The resultant dried DMA slides were subsequently stored for approximately 3 months in a falcon container that had been opaque and shrink-wrapped.

2.6 Live/Dead fluorescent staining

To assess the viability of cells and investigate the impact of drugs, a fluorescence-based method is employed. The method involves staining cells with three distinct dyes, including Hoechst H3570, Calcein AM, and Propidium iodide (PI). Hoechst dye is used to label DNA in the nucleus of all cells. It binds specifically to the minor groove of DNA, particularly in adenine-thymine (A-T) rich regions and produces a blue fluorescence when excited at around 350 nm. This allows the visualization and identification of nuclei in both living and dead cells. Calcein, in its form as Calcein-AM, stains live cells by becoming fluorescent only after conversion by intracellular esterase that are active in viable cells. This conversion results in green fluorescence when excited at approximately 494 nm, highlighting live cells. Whereas Propidium iodide (PI) labels dead or damaged cells by penetrating and binding to DNA in cells with compromised membranes, resulting in red fluorescence when excited at around 535 nm. This combination of dyes allows researchers to assess cell viability, distinguish between live and dead cells, and visualize all cell nuclei in a single assay. The cells are printed onto the DMA slide using the cell printer and are then incubated for varying durations. Subsequently, 50 nl of the fluorescent dyes are printed on top of the cells. The LEICA Thunder 3D Imager microscope (Leica BioSystems) is utilized to capture images of the DMA spots, while the Keyence microscope (Keyence GmbH) is employed for the plate control. The resulting images are analyzed using ImageJ, and the viability is calculated using Excel and presented in graphs. Control samples are prepared by adding 7.5 μL of fluorescent dye to 22.5 μL of cell suspension in a 384 well-plate. Following a 15 min incubation, a sticky chamber is attached to prevent evaporation during microscopy.

2.7 Image analysis

Automated image analysis is employed for the drug screen on the DMA platform. Kaida (KIT Artificial Intelligence-based Data Analysis) is an image analysis platform designed for high-throughput, automated processing of biological images, particularly in drug screening applications. It offers a reliable tool for personalized oncology research and high-throughput screening protocols. Kaida integrates deep learning methodologies, including convolutional neural networks (CNNs), to enhance the accuracy of cellular image segmentation and

classification. By combining advanced algorithms with a robust image processing pipeline, it automates the identification of viable and non-viable cells using markers like Hoechst, Calcein, and Propidium Iodide (PI).[210]

Kaida's flexibility allows for efficient annotation and processing of large datasets, optimizing drug response analysis on the DMA platform while simultaneously reducing human error in cell viability determination. Specifically, it employs a combination of deep learning for initial cell segmentation and the k-Nearest-Neighbor (k-NN) algorithm for accurately distinguishing live cells, which are Hoechst and Calcein positive but PI negative. Additionally, Kaida handles sample segmentation based on uniform intensity and size criteria, with cells being masked with corresponding colors for better visualization. Furthermore, cell identification is further refined through centroid detection.[210]

Fluorescent staining for live/dead is represented as follows: live cells are denoted by green crosses, indicating positive signals for Hoechst and Calcein while being negative for PI. Conversely, deceased cells are marked by red crosses, displaying positive signals for Hoechst, Calcein, and PI.

2.8 CellTiter-Glo luminescent cell viability assay

The CellTiter-Glo® Luminescent Cell Viability Assay is a widely used method for quantifying cell viability by measuring the amount of ATP, a marker of metabolically active cells. The assay generates a luminescent signal proportional to the ATP concentration, which correlates with the number of viable cells in the sample. This method is highly sensitive and is particularly useful for high-throughput screening, as it allows for rapid and accurate assessment of cell viability across many samples simultaneously.[211, 212]

To measure cell viability using the CellTiter-Glo® assay in a 384-well plate, 15 µl of the CellTiter-Glo reagent is added to each well containing 25 µl of cell suspension. The reagent lyses the cells, releasing ATP, which then interacts with the luciferase enzyme in the reagent to produce a luminescent signal. After an incubation period of 20 minutes at room temperature, allowing the reaction to reach its maximum luminescence, the luminescence is measured using the ClarioStar plate reader. This luminescent signal is directly proportional to

the amount of ATP present, and therefore to the number of viable cells. The assay is highly sensitive, detecting even low levels of ATP, making it an ideal choice for determining cell viability in various experimental conditions, including cytotoxicity testing, proliferation assays, and drug screening.

2.9 Ki-67 Immunofluorescence proliferation assay

The Ki-67 protein is a widely recognized marker of cellular proliferation, expressed specifically in the nuclei of cells during the active phases of the cell cycle—G1, S, G2, and M phases—while being absent in quiescent cells in the G0 phase. This expression pattern makes Ki-67 an essential indicator for identifying proliferating cells, particularly in cancer research and pathology. To detect Ki-67, an immunofluorescence assay is conducted, involving several key steps. First, cells are fixed and permeabilized to preserve cellular structures and allow antibodies to access intracellular targets. A primary antibody specific to Ki-67 is then applied, binding to the protein within the nuclei of proliferating cells. This is followed by the application of a fluorescently-labeled secondary antibody that binds to the primary antibody, enabling visualization of Ki-67-positive cells under a fluorescence microscope. The fluorescent signals observed correspond to the active phases of the cell cycle, where Ki-67 is expressed, and can be quantified to assess the proliferation rate within a cell population. This assay is extensively used in cancer research, where Ki-67 serves as a prognostic marker, and in cell biology for studying cell cycle dynamics. Additionally, in tissue pathology, Ki-67 staining aids in the diagnosis and grading of tumors by assessing cell proliferation in tissue sections. [213, 214]

Initially, cells are embedded within hydrogel on a DMA slide using the previously outlined procedure. Following an incubation period of either 3 or 6 hours, the cells are fixed onto the DMA slide using formalin for a duration of 20 minutes. Once fixation is complete, the cells are treated with Triton X-100 for 30 minutes to permeabilize them. To prevent non-specific antibody binding, a blocking solution called PowerBlock is applied onto the hydrogels and allowed to incubate for 10 minutes. Subsequently, 150 µL of the primary antibody is applied and left to incubate overnight at a temperature of 4 degrees Celsius. The following day, the slide is washed using PBS with Tween 20 to eliminate unbound antibodies. In the final step,

150 µL of the secondary antibody is applied to the DMA slide, undergoing a 2-hour incubation at room temperature in a dark environment. next, fluorescence images of both Hoechst and the secondary antibody are captured using a microscope.

The proliferation rate is then determined by employing the following calculation method:

$$Proliferation = \frac{\text{Number of cells with Ki} - 67 \text{ signal}}{\text{Cells with Hoechst signal}}$$

2.10 Sample preparation and cDNA generation on DMA platform

Before starting the experiments, it is essential to sterilize the clean bench with RNASeZap and to work in an aseptic environment. All reagents used in this experiment were thawed on ice unless otherwise specified in the kit manufacturer's protocols. The experimental procedure was done according to the following instructions. To prevent evaporation during sample preparation, water droplets were spotted around the droplets with the experiment (4, 2 or 1 droplets), leaving 1 row of droplets empty around the sample to simplify manual collection of the droplets. Then 100 nL of the cell suspension with the desired cell concentration was printed in four two or one droplets according to the scheme. Images were captured using Keyence BZ-X810 to verify the number of cells per spot prior to lysis. The method of limited dilution was used for obtaining a single cell per droplet. The presence of a single cell in the droplets was verified by microscopy. Once the positions of the single cells were identified, a protocol was created on the I-DOT One to dispense reagents only into the droplets containing single cell. Subsequently, 100 nL of cell lysis buffer containing Proteinase K (Table 9) was added to each droplet with single cell, followed by the addition of 10 nL of E3V6NEXT primer (2 µM). The DMA slide was then transferred to a PCR humidity chamber. A PCR humidity chamber was assembled with a metal adapter for a 96-well thermocycler (Bio-Rad Laboratories GmbH, Germany). Tissue pads were cut into strips and placed around the edges to allow space for a DMA slide. These pads were moistened with a total of 4 ml of water. The chamber was sealed with a custom 3D-printed lid made of heat-resistant polyamide to maintain adequate humidity during the temperature steps. This chamber containing the DMA slide was placed in the thermocycler for a 15-minute for Proteinase K digestion at 50°C,

followed by a 12-minute heat inactivation step at 80°C. During the cell lysis process, the reverse transcription (RT) mix was prepared according to Table 10. Upon completion of the cell lysis process, the PCR humidification chamber containing the DMA slide was placed on ice for 2 minutes. Cell lysis was checked under the microscope. Subsequently, 150 nL of reaction mix was added per spot. The DMA slide was then placed in a PCR thermocycler for conversion of mRNA to cDNA, which was performed at 42°C for 100 minutes. Upon completion of the reverse transcription step, the PCR humidity chamber was placed on ice for 2 minutes. Next, 10 µL of water was pipetted onto each experimental droplets (4, 2 or 1) to manually collect the cDNA samples from the DMA and transfer them to PCR microtubes. The single-stranded cDNA (ss-cDNA) was then purified using AMPure XP beads according to the Agencourt AMPure XP manufacturing instructions. After purification, excess of primers, salts, enzymes and nucleotides were removed by a washing procedure, and then ss-cDNA was subjected to exonuclease treatment (Table 11) with exonuclease I at 37°C for 20 min, followed by a heat inactivation step at 80°C for 10 min. The cDNA amplification mix (Table 12) was then added to the exonuclease I digested samples. sscDNA was amplified using the following settings: initial denaturation at 98°C for 3 minutes, followed by 21 cycles of denaturation at 98°C for 15 seconds, annealing at 65°C for 30 seconds, extension at 68°C for 4 minutes and a final extension at 72°C for 10 minutes. The samples were then cooled at 8°C and stored at -20°C. The concentration of ds-cDNA was measured using a Nanodrop 2000 UV-vis spectrophotometer (Thermo Fisher Scientific) and quantified by absorbance measurements and 260/280 and 260/230 ratio analysis. Finally, the complete double-stranded cDNA (dscDNA) was purified with AMpure XP beads using the same procedure as for sscDNA. The resulting dscDNA was checked for quality using standard PCR and gel electrophoresis, RT-PCR and bioanalysis to confirm correct sample preparation on the DMA platform. For sample preparation in hydrogel arrays, an additional lysis step was introduced to ensure complete lysis of the cells within the hydrogels. Lysis was performed in a thermocycler for 15 minutes at 50°C, followed by 12 minutes of proteinase K inactivation at 80°C. The lysis step was repeated by adding 100 nl of lysis solution, followed by 15 min at 50 °C and 12 min at 80°C. After the lysis step, the protocol was carried out as previously described for liquid medium.

2.11 Gene expression analysis after drug treatment (proof of concept)

Doxorubicin was administered at the following concentrations: 5 µM, 1 µM, 0.2 µM, 0.04 µM and 0.008 µM. It was dispensed onto 672 DMA slides using the Scienion sciFLEXARRAYER S11 liquid dispenser (Germany). For 384-well plate treatment, the same drug concentrations were prepared to be pipetted in 2.5 µL volumes per well. 10,000 SU-DHL-4 cells were used per well in 22.5 µL of medium. For the DMA chip, 100 SU-DHL-4 cells in medium and 2,000 CLL cells in hydrogel were used per spot in 150 nL volumes. The cells were treated with doxorubicin for 48 hours. Cell viability was assessed by live/dead fluorescent staining including Hoechst, Calcein and PI. IC50 was determined using GraphPad Prism software. To assess *SYK* and *GADD45β* gene expression levels, cells were exposed to IC50 concentrations of doxorubicin for 48 hours, followed by the sample preparation protocol described in "Sample preparation and cDNA generation on DMA chips".

2.12 PCR and gel electrophoresis

Polymerase Chain Reaction (PCR) and gel electrophoresis are fundamental techniques in molecular biology used to amplify and analyze specific DNA sequences. PCR allows for the selective amplification of target DNA regions, while gel electrophoresis enables the separation and visualization of these amplified fragments based on their size. Together, these methods are essential for verifying the presence, size, and purity of DNA fragments in research and diagnostics.[215, 216]

In this study, two housekeeping genes, *GAPDH* and *ß-actin*, were selected as internal controls to assess the quality and consistency of the cDNA obtained. For quality control, a positive control sample was used alongside nuclease-free water (NFW) as a negative control to ensure the specificity of the PCR amplification. Primer sequences for these PCR reactions are detailed in Table 7. The PCR reactions were performed using Taq PCR Mix (Qiagen, Germany), with all reagents thawed on ice to maintain their integrity. (Table 14) The PCR protocol included an initial denaturation step at 94°C for 3 minutes to separate the DNA strands. This was followed by 35 cycles of the following steps: Denaturation at 94°C for 30 seconds to ensure the DNA strands remain separated. Annealing at 54°C for 30 seconds, during which the primers bind

to their complementary sequences on the template DNA. Following by Extension at 72°C for 45 seconds, where the Taq polymerase enzyme synthesizes the new DNA strand by adding nucleotides to the 3' end of each primer. After these cycles, a final extension step at 72°C for 3 minutes was included to ensure complete synthesis of all DNA fragments. The reaction was then cooled to 8°C, where it could be held indefinitely until further processing.

The PCR products were subsequently analyzed using gel electrophoresis to verify the success and specificity of the amplification. The amplified DNA fragments were loaded into a 1.5% agarose gel, prepared to provide a suitable matrix for separating the DNA based on size. The gel was run at 100 volts for 75 minutes in a gel electrophoresis apparatus (Bio-Rad Laboratories GmbH, Germany). DNA migration through the gel was driven by an electric current, with smaller DNA fragments moving faster through the agarose matrix compared to larger fragments. After the electrophoresis, the DNA bands were visualized by staining the gel with SYBR™ Safe DNA Gel Stain, a safer alternative to ethidium bromide, which binds to DNA and fluoresces under UV light. The stained gel was then imaged using a UV transilluminator (Bio-Rad Laboratories GmbH, Germany), allowing for the identification and analysis of the PCR products. The size of the PCR products was confirmed by comparing them to a DNA ladder, ensuring that the expected amplification occurred.

2.13 Quantitative PCR (qPCR)

qPCR also known as real-time PCR, is a powerful technique used to amplify and simultaneously quantify a targeted DNA molecule. It enables the precise quantification of gene expression levels by measuring the amount of amplified product in real-time during the PCR process. For this study, the qPCR analysis was conducted using the GoTaq® qPCR Master Mix (Promega, USA), following the standard protocol provided by the manufacturer. This master mix contains all the necessary components for the PCR reaction, including Taq polymerase, dNTPs, $MgCl_2$, and a proprietary buffer system, with the addition of a fluorescent dye (such as SYBR® Green) that binds to the DNA, allowing for the detection and quantification of the amplified product. Gene-specific primers used in the qPCR reactions are detailed in Table 7. These primers were carefully designed to ensure specificity to the target genes, minimizing the potential for non-specific amplification. The qPCR reactions were

performed on a StepOne Real-Time PCR System (Life Technologies GmbH, Germany), which is equipped with the capability to monitor the fluorescence intensity of the DNA-dye complex during each cycle of the PCR. This allows for the continuous measurement of DNA amplification, enabling accurate quantification of gene expression. The qPCR protocol begins with an initial denaturation step to separate the DNA strands. This is followed by cycles of denaturation, annealing and extension. During each cycle, the fluorescence emitted by the dye increases in proportion to the amount of DNA amplified, and the system records this increase in fluorescence in real time. Cycle threshold (Ct) values is determined for each gene, representing the point at which the fluorescence signal exceeds the background level and is directly related to the initial amount of target DNA in the sample. Gene expression analysis was performed as previously described. This typically involves normalizing the Ct values of the target genes to those of a housekeeping gene (internal control) to account for variability in sample preparation and loading. The relative expression levels of the genes of interest were calculated using the $2^{-\Delta\Delta Ct}$ method or similar quantitative approaches, providing insights into the differential expression of genes under various experimental conditions.[217, 218]

2.14 Nanodrop spectrophotometer

The double-stranded DNA (dsDNA) samples were first quantified for concentration and purity using a Nanodrop spectrophotometer, a widely utilized instrument in molecular biology labs for its simplicity and accuracy. The Nanodrop operates by measuring the absorbance of nucleic acid samples at specific wavelengths, which provides vital information on both the concentration and purity of the DNA. The absorbance at 260 nm is critical for determining the concentration of nucleic acids, as DNA absorbs UV light most strongly at this wavelength due to the presence of aromatic bases. The Beer-Lambert law is applied here, where absorbance at 260 nm is directly proportional to the concentration of DNA in the sample. This measurement is particularly useful because it allows for the rapid quantification of DNA without the need for additional reagents or sample preparation. In addition to concentration, the Nanodrop also assesses the purity of the DNA samples by measuring absorbance at 280 nm and 230 nm. The 260/280 ratio is used to evaluate protein contamination; pure DNA typically has a ratio of approximately 1.8, while lower ratios may indicate the presence of

protein contaminants like phenol, which absorb at 280 nm. Similarly, the 260/230 ratio is an indicator of contamination from organic compounds such as phenol, carbohydrates, or residual reagents from nucleic acid extraction processes, with pure DNA samples usually showing a ratio in the range of 2.0 to 2.2. These spectrophotometric measurements are essential to ensure that the DNA samples are of high quality and free from significant contaminants, which is crucial for the success of downstream applications such as PCR, sequencing, or cloning.[219, 220]

2.15 Bioanalyzer

After the initial quantification, the dsDNA samples were analyzed on the Agilent 2100 Bioanalyzer, an advanced microfluidics-based platform that is widely recognized for its ability to provide a detailed and accurate assessment of nucleic acids. The Bioanalyzer system utilizes lab-on-a-chip technology that enables automated, high-throughput analysis of DNA, RNA and proteins. The preparation of the Bioanalyzer chips is a critical step in the process and requires precise handling of the reagents in order to ensure the integrity of the samples. It is essential for reliable and reproducible results that the chips are loaded with sample buffer, marker dye and ladder solutions according to the manufacturer's guidelines. It uses capillary electrophoresis, in which an electric field is applied across microchannels in the chip to separate DNA fragments on the basis of their size. This method is highly sensitive. It allows fragments to be separated with single-base resolution. As the DNA fragments migrate through the capillaries, they are detected by laser-induced fluorescence, generating detailed electropherograms for each sample. These electropherograms provide a visual representation of the DNA fragments, showing peaks corresponding to different fragment sizes. The accompanying data reports generated by the Bioanalyzer provide comprehensive information on the quality, size distribution and concentration of the DNA. A key aspect of quality assessment is the DNA Integrity Number (DIN), which is calculated based on the size distribution of the DNA fragments. A higher DIN indicates higher quality, intact DNA, while a lower DIN may indicate degradation. In addition, the reports identify any degradation products, providing insight into the overall integrity of the sample. This information is particularly important for downstream applications such as NGS or qPCR, where the quality

and size distribution of the DNA can have a significant impact on the accuracy and reliability of the results.[221-223]

2.16 Statistical analysis

All experiments were conducted with three technical replicates per sample to assess technical precision and at least 3 biological replicates to account for biological variability. Statistical analysis was performed using biological replicates unless otherwise stated. Data were analyzed using GraphPad Prism, widely used for statistical analysis in biomedical research. All data are expressed as mean ± SEM (Standard Error of the Mean), which provides an estimate of sample mean variability, allowing more accurate comparisons between groups. Statistical significance was determined using one-way analysis of variance (ANOVA), a robust statistical method for comparing the means of three or more independent groups to assess whether they differ statistically. ANOVA helps to control for type I errors (false positives) that can occur when multiple comparisons are made. In cases where ANOVA indicated significant differences, a post-hoc test such as Tukey's or Dunnett's (depending on software settings and study design) was performed to identify the specific group differences. P-values were reported to indicate the level of statistical significance, with thresholds set as follows ****$P < 0.0001$, ***$P < 0.001$, **$P < 0.01$. These levels indicate highly significant differences between groups, indicating strong evidence against the null hypothesis. Conversely, 'NS' indicates a non-significant statistical difference ($P > 0.05$), indicating that the observed differences between the groups are likely due to chance and are not statistically significant. To ensure the reliability and reproducibility of the results, the assumptions of ANOVA, such as normality and homogeneity of variances, were checked using appropriate diagnostic tests.[224, 225]

2.17 Barcoded cDNA library preparation

As mentioned in Section 3, the cDNA was generated per spot using different barcoded oligo(dT) primers (Table 8). The next steps involve preparing the dsDNA for tagmentation, a process that fragments the DNA and attaches sequencing adapters in a single reaction. Following tagmentation, the library is prepared through a polymerase chain reaction (PCR)

that amplifies the fragments and incorporates indexing sequences to identify each sample. After library amplification, a 3' enrichment PCR is performed to selectively amplify the regions of interest, enhancing their representation in the final library. The prepared libraries are then quantified using a suitable assay, such as Qubit, with successful libraries typically exceeding a concentration of 3-5 ng/µl. The libraries are diluted to the recommended molarity, usually around 2 nM, as per Illumina's guidelines, and then sequenced on a compatible Illumina sequencer. For sequencing, the paired-end read-length settings should be configured as follows: Read 1 with 16 cycles for cell barcode and UMI, Index 1 with 8 cycles for i7 Index, Read 2 with 50 cycles for cDNA fragments, with Index 2 set to 0. After sequencing, transfer the raw data from the sequencer and perform primary data processing using zUMIs. Finally, run bcl2fastq to convert the BCL files into FASTQ format, ensuring that demultiplexing is not performed during this step, as zUMIs will handle it.

Chapter 3. Results and discussion

3.1 Hydrogel-integrated droplet microarray for improved viabiltiy for drug sensitivity screening using patient-derived Chronic Lymphocytic Leukemia cells

Functionally personalized oncology (FPO) involves the use of functional assays and techniques to customize cancer treatment for individual patients based on the unique characteristics of their tumor cells. FPO involves the analysis of specific molecular and genetic characteristics of a patient's tumor to identify the most effective treatment options for personalized care. By assessing the functional properties of tumor cells, such as their response to drugs or targeted therapies, clinicians can determine the most appropriate therapies for each patient, thereby improving treatment outcomes and potentially increasing patient survival.[226, 227] However, functional personalized oncology has some limitations and challenges. A major challenge is the scarcity of tumor cells available for analysis, particularly in cases where needle biopsies are taken from original tumors or metastatic sites, especially when the tumors are small or in advanced metastatic stages. Obtaining a sufficient number of viable tumor cells for in vitro functional assays is a significant challenge. In addition, intra-tumor heterogeneity further complicates the analysis process, as different subpopulations of cells within a tumor may respond differently to treatment interventions.[228]

FPO has potential in both blood cancers and solid tumors. However, there are specific considerations for its implementation. Blood cancers, such as CLL, generally provide a sufficient amount of cells for functional testing using Microtiter Plate (MTPs). However, certain blood cancers, including multiple myeloma (MM) and myelodysplastic syndromes (MDS), present a limited number of cells available for analysis.[229, 230] The inability to culture blood cells in vitro, primarily due to their lack of proliferation and tendency toward spontaneous apoptosis, poses a significant challenge for functional testing in blood cancers.[231] This contrasts with solid tumors, where patient-derived organoids (PDOs) have been successfully explored for such testing. PDOs mimic tumor characteristics and allow larger cell populations for functional testing. However, while organoid models for blood

cancers are still in their early stages of development, they have shown potential in recent studies. Overcoming the current limitations of these models is critical for personalized oncology, and researchers are actively investigating strategies to optimize functional assays for both blood cancers and solid tumors to facilitate customized cancer treatments.[232, 233] Many methods are used for personalized medicine, including 2D cell cultures, which provide a simplified and cost-effective model for studying cellular behavior, but they lack the complexity and physiological relevance of the in vivo environment. In contrast, 3D cultures and organoids better mimic the architecture and interactions of tissues, allowing a more accurate representation of disease mechanisms, drug responses and personalized treatment strategies. However, these models can be more challenging to establish, maintain, and standardize, and their interpretation can be complex due to the heterogeneity and dynamic nature of 3D structures.[232, 234, 235]

In our study, we utilize patient-derived CLL cells to perform drug screening within a hydrogel matrix using the Droplet-Microarray (DMA) as a versatile method for HTS. To validate the efficiency of the DMA platform, we chose CLL cells as a model of blood cancer. CLL is a common form of leukemia in adults. It is characterized by the accumulation of abnormal lymphocytes in the blood, bone marrow and lymph nodes.[236] CLL cells undergo early apoptosis and are difficult to culture in-vitro without the use of co-culture conditions. Although coculturing with stromal cells or adding soluble factors can increase and prolong the survival of CLL cells, no existing systems allow long-term expansion of CLL cells in vitro.[237] Our previous studies have demonstrated low viability of CLL cells on the DMA platform. Therefore, we used hydrogels to enhance the viability of CLL cells and carried out our screening within the hydrogel matrix on DMA. Importantly, we demonstrated that the hydrogel did not interfere with our drug screening results. The abundance of CLL cells readily available for analysis allows us to compare and validate the performance of the DMA method in capturing their unique characteristics and responses compared to traditional MTPs. We assessed the viability of CLL cells on a 672 DMA slide and performed drug screening experiments using the drug library DMA slides and validated the results by comparing them with those obtained from MTPs.

3.1.1 Assessing viability involving varying cell quantities on DMA after 24 and 48 hours of culturing

The aim of this study was to determine whether variations in cell number, medium volume and incubation time affect the viability of patient-derived CLL cells on 672 and 320 DMA slides and in 384-well plates. The cell viability was assessed after 24 and 48 hours of incubation using live/dead fluorescence staining and cell titer GLO as a readout method. (Appendix Figure A 1) Figure 10 A shows the assessment of patient-derived CLL cell viability at different volumes and cell numbers on DMA platform whereas the data for the 384-well plate experiments are shown in the Appendix Figure A 1.

This work was previously conducted by a bachelor student, Annika Strauß, under my supervision. Different cell numbers (ranging from 200 to 650) in a total medium volume of 150 nL and 200 nL on a 672 DMA slide (represented in Figure 10 A legend in purple). Meanwhile, cell numbers ranging from 500 to 1250 cells were plated in total medium volumes of 750 nL and 1000 nL on a 320 DMA slide (represented in Figure 10 A legend in blue) and incubated for 24 and 48 hours (indicated by clear and striped legends, respectively). In 384-well plates, 4800 patient-derived CLL cells were seeded in a total medium volume of 50 uL. The cell concentration for each condition is shown in Appendix Table A 1.

The results shown in Figure 10 A illustrate the average viability after 24 hours of incubation for all four volumes and cell counts, ranging from approximately 20% to 50%, while after 48 hours of incubation, the viability for all four volumes ranges from 10% to 35%, indicating a decrease compared to the 24-hour incubation.

The viability of CLL cells cultured in the 384-well plate was significantly higher after 24 hours, ranging from 65% to 85%, whereas after 48 hours of incubation, the viability in the 384-well plate varied between 45% and 90%. There is a significant difference in the maximum deviation of all viability measurements between the two different incubation periods: after 48 hours the maximum deviation is 45% (ranging from 45% to 90%), whereas after 24 hours incubation the maximum deviation is 20% (ranging from 65% to 85%). This can likely be attributed to the greater volume available in each well, affording the cells a more substantial supply of essential nutrients and a stable environment, which are both crucial for promoting cell growth and proliferation.[238]

This work was done in collaboration with Berit Brinkmann from the Department for Hematology, Immunology, and Clinical Oncology, Heinrich-Heine-University Düsseldorf, Germany. Figure 10 B shows the viability variation of control spots with DMSO conditions on the 672-DMA slide tested with 21 different CLL patients. The 672-DMA slide consists of 48 columns and 14 rows, as shown in the schematic (Figure 10 C). The data from the viability assessment highlight the impact of the position of CLL patient-derived cells on the slide, with distinct variations observed across different columns and rows as well as among different patients. Each point per column represents the CLL cells viability across 21 patients compared across different rows (B, J and F). Cell viability was measured after one day of culture under control (DMSO) conditions, providing insight into how the DMA slide layout influences the response of CLL cells. For example, viability in Row B ranged from approximately 0.04 (4%) to 0.60 (60%), with notable variations across different patients and columns. In Row F, some columns exhibited the highest viability (e.g., columns 15, 31, and 35, with values above 0.60 (60%), while others showed the lowest viability, around 0.10 (10%) (e.g., columns 11, 15, and 45). As another example, in Row F, viability varied from 0.075 (7.5%) in column 3 to 0.690 (69%) in column 19, with other values falling between 0.150 (15%) and 0.680 (68%) in column 23. In Row J, the viability in column 19, 23 and 27 ranged from 0.15 (15%) to 0.70 (70%), suggesting that patient-specific responses may contribute to overall viability differences. These data indicates that the positioning of cells on the slide, whether in specific columns or rows, could play a significant role in the variability of cell behavior. Furthermore, Figure 10 D presents the average viability of patient-derived cells in different rows of the DMA slide, highlighting the differential response of CLL cells under identical culture conditions. The average viability data reveal that, despite the significant variability in the responses of the 21 patient-derived samples, the majority of the data points in Row B fall within a range of 0.25 (25%) to 0.30 (30%) viability. Row F shows a higher viability range, from 0.35 (35%) to 0.40 (40%), while Row J exhibits a slightly higher range, up to 0.42 (42%), as shown in Figure 10 D. This indicates that viability variability is influenced by the positioning on the DMA slide, with lower viability observed at the outer edges (Row B) compared to the inner rows (Row F and J). Further investigation into the specific rows showing the lowest or highest viability may provide valuable insights into potential experimental conditions affecting cell behavior. Factors such as the impact of specific regions on the DMA slide, spatial effects, and potential

evaporation should be considered, as they are essential for optimizing experimental conditions in CLL drug sensitivity testing using the DMA platform.
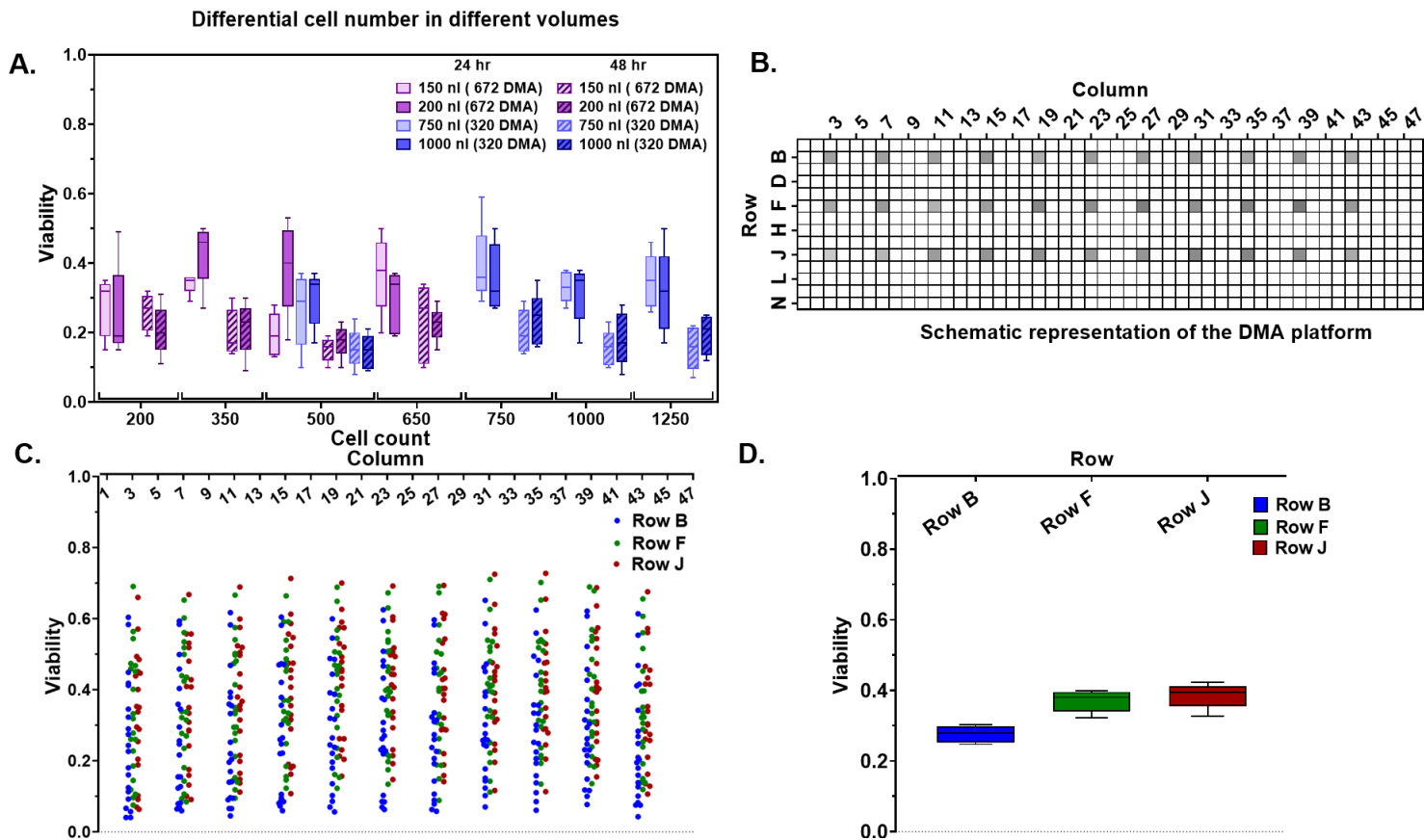

Figure 10. Viability assessment on different DMA platforms and comparison of column vs. row effects in CLL patient-derived cells cultured on DMA.

Assessment of cell viability using different cell numbers and volumes on DMA slides (672- and 320-spot formats) after 24 and 48 hours. The legend in purple represents data from the 672-spot DMA slide, while blue represents data from the 320-spot DMA slide. Clear bars indicate data from the 24-hour incubation period, while striped bars represent data from the 48-hour incubation period. (B) Schematic representation of the DMA slide, illustrating the column and row layout and the positioning of the DMSO control condition. (C) Viability assessment of 21 patient-derived CLL cell samples after 1 day in culture on the 672-spot DMA slide under control conditions (DMSO) in specific columns and rows of the DMA slide. (D.) Average viability of patient derived cells in rows on DMA. The presented results were obtained in collaboration with the Department of Hematology, Oncology, and Clinical Immunology at Heinrich Heine University Düsseldorf, Germany.

3.1.2 Drug sensitivity and resistance test using 33 drugs conducted on both DMA slides and in 384-well plates

In this experimental section, a miniaturized drug screening on DMA slides is established, utilizing both the SU-DHL-4 cell line and 8 patient-derived CLL cells. The viabilities results of patient-derived CLL cells treated with a library containing 33 anti-cancer drugs (Table 2) were compared between the 672 DMA slide (150 nL) (Appendix Figure A 2) and the 384-well plate (25 µL) (Appendix Figure A 3) after 24 hours of incubation. As well as in comparison using the cell line SU-DHL-4 results on both platforms are represented in Appendix Figure A 4. All drugs were subjected to three repetitions on both the DMA slide and the 384-well plate, with DMSO serving as the negative control Figure 11 (A 1 and 2 respectively). Each drug repeat is dispensed at a different position on the DMA slide to ensure that there is no bias regarding the drug's position per droplet on the DMA slide. (Appendix Figure A 5)

Appendix Figure A 6 illustrates the experimental workflow for the drug screen on DMA slides and plates. These experiments were conducted in Düsseldorf, and the drug response data was compared with existing databases, where responses were measured after 48 hours using the CellTiter-Glo assay. The viability across both platforms DMA and plates are represented in Figure 11 B across 21 different CLL patients. The viability in MTP ranges between an average of 25-80% across various patients while those on DMA ranges between an average of 15-65%. This can likely be attributed to the greater volume available in each well, affording the cells a more substantial supply of essential nutrients and a stable environment, which are both crucial for promoting cell growth [238] Figure 11 D represent the DSRT comparison between DMA and MTPs where green indicates a similar drug response on both platforms, red represents differing drug response effects, while white denotes cases where no comparison was possible. Out of the 33 drugs analyzed, 6 could not be tested in DMA due to limited availability of the drugs to be prepared for DMA drug library, making a comparison with MTP results unavailable. Across the 27 drugs, only 4 drugs showed different result between the 2 platforms. Certain drugs, like BCL2-inhibitors venetoclax and navitoclax, exhibit a noticeable impact on viability of CLL cells both in the 384-well plate and on the DMA slide. Notably, the viability observed for these two drugs on the DMA slide was consistently below 100% across

all patients, as was the case in the plates. In contrast, other drugs such as idelalisib, lenalidomide, and ruxolitinib do not influence the viability of B-lymphocytes either in the 384-well plate or on the DMA slide. In these cases, viability remained at 100% across different concentrations on both platforms. There are also instances where the effects of drugs differ between MTPs and DMA slide, exemplified by drug vorinostat, selinxor, palbociclib, and daunorubicine, particularly after 24 and 48- hours of incubation. In this study, we screened 27 drugs using both DMA platform and traditional plates. Out of these, 4 drugs (approximately 15%) did not show similar results across the two platforms as shown in Figure 11 D. Furthermore, patient responses can vary widely even when the same drug is administered. For instance, in Figure A 3, which depicts DSRT for CLL in plates using bendamustine, the variance in responses across the 8 tested patients is notable. Bendamustine works by cross-linking DNA, leading to cell cycle arrest and apoptosis in malignant cells. In this case, Patient 1 did not respond to bendamustine at all, while Patient 8 exhibited a strong response. Meanwhile, Patients 6 and 7 showed partial responses, highlighting the heterogeneity in drug efficacy among different individuals. This discrepancy in drug response underscores the significant influence of individual patient variability, which appears to be independent of the platform used. The variability in patient responses to drug treatments is largely influenced by individual heterogeneity, including genetic(such as mutations in specific genes), metabolic pathways (like drug metabolism and clearance), and environmental factors(including lifestyles and comorbidities).[239] This underscores the importance of personalized medicine approaches to optimize therapeutic outcomes. Additionally, this inconsistency may stem from experimental variables, such as sample handling.[240] In this study, Figure 11C shows the correlation graph of data from patient number 016, revealing a positive correlation with a coefficient of R = 0.8356 between the viability assessed on both the DMA platform and in plates. The correlation was plotted by comparing the normalized viability data from both platforms, where each data point represents the average viability value from three technical replicates for each drug, normalized to the DMSO control across five different concentrations. The viability measurements from the DMA and plate assays were plotted against each other, and the linear regression analysis was performed to determine the correlation coefficient (R). This high correlation indicates that the DMA platform and the traditional plate-based assays are both reliably capturing the same biological response in this patient's cells, despite

potentially different methodologies and scales. This positive correlation is important as it validates the use of the DMA platform in reflecting true biological responses, similar to established methods. Additionally, the DMA platform offers a more dynamic and high-throughput measurement compared to traditional plates, yet still aligns well with plate-based measurements in this instance. Nevertheless, it's important to note that correlation vary across different patients, as illustrated in Appendix Figure A 7.
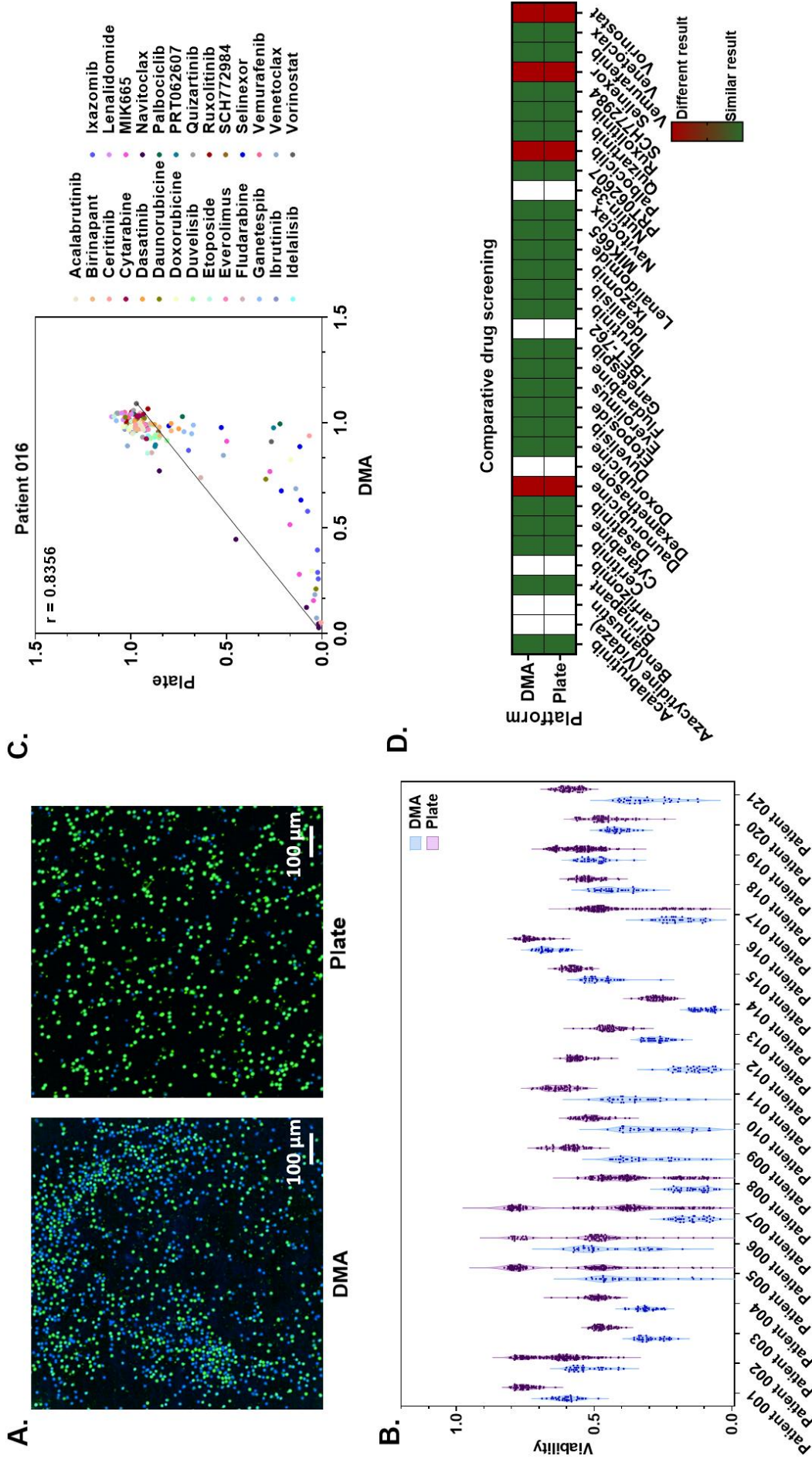
Figure 11. Differential Performance and Effectiveness of the DMA and MTP Platforms for Viability Assessment, Drug Screening, and Personalized Medicine Applications Tested Across Different Patient Derived CLL Cells

A) Representative images of patient-derived CLL cells stained using live/dead fluorescent staining on both the DMA platform and the MTP platform in the DMSO control. The staining includes Hoechst (blue, staining nuclei) and Calcein AM (green, indicating viable cells). Image (1) shows CLL cells on the DMA platform from patient one, while image (2) depicts CLL cells on the MTP platform. (B) Comparison of CLL cell viability between the DMA and MTP platforms in the DMSO control, showcasing results obtained from 21 different patients. (C) Normalized viability-based drug screening comparison of 27 different drugs conducted on both the DMA and MTP platforms using patient 016. (D) Heatmap illustrating the concordant and discordant effects of a drug library in DMA vs. MTP, with notable exceptions where Green indicates a similar effect on both platforms, red represents different results, and white denotes no result of drugs tested only in MTP and not in DMA. (A), (B), and (D) The presented results were obtained in collaboration with the Department of Hematology, Oncology, and Clinical Immunology at Heinrich Heine University Düsseldorf, Germany.

3.1.3 Cell viability across various time points: comparing patient-derived CLL cells cultured on DMA slides in both medium and hydrogel
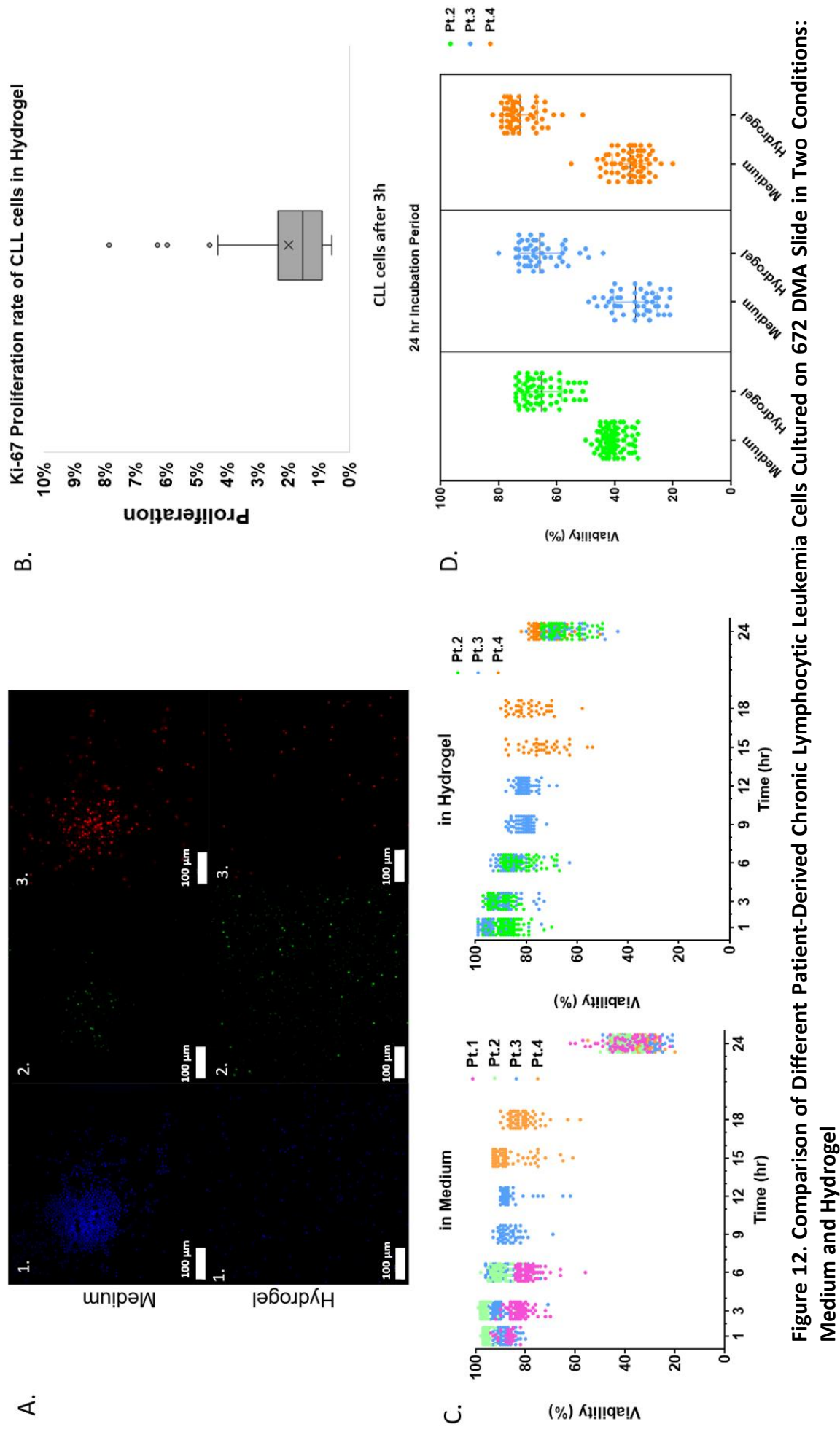
The primary objective of this experiment, conducted by my student Tobias Gärtner under my supervision, is to enhance the viability of patient derived CLL cells on DMA platform. In previous experiments, patient-derived CLL cells were cultured for only 24 and 48 hours due to their significant viability decline after 24 hours, which limited further experimentation. Therefore, there is a need for improved viability on the DMA slide to extend the culture duration and allow for more comprehensive analysis. To determine the optimal culture conditions for sustained cell viability, we tested patient-derived CLL cells on DMA slides in both liquid medium and 3D Life Dextran-PEG Hydrogel across different time points. Figure 12 A represent patient derived CLL cells cultured on 672- DMA in hydrogel vs medium condition in DMSO control, stained with Hoechst, Calcein and PI. Figure 12 C and D represent the viability comparison between cell cultured in 2 conditions, in liquid medium and hydrogel, across time points of 1, 3, 6, 9 ,12 15, 18 and 24 hrs. In patient 1, the average viability of CLL cells in medium began at 95% after 1 hour but steadily declined to 92% after 3 hours, further dropping to 91% after 6 hours. Between 6 and 24 hours, a significant decrease in viability was observed, dropping to average 35% (Figure 12C). The variation in viability across these time points was minimal, indicating a relatively consistent decrease in viability over time. For patient 2, cell viability remained consistent at around 93% during the 1-hour, 3-hour, and 6-hour time points. However, after 24 hours, the viability dropped to 42%, with minimal variation in the data at any of the time points. This suggests that the viability of CLL cells from patient 2 was relatively stable over short incubation periods but declined sharply after 24 hours. In patient 3, the viability of CLL cells started at 94% after 1 hour and slightly decreased to 91% at 3 and 6 hours. The data exhibited more variability during these time points compared to patients 1 and 2. After 24 hours, a significant drop in viability to 42% was observed, indicating that CLL cells from this patient were more sensitive to extended culture times (Appendix Figure A8). The observed differences in viability across the 3 different patients may be due to a combination of patient-specific biology, cellular sensitivity to culture conditions, and extended culture stress. Figure 12 C presents a comprehensive comparison of

viability outcomes for patient-derived CLL cells cultured in both liquid medium and hydrogel across various time points. In medium, patient 1's cells showed a steady decline from 86% after 1 hour to 39% after 24 hours, with significant outliers observed at the 24-hour mark. In hydrogel, viability started at 86% after 1 hour but decreased more gradually, reaching 44% after 24 hours. Variability was observed at the 6-hour incubation point, but hydrogel conditions provided a more stable environment for cell viability. For patient 2, cell viability in medium peaked at 96% after 1 hour but decreased to 40% after 24 hours, with noticeable outliers at early time points. In hydrogel, viability increased from 85% at 1 hour to 90% at 3 hours before declining to 67% at 24 hours. This pattern shows that hydrogel conditions may support better viability for CLL cells over longer incubation periods compared to liquid medium. For patient 3, the highest recorded viability in medium was 92% after 3 hours, but it steadily decreased to 33% by 24 hours, with significant outliers observed between 3 and 12 hours. In hydrogel, the highest viability was recorded at 95% after 1 hour, but after 24 hours, it dropped to 67%, with the most significant dispersion occurring at the 24-hour time point. This suggests that, while hydrogel conditions improve viability compared to medium, there is still considerable variability depending on the patient. For patient 4, the peak viability in medium was 88% after 15 hours, and after 18 hours, it was 80%. However, at 24 hours, the viability dropped to 35%. In hydrogel, the viability increased from 75% after 15 hours to 80% after 18 hours, but the lowest observed value, 76%, occurred at 24 hours. This patient exhibited the least variability across time points, especially in hydrogel conditions. Additional information regarding the viability graphs can be found in Appendix Figure A 9 And Figure A 10. Figure 12 D further compares viability across patients, cultured in medium versus hydrogel conditions after 24 hours. Patient-derived CLL cells cultured in hydrogel showed a marked improvement in viability, with an average of 68% across three replicates, compared to a decline to 38% in medium. Specifically, patient 2 had 40% viability in medium and 70% in hydrogel, patient 3 had 30% viability in medium and 70% in hydrogel, and patient 4 had 30% viability in medium and 80% in hydrogel. This stark contrast emphasizes the advantage of hydrogel conditions in promoting cell survival.

The results indicate that CLL cell viability decreases over time, but the rate and pattern of this decline vary between patients. Patient 1's cells showed a steady, consistent decrease,

suggesting a gradual loss of cell viability with extended culture. Patient 2's cells remained stable for the first 6 hours but became highly susceptible to prolonged culture stress, with a sharp decline at 24 hours. Patient 3's cells exhibited more variability in viability over shorter time periods and were also sensitive to extended culture, showing a significant drop at 24 hours.

These differences highlight the importance of patient-specific factors in determining cell behavior and viability over time. The results suggest that prolonged incubation may induce stress that affects all patients' CLL cells, but the degree of sensitivity to this stress varies. While the exact mechanisms behind this enhanced viability are not fully investigated in this study, several factors likely contribute. First, the hydrogel provides a 3D scaffold that mimics the natural extracellular matrix (ECM), supporting cell-matrix interactions crucial for survival. Second, the hydrogel may reduce stress caused by evaporation and changes in osmolarity, which are more prevalent in standard medium conditions. This stable environment could help maintain cell viability, especially during longer incubation periods, thus improving the outcomes of drug sensitivity testing.[241, 242]

Figure 12. Comparison of Different Patient-Derived Chronic Lymphocytic Leukemia Cells Cultured on 672 DMA Slide in Two Conditions: Medium and Hydrogel

(A) Representative images of CLL cells cultured for 24 hours per spot on DMA Slide in Medium and Hydrogel stained with Live-Dead Fluorescent Dye. (1) Hoechst Channel (2) Calcein Channel (3) PI Channel cells (B) KI67 Proliferation Rate for CLL cells in hydrogel after 3 hours from patient 4. (C) Scatter Plots of cellular viability (%) for CLL Cells from four different patients in medium and in hydrogel respectively at different Time points in hours. (D) Comparison of cellular viability from 3 different patients in medium vs. hydrogel after 24 hr incubation period.

3.1.4 Proliferation rate of patient derived CLL cells in hydrogel on 672 DMA

The microenvironment plays a critical role in influencing B cell proliferation, though no further investigations were conducted to delve into the specifics of this influence. It is important to note that CLL cells do not proliferate in vitro. Therefore, the results observed in this study regarding proliferation rates are consistent with typical findings in standard in vitro culture conditions, where CLL cells often exhibit limited or no proliferation.[243] To explore the proliferation of CLL cells within hydrogels, a study was undertaken using the 672 DMA—a novel approach using Ki67 staining, conducted for the first time on a DMA slide in a nanoliter format. This methodology allows for the effective application of Ki67 staining within hydrogels, which is enabled by the hydrogel's unique properties. The hydrogel matrix minimizes the impact of washing steps, facilitating accurate assessment of cell proliferation. By utilizing this innovative technique, insights into the proliferation dynamics of CLL cells can be obtained, contributing to a better understanding of their behavior in a more physiologically relevant microenvironment. Figure 12 B illustrates the proliferation rates after two replications over a 3-hour incubation period. Proliferation of CLL cells within the hydrogel was assessed using Ki67 staining at both the 3-hour and 6-hour marks, as cell viability remained relatively high during these intervals. In the initial experiment, the majority of proliferation rates were modest, ranging between 1% and 2%. However, outliers showed higher proliferation rates, ranging between 6% and 8%. Notably, when attempts were made to assess CLL cell proliferation after 6 hours, no Ki-67 signal—an indicator of cell proliferation—was detected, leading to a recorded proliferation rate of 0% in both cases. This absence of a Ki-67 signal after 6 hours suggests that CLL cells might have entered a non-proliferative state or experienced a rapid decline in viability, possibly due to the limitations of the culture conditions or the sensitivity of the assay in detecting low proliferation rates over extended periods. Further studies would be necessary to fully understand these dynamics and optimize the culture conditions for sustained proliferation.

3.2 Drug-induced differential gene expression analysis (DGEA) on nanoliter Droplet Microarrays: enabling tool for functional precision oncology

In the dynamic field of cancer research and treatment, DGEA plays a crucial role. The study of gene expression patterns through transcriptomic analysis is used to decipher the molecular signatures that characterize different types of cancer or the mechanism of drug response and resistance of individual tumor types.[244, 245] DGEA, especially with the possibility of parallel phenotypic analysis using microscopy, can be an indispensable tool for uncovering the molecular basis of phenotypic changes in cells upon drug treatment and ultimately for understanding the mechanisms of drug response. Post-drug treatment transcriptomics using qPCR and mRNAseq has been applied in multi-well plates,[246] but it is challenging due to the high cost and labor-intensive multi-step sample preparation protocols. Performing DGEA on cancer cells derived from patient biopsies is especially important, since the insights obtained from molecular profiling of unique patient-derived samples upon drug treatment in vitro, are indispensable for understanding the individual tumor response to anti-cancer drugs. However, the use of primary cells poses increased challenges due to the scarcity of available cells, requiring miniaturized and low-input protocols.

In our research group, we have previously demonstrated a protocol for mRNA isolation from cells on the DMA chip using oligo d(T) magnetic beads followed by conversion to cDNA using as low as a single cell.[2] In this study, I have refined the protocol by eliminating the need for oligo d(T) magnetic beads, thereby further simplifying the process and for the first time have demonstrated the ability to detect changes in gene expression following drug treatment on a chip, demonstrating the application of the protocol on patient-derived CLL cells. By miniaturizing the entire workflow from cell culture to cDNA synthesis in nanoliter volumes, reagent and cell consumption were reduced by a factor of 300 and 100, respectively, compared to a 384-well plate. The methodology established here serves as a critical foundation for performing DGEA on limited numbers of cells, offering potential applications in functional precision oncology.

3.2.1 Concept and experimental workflow of drug-induced DGEA on DMA chip

In this study, we introduce a concept and methodology for performing drug-induced DGEA as a read-out method in addition to microscopy for in-depth characterization of gene expression changes in cells upon drug treatment, in nanoliter format on the DMA platform. Figure 13 shows the concept and objectives of this study. The workflow was optimized on DMA, which contains an array of 672 square 1 mm2 hydrophilic spots separated by hydrophobic borders. This array allows for the formation of an array of nanoliter droplets, working volume from 150 to 200 nL, on a planar surface, serving as nano-wells for cell culture and drug screening (Figure 13 A). Due to the dramatic miniaturization of the culturing reservoirs, the DMA platform is advantageous for low cell number experiments, which is essential, for example, in the case of patient-derived cancer cells. In this study, as a model cell type we chose patient-derived CLL. As shown in Figure 13 B, the patient-derived cells can be exposed to a panel of anticancer drugs pre-printed on the DMA chip. Both image-based analysis, such as live/dead fluorescence staining to determine cell viability, and DGEA can be performed as a read-out for drug effect (Figure 13 B). The protocol for DGEA involves lysis of cells, isolation of mRNA and conversion of mRNA to cDNA, all in nanoliter droplets on the DMA chip (Figure 13 C). The cDNA generated from each nanoliter droplet on the DMA platform was characterized by a capillary gel electrophoresis (Bio-analyzer), polymerase chain reaction (PCR) and quantitative PCR (qPCR).
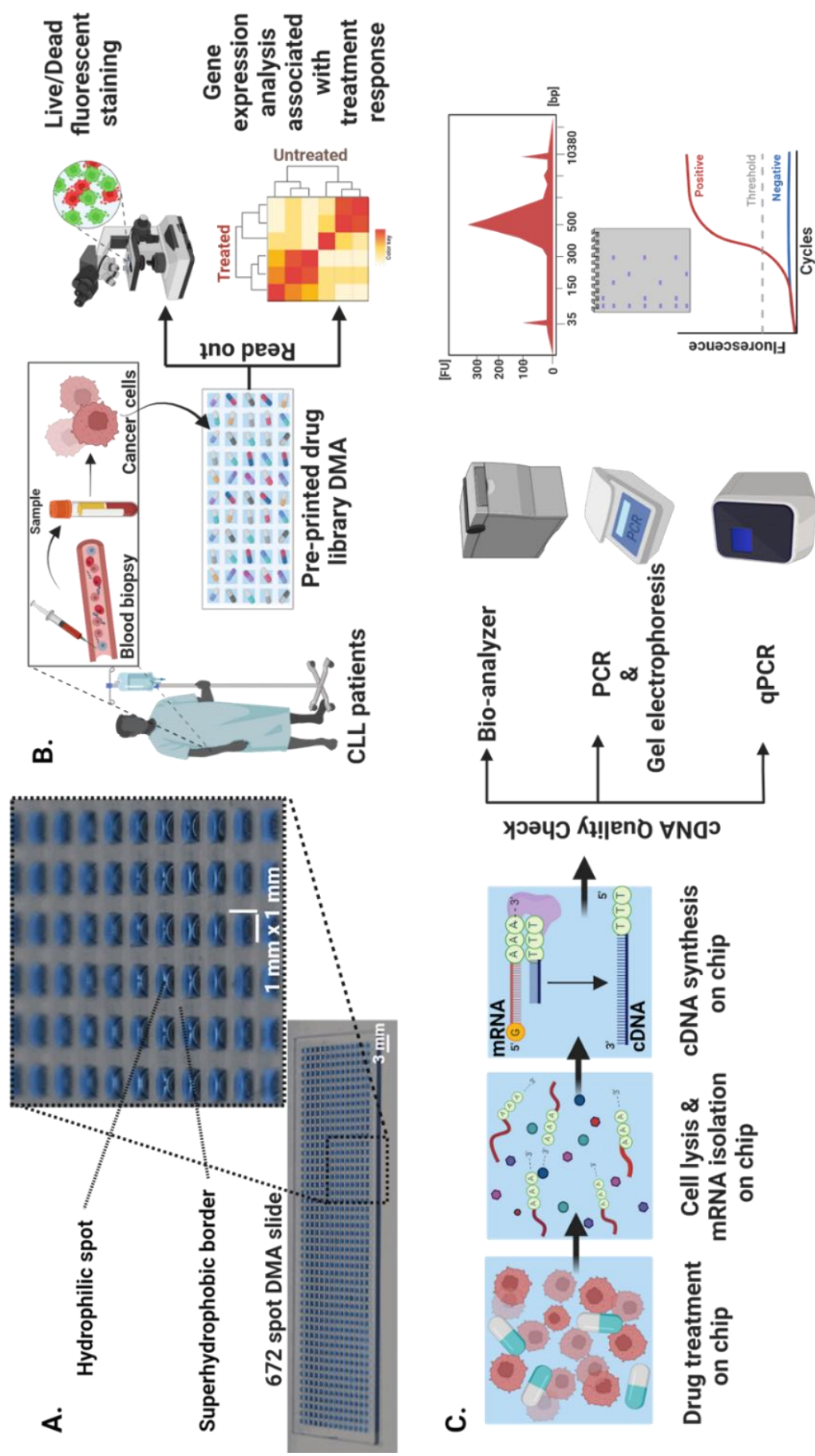
Figure 13. Concept and Experimental Workflow of Drug-Induced DGEA on DMA Chip

(A) The DMA platform with 672 hydrophilic spots separated by a superhydrophobic background, each spot measuring 1 mm x 1 mm. (B) Blood biopsy-derived chronic lymphocytic leukemia (CLL) cells are applied to individual spots on a pre-printed DMA slide containing a drug library. Following a 24-hour incubation period, live/dead fluorescent staining (utilizing Calcein, Hoechst, and propidium iodide) to estimate cell viability and DGEA can be performed to analyze the drug response. (C) The sample preparation protocol for DGEA includes the lysis of cells treated with drugs with a lysis buffer, causing the release of mRNA from the cells into the droplets, which then is converted into complementary DNA (cDNA) via reverse transcription. The resulting cDNA is collected from the DMA chip and subjected to quality checks, including capillary gel electrophoresis (Bio-analyzer), polymerase chain reaction (PCR) and quantitative PCR (qPCR).

97

3.2.2 Validation of the protocol for DGEA on DMA chip

As a first step, we optimized the protocol for cell lysis and conversion of mRNA into cDNA using the suspension SU-DHL-4 cell line. SU-DHL-4 is a B-cell lymphoma cell line, representing one of the most diverse malignancies arising from B-lymphocytes. Previously, we published a protocol using oligo d(T) magnetic beads for mRNA extraction and purification on DMA chip using adherent cell lines.[2] In comparison with the previously published protocol we removed the step of mRNA purification on DMA chip using oligo d(T) beads and changed the RNA later lysis (RLT) buffer to Proteinase K enzyme. The current protocol is optimized and validated for the analysis of suspension cells. The detailed sample preparation protocol is shown in Figure 14. It includes the following steps: (1) lysis of cells using proteinase K and dispensing of oligo-dT primers, (2) dispensing of RT (Reverse Transcription) mix followed by incubation of the DMA chip at 42°C for conversion of mRNA to cDNA, (3) collecting the resulting sscDNA (single-stranded cDNA) synthesized in a total volume of 260 nL from the DMA into a PCR tube, (4) exonuclease treatment, (5) amplification of sscDNA into dscDNA, (6) purification of the final DNA product (dscDNA) using AMPure XP beads. As indicated, steps 1 and 2 are performed on the DMA chip, while steps 4 to 6 are performed in a tube using standard protocols. In this study, we transferred samples from the DMA chip to the tubes (step 3) using manual pipetting. In our recent study, we demonstrated automated collection and transfer of sscDNA synthesized on the DMA chip using the in-house developed automated nanoliter droplet selection and collection device ANDeS.[247] Automated collection of the droplets opens the possibility of performing high-throughput workflows on the DMA chip utilizing drug-induced DGEA as a read-out.

In order to validate the cell lysis protocol on a DMA platform for efficient mRNA extraction and subsequent conversion to cDNA, a series of experiments were performed comparing different lysis conditions. (Appendix Figure A 11) The aim was to identify the most effective combination of Proteinase K treatment time, heat inactivation time, both with and without RNAse inhibitor, across different cell numbers. Tube control was performed under standardized conditions (10 min Proteinase K treatment and 10 min heat inactivation with RNAse inhibitor) to serve as a benchmark for comparison. (Appendix Figure A 11) The efficiency of lysis and subsequent RNA extraction was quantitatively assessed by measuring

the concentration of obtained nucleic acids (ng/µL) and the mean quantification cycle (Cq) values in a real-time PCR setup using the GAPDH gene (Appendix Figure A 11) The experiments yielded a range of nucleic acid concentrations and Cq values, with 30 minutes Proteinase K lysis and 10 min heat inactivation with RNAse inhibitor showing comparable values to the tube control. (Appendix Figure A 11)

To demonstrate the optimized protocol, we first dispensed 100 SU-DHL-4 cells in an initial volume of 150 nL and performed step 1 and 2 of the protocol (Figure 14 and Appendix Figure A 12). We then collected sscDNA from 4 (400 cells), 2 (200 cells) and a single (100 cells) droplets into the tubes and performed steps 4 to 6 (Figure 14 and Appendix Figure A 12). We obtained from about 7000 pg/µL and 1500 pg/µL of dscDNA from 400 and 100 cells, respectively (Appendix Figure A 13). We then assessed the quality of the dscDNA using capillary gel electrophoresis, PCR and qPCR. As shown in Figure 14 B, we obtained the expected size distribution of dscDNA, from about 300 and 1000 bp, as shown by the electrophoresis results using the high sensitivity Agilent 2100 Bioanalyzer (Figure 14 B). Next, we demonstrated successful amplification of short fragment (112 bp) of glyceraldehyde-3-phosphate dehydrogenase (GAPDH) and long fragment (1045 bp) of ACTB (β-actin) genes, indicating intact cDNA obtained from the DMA chip (Figure 14 C- E). The qPCR analysis of the relative gene expression of GAPDH gene showed a statistically significant proportional increase from 100 to 400 cells (Figure 14 F). Importantly, minimal spot-to-spot variability in the relative expression of GAPDH was observed, as indicated by the standard error of the mean for each group, indicating robustness and reproducibility of the developed protocol (Figure 14 F). As a next step, we aimed to check the sensitivity of our method and performed the same analysis using only a single cell. As shown in Figure 14 B and E, we were able to detect dscDNA obtained from a single cell by capillary electrophoresis and successfully amplify GAPDH and β-actin genes by PCR (Figure 14 A-B and E). Thus, our results show the accuracy and sensitivity of the developed method and demonstrate the successful generation of high-quality cDNA suitable for various downstream DGEA methods, including qPCR and potentially next generation sequencing (NGS).
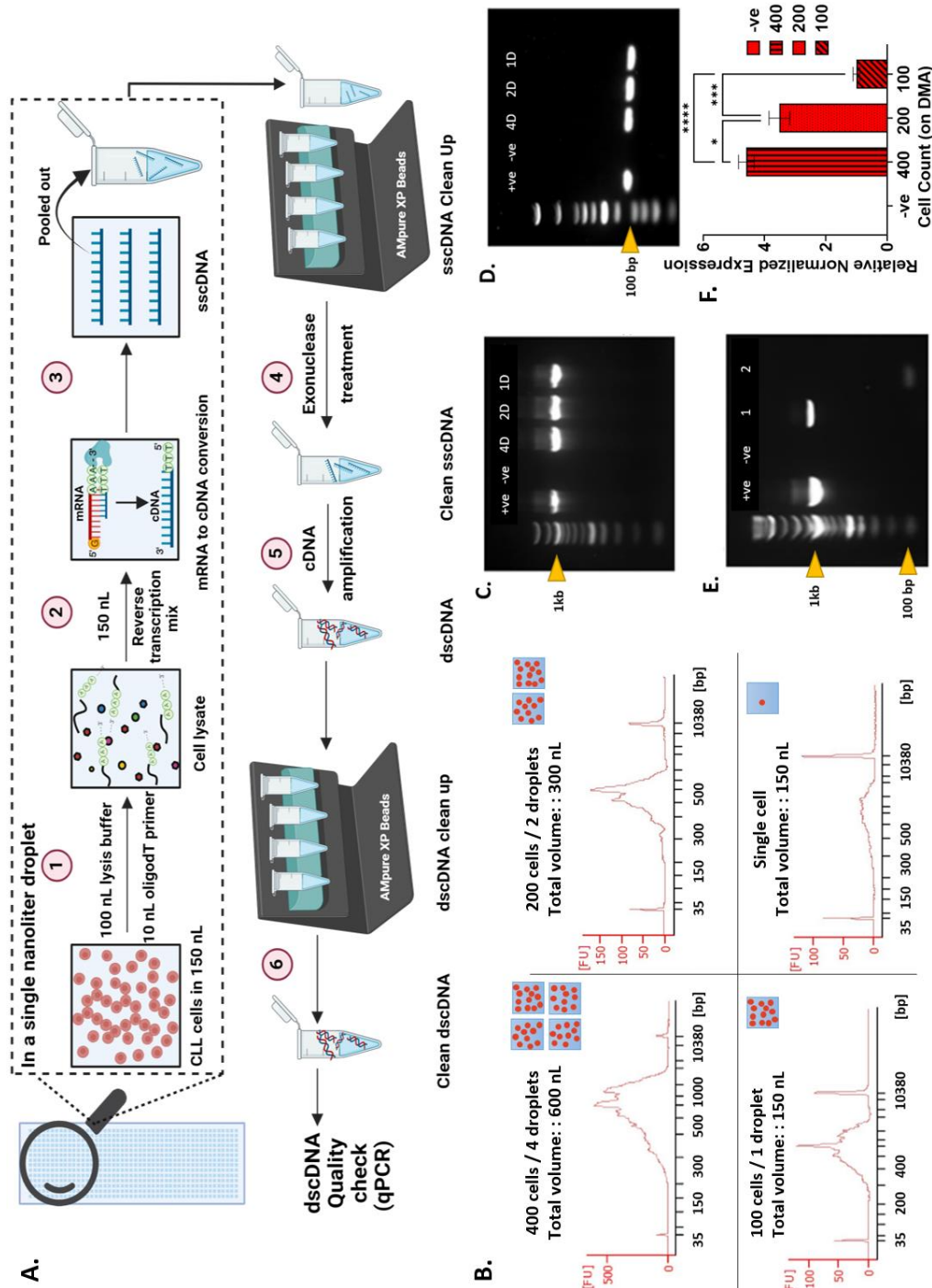
Figure 14. Validation of the Protocol for DGEA on DMA Chip

(A) Schematic representation of the workflow of protocol for cDNA synthesis in individual droplets on DMA slide. (B) Qualitative assessment of the cDNA prepared on the DMA chip from cells using the Agilent 2100 Bioanalyzer. This analysis encompasses samples collected from 4, 2 and 1 droplet, containing in total 400, 200 and 100 cells, respectively, as well as a single cell per droplet. Results from a total of three experiments are shown. (C-E) Gel electrophoresis of amplified *β-actin* (B, product size = 1045 bp) and *GAPDH* (C, product size = 112 bp) genes from cDNA obtained from 4 (4D), 2 (2D), and 1 (1D) droplet. (D) Gel electrophoresis of amplified *β-actin* (lane 1, product size = 1045 bp) and *GAPDH* (lane 2, product size = 112 bp) genes from cDNA obtained from a single-cell from DMA chip. The "+ve" lane contains positive control, which is cDNA synthesized from SU-DHL-4 cells using the standard protocol, whereas the "-ve" lane contains negative control with no template. (F.) Graph illustrating *GAPDH* relative gene expression in samples prepared from 4 droplets, 2 and 1 droplets. The error bars represent the mean ± SEM from 3 technical repeats. Statistical significance was determined using ordinary one-way ANOVA, revealing highly significant differences ****P < 0.0001, ***P < 0.001, *P < 0.01 between consecutive groups, 'NS' indicates non-significant statistical differences between the analyzed groups.

100

3.2.3 Towards drug-induced DGEA from DMA chip: SU-DHL-4 cells

To demonstrate the application of the established DMA protocol for drug-induced DGEA, we have characterized the expression of the genes *SYK* (Spleen Tyrosine Kinase) and *GADD45β* (Growth Arrest and DNA Damage-inducible, beta) following treatment with a cytotoxic anticancer drug on a DMA chip. Both genes play an important role in the regulation of cell survival and apoptosis in CLL, and their study is essential to elucidate the molecular mechanisms driving CLL carcinogenesis, identify potential therapeutic targets and improve prognostic assessment.[248-251] Understanding the role of *SYK* in aberrant B-cell receptor signaling and *GADD45β* in stress response and DNA damage repair provides valuable insights that will guide the development of targeted therapies and advance personalized treatment strategies in CLL. The study by Baudot et al. sheds light on the role of *SYK* in coordinating survival pathways in CLL cells, particularly through mechanisms that modulate the expression of Mcl-1, an essential anti-apoptotic protein.[248] In addition, research by Woyach et al. highlights the importance of B-cell receptor signaling in CLL, with *SYK* emerging as a key component of this pathway and a promising therapeutic target,[252] and research by Salvador et al. elucidates the role of *GADD45β* in cellular stress responses, including DNA damage repair, which has important implications in the context of CLL carcinogenesis and therapeutic response.[250, 251]

First, we have optimized and validated the protocol for drug-induced DGEA on DMA using SU-DHL-4 cell line with the cytotoxic drug doxorubicin on the DMA chip and in 384-well plates. For dose-response assessment, cell viability was assessed by treating cells with doxorubicin over a concentration range from 0.008 µM to 5 µM for 48 hours. Live-dead fluorescence staining and image-based analysis were used for evaluation of drug response (Figure 15 and Appendix Figure A 14). Figure 15A presents representative images of SU-DHL-4 cells stained with live/dead fluorescent dyes on both the 384-well plates and the DMA platform, with DMSO control after 24-hr incubation. The dose-response and IC50 values determined for DMA were comparable to the dose-response obtained from 384-well plates, being 2.1 µM and 2.5 µM for plates and DMA, respectively (Figure 15 B). We then generated cDNA samples from cells treated with 1 µM doxorubicin on DMA and plates to assess the relative gene expression of *SYK* and *GADD45β* genes. To verify the presence of cDNA in our sample preparation within

the droplets, we detected amplification of the housekeeping gene *GAPDH* (Appendix Figure A 14 B and C). Afterwards, the relative gene expression of *SYK* and *GADD45β* genes was analyzed by qPCR as shown in Figure 15 C. We have shown an upregulation of both genes in response to doxorubicin treatment in SU-DHL-4 cells (Figure 15 C). The results obtained on the DMA chip were comparable to those obtained in the 384-well plate. Treatment with doxorubicin lead to a significant upregulation of both *SYK* and *GADD45β* genes in both DMA and well plate. Specifically, *SYK* expression was upregulated 1.5-fold in DMA and 2-fold in plate, while the *GADD45β* gene shows a significant upregulation in response to doxorubicin, with a 20-fold increase in DMA and a 15-fold increase in plate. Thus, we have demonstrated the successful adaptation and reliable performance of the drug-induced DGEA protocol on the DMA platform using the SU-DHL-4 cell line. The results obtained from both DMA and conventional 384-well plates were highly comparable, validating the efficacy of our methodology for high-throughput drug screening applications.
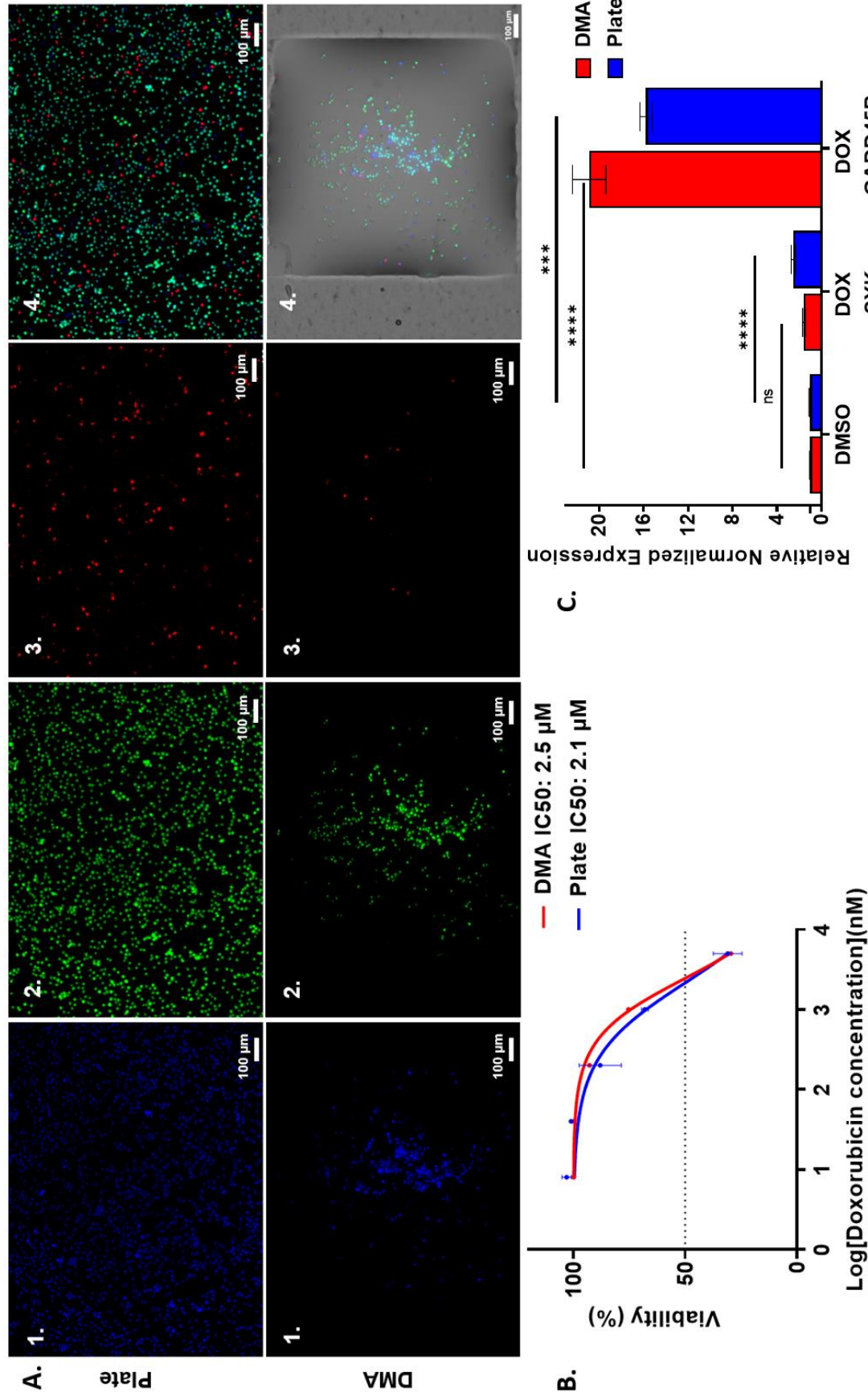
Figure 15. Comparative Analysis of SU-DHL-4 Cell Responses to Doxorubicin (DOX) Treatment in 384-Well Plate and on 672-Spot DMA Slide

(A) Representative images of SU-DHL-4 cells stained using live/dead fluorescent staining on both platform plates and the DMA in DMSO control. The staining includes (1) Hoechst, (2) Calcein, and (3) PI. (4) An overlay of the three channels. Images were captured using the Keyence BZ-X810 microscope. (B) Graph showing dose-response of SU-DHL-4 cells to doxorubicin and estimated IC50 values obtained from DMA and 384-well plate. (C) Relative gene expression analysis of *SYK* and *GADD45β* genes in cells exposed to a vehicle control (DMSO) and 1 µM of DOX. Error bars represent the mean ± SEM from three technical repeats (n=3). The bar graphs illustrating the relative gene expression of *SYK* and *GADD45β* from the samples. Statistical significance was determined using one-way ordinary ANOVA, with highly significant differences ****P < 0.0001, ***P < 0.001, *P < 0.01 for comparison between consecutive groups, 'NS' 'NS' indicates non-significant statistical differences between the analyzed groups.

103

3.2.4 Towards drug-induced DGEA from the DMA chip: patient-derived CLL cells

To demonstrate the applicability of the developed protocol for use with patient-derived cancer cells, we used CLL cells obtained from patient blood biopsies. In vitro testing of CLL cells for sensitivity to anticancer drugs is an important application that shows good correlation with patient response.[253] DGEA is applied to CLL to assess gene expression changes resulting from drug treatment, providing insight into the molecular mechanisms underlying drug response and identifying potential therapeutic targets in CLL. In this study, we aim to demonstrate the feasibility of performing drug-induced DGEA on patient-derived CLL cells from the DMA chip, where drug screening and sscDNA preparation are performed on the DMA chip in a nanoliter format.

As mentioned earlier in chapter 3.1 , we have shown that CLL cells can be cultured and tested on DMA chips and that the viability of CLL cells is higher and more stable when cultured in hydrogel pads on DMA instead of liquid media (manuscript in preparation). Therefore, we cultured CLL in 150 nL of commercially available dextran-based hydrogel (Cellendes) with 150 nL of medium on top of each hydrogel pad. Therefore, we first adapted the protocol for sscDNA sample preparation using SU-DHL-4 cells in 150 nL hydrogel pads on DMA (Appendix Figure A 15), successfully demonstrating the expected size distribution of obtained cDNA, spanning between 300 and 1000 bp and amplification of *GAPDH* housekeeping gene (Appendix Figure A 15)

Having optimized the protocol for DGEA on hydrogel pads on the DMA chip, we proceeded to test this protocol on patient-derived CLL cells. First, we tested obtaining cDNA from different numbers of cells ranging from 100 to 2000 cells (Figure 16 A-D). Using qPCR analysis, we observed a consistent decrease in *GAPDH* expression with decreasing numbers of primary cells both in tubes and on the DMA chip (Figure 16 C and Appendix Figure A 17). This assessment was performed on samples from three different patients, ensuring the robustness of the protocol across different CLL patient samples (Figure A 17). Next, we analyzed the expression levels of the *SYK* and *GADD45β* genes in CLL cells obtained from three patients after treatment with doxorubicin on DMA slide. The IC50 values for doxorubicin in the three

different patients were 3.209 μM, 3.109 μM and 2.141 μM, respectively (Figure 16 B, Appendix Figure A 16). We then exposed CLL cells to 1 μM doxorubicin in 150 nl hydrogel pads for 24 hours, as represented in Figure 4 A. Afterwards, cells were subjected to the protocol for cDNA generation. In all three CLL patient-derived samples tested, relative gene expression analysis revealed upregulation of the *SYK* and *GADD45β* genes, as shown in Figure 16 D and Appendix Figure A 18. In our study, we observed different patterns of gene expression for both *SYK* and *GADD45β* in the different patient samples when compared to the control (DMSO). Patient 1 showed a 1.4-fold upregulation of *SYK*, indicating a modest increase in expression. In contrast, patient 002 showed a more significant increase with a 2-fold increase while patient 003 showed an even higher upregulation with a 3-fold increase. These results indicate that the level of *SYK* expression varies between patients, suggesting potential heterogeneity in molecular responses with potential clinical implications. Our observations showed that the degree of up-regulation in the relative amount of the *GADD45β* gene varied between the patient samples. Specifically, patient 1 showed a remarkable upregulation with a relative abundance of 2.2-fold. In contrast, patient 002 showed a dramatic upregulation of 8000-fold, while patient 003 showed a moderate increase of 3.5-fold compared to the DMSO control. These results underline the existence of patient-specific responses to the experimental conditions and highlight the need for tailored therapeutic strategies to target *GADD45β* expression. In conclusion, our study reveals a consistent upregulation of *SYK* and *GADD45β* genes in patient-derived CLL cells treated with doxorubicin, highlighting the potential importance of these molecular changes in the context of therapeutic responses, and providing valuable insights for future investigations into CLL treatment strategies. These results demonstrate the feasibility of performing such protocols on patient-derived cells, thereby facilitating the exploration of personalized medicine approaches to CLL treatment.

To date, no previous research has investigated the direct effect of the drug doxorubicin on the *SYK* and *GADD45β* genes in the SU-DHL-4 cell line or CLL patient-derived cells. However, our results are consistent with previous research showing that DNA damage in cancer cells induced by chemical inhibitors of *SYK* leads to an upregulation of *SYK* expression, accompanied by an increase in p53 expression in the HCT116 and HT1080 cell lines.[254] According to Wiest et al, the GADD45 family of proteins, consisting of *Gadd45a*, *Gadd45β* and *Gadd45g*, serve as stress sensors, particularly in response to oncogenic stress, and

regulate various cellular processes such as cell cycle, DNA replication/repair and survival through interactions with other proteins.[255] Guo et al. demonstrated the effects of GADD45g overexpression, showing its role in inducing apoptosis, differentiation, growth inhibition and enhancing chemosensitivity in primary leukemia cells from patients with AML.[251]Our findings are consistent with previous research and support the involvement of *GADD45β* in stress response and DNA damage repair, as evidenced by its significant upregulation in response to doxorubicin treatment in both DMA and plate platforms.
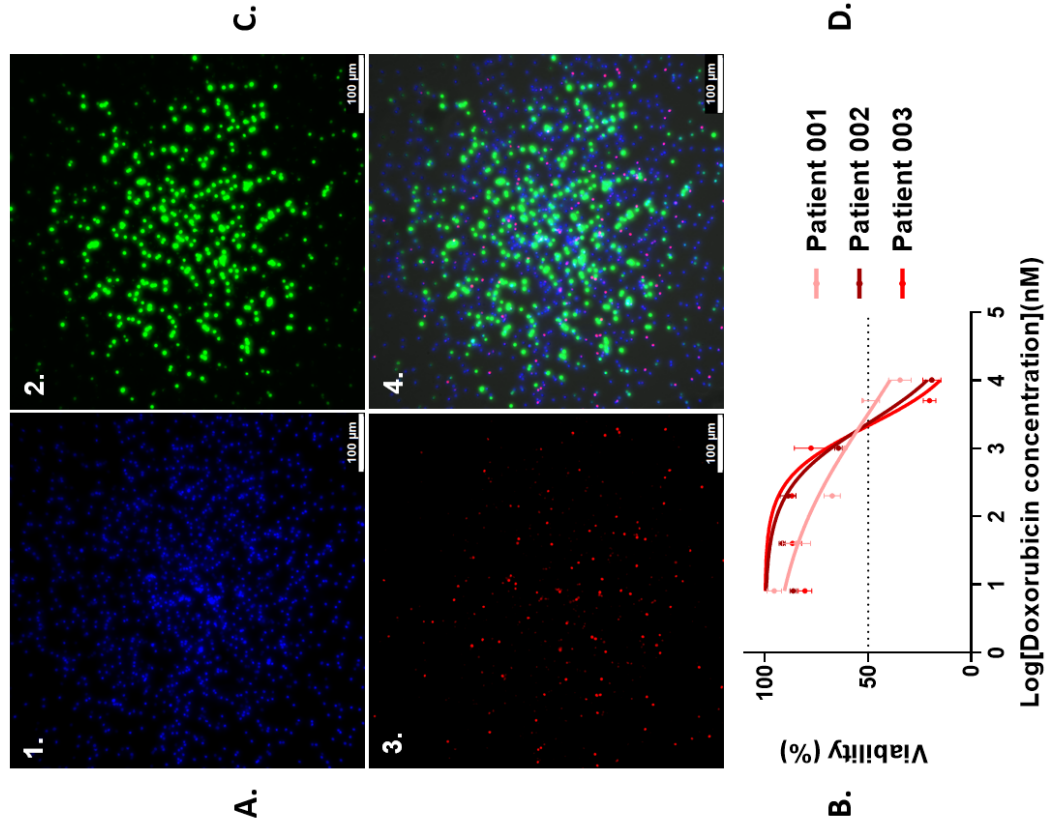
Figure 16. Evaluating Viability, cDNA Quantity, and Gene Expression of 3 Patients -derived CLL Cells on DMA slide

(A.) Representative mages of CLL patient-derived cells (patient 003) following 24 hours of incubation with 1 μM doxorubicin (DOX) on a DMA slide, stained using live/dead fluorescent staining. The images displayed are: (1) Hoechst, (2) Calcein-AM, (3) PI, and (4) overlay of the three channels. Images were captured using the Leica Thunder 3D Imager. (B.) Comparison of IC50 viability percentages for three different CLL patient-derived cells indicating their drug sensitivity to DOX treatment. (C) Quantification of *GAPDH* gene expression in CLL patient-derived cells (patient 003) by qPCR at different cell numbers ranging from 2000 to 100 cells. (D) Analysis of SYK and GADD45β gene expression by qPCR in CLL cells treated with 1uM DOX. Statistical analysis showed significant differences (p < 0.05) between cell counts and sample preparation methods. Error bars represent the mean ± SEM from three technical repeats (n=3).

3.3 Seq-on-a-Chip: multiplexed sample preparation for global transcriptomic analysis in nanoliter reservoirs on droplet microarray

The data and findings presented in this section are part of an ongoing project. The manuscript is currently in the process of being written and is expected to be submitted for publication soon. Therefore, the information provided here is preliminary and subject to further refinement.

Microfluidic-based platforms, which have been successfully applied to single-cell sequencing, are well-suited for multiplexing, parallelization, and miniaturization of sequencing protocols. However, they are not compatible with high-throughput screenings, where cells need to be treated with different factors and incubated under specific conditions (e.g., 2D, 3D, scaffolds, different coatings) for days before RNA sequencing. A platform that enables miniaturized high-throughput screening of live cells in a physiologically appropriate environment, followed by transcriptome analysis of each tested condition, would be a valuable tool, expanding possibilities in both fundamental and applied biological research.

Our group has previously developed the DMA platform, which utilizes hydrophilic-superhydrophobic patterning to create wall-less arrays of separated nanoliter droplets.[201, 256] Over the past few years, we have successfully used this platform for culturing various cell types and have established protocols for compound and transfection-based screenings, as well as transcriptomic studies.[1, 2, 200, 257] Building upon these advancements, the present study focuses on expanding the DMA platform's capabilities for transcriptomic analysis of cells exposed to different stimuli within nanoliter droplets. To achieve this, a miniaturized mRNA sequencing protocol was developed and optimized directly on the DMA platform, integrating unique molecular identifiers (UMIs) to enable precise tracking of individual conditions.

Following the successful generation of high-quality cDNA from both cell lines and patient-derived cells and the accurate determination of gene expression, as demonstrated in Chapter 3.2, efforts were directed toward further developing a high-throughput transcriptomic

analysis approach. This led to the establishment of a novel Seq-on-a-Chip protocol using the DMA platform, designed to enhance RNA sequencing efficiency and precision, particularly in scenarios where sample availability is limited, or large-scale screening is required. By miniaturizing the sample preparation process and incorporating barcoded oligo-dT primers with UMIs, the DMA platform offers substantial improvements over conventional PCR tube-based methods in terms of detection, specificity, and sensitivity. Notably, the platform demonstrates superior transcriptome coverage, particularly for complex transcriptomic features such as intronic and ribosomal RNA sequences, while also reducing reagent consumption and increasing throughput.

The proposed Seq-on-a-Chip protocol is based on the previously established SCRB-Seq procedure, adapted for the DMA platform .[177, 258] In this study, we used a DMA with 672 hydrophilic square spots, each 1 mm inside length, capable of holding up to 200 nL of reaction volume per spot. The proposed protocol is illustrated in Figure 17. Briefly, 100 cells are seeded into each hydrophilic spot on the DMA using a non-contact nanoliter dispenser. Substances of interest, such as siRNA or drugs, can then be added to the droplets containing cells, followed by incubation as required by the assay. After the appropriate incubation period, cells are lysed in separate spots by adding cell lysis buffer. Simultaneously, mRNA from lysed cells in each droplet is barcoded with different E3V6NEXT primers,[259] which are barcoded oligo-dT primers containing a 6 bp UMI. cDNA synthesis is then performed in nanoliter droplets on the DMA using a previously described setup, along with the addition of a template-switching oligo (E5V6NEXT). Subsequent steps involve pooling the first-strand cDNA from multiple spots into a single PCR tube, followed by exonuclease treatment, purification, and single-primer (SINGV6) PCR amplification. The resulting double-stranded cDNA is then purified and used for library preparation and sequencing. The inclusion of UMIs ensures precise identification of genetic material from each nanoliter droplet during sequencing data analysis.

3.3.1 Development of the droplet microarray as a Seq-on-a-Chip platform for transcriptomic analysis
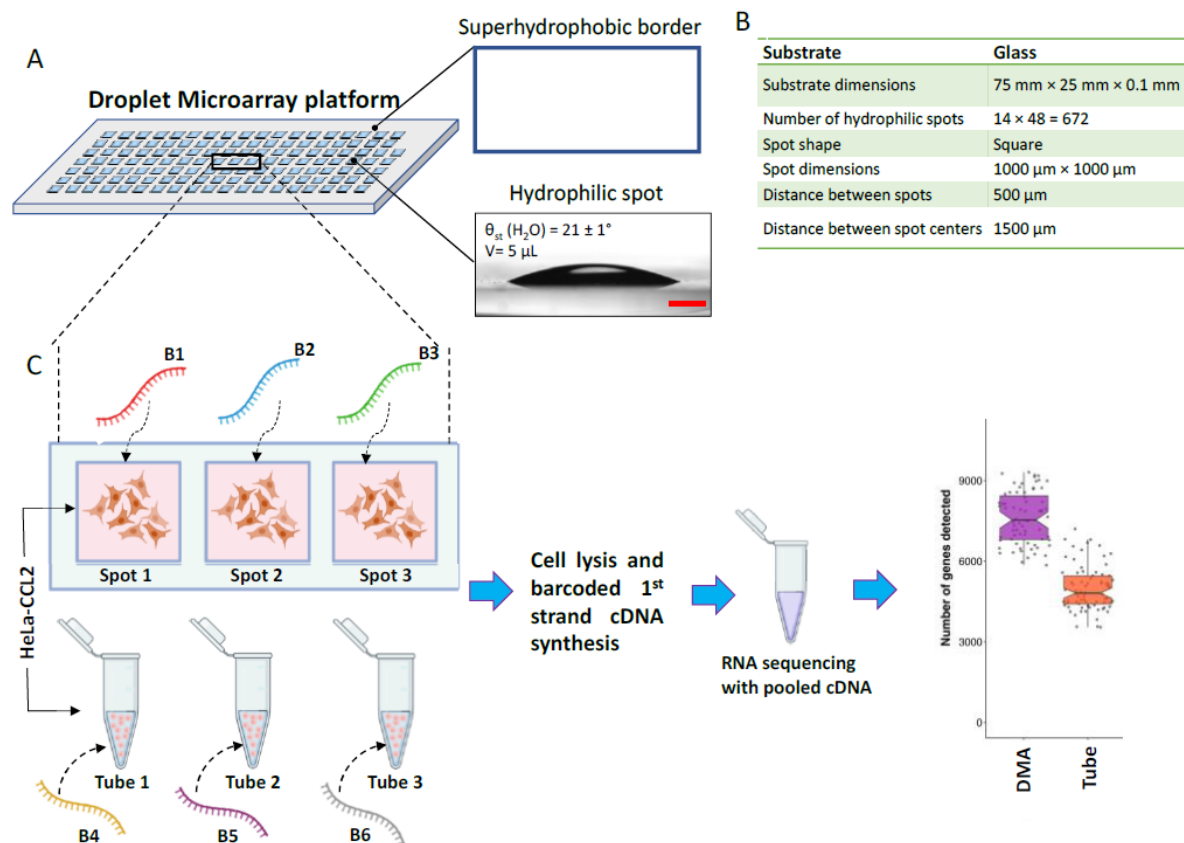

Figure 17. DMA Platform as Seq-on-a-Chip Platform

(A) Schematic representation of the 1 mm x 1 mm spot DMA, showing the water contact angles for both the super-hydrophobic edges and the hydrophilic spots. (B) Detailed description of the properties of the platform. (C) Schematic overview of the study design, comparing the DMA and PCR tubes for the preparation of barcoded cDNA ready for sequencing.

The primary objective of this research is to establish a robust protocol for the preparation of high-quality cDNA in a miniaturized format using a 672-spot DMA slide, with the aim of performing RNA sequencing to detect and distinguish between various barcoded oligo-dT primers and UMIs assigned to different spots on the slide. This approach allows for the simultaneous analysis of multiple experimental conditions within a single sequencing run, enhancing both the throughput and precision of transcriptomic studies. By incorporating barcoded oligo-dT primers and UMIs for each spot, we can accurately track and identify the

cDNA generated from each nanoliter droplet, enabling a detailed comparison of gene expression profiles across different experimental conditions. Using a 672 spot DMA slide, the primary objective of this research is to establish a robust protocol for producing high quality cDNA in a miniaturized format. As shown in Figure 17 A, each spot on this slide measures 1 mm x 1 mm. The DMA slide described in sections 3.1 and 3.3 is designed to be 75 mm x 25 mm x 0.1 mm. This is the standard size of a conventional microscope slide. As shown in Figure 17 B, each hydrophilic spot on the DMA slide is exactly 1000 μm x 1000 μm, with 500 μm between adjacent spots and a center-to-center distance of 1500 μm.

Our aim in this study was to synthesize cDNA directly on the DMA slide, spot by spot, and to compare the resultant cDNA with that synthesized in conventional PCR tubes. In order to ensure specificity and to allow for accurate tracking, we used a unique barcoded oligo-dT primer for each spot on the DMA slide. For example, SK-MEL-28 cells were seeded into spot 1 barcoded B1, spot 2 barcoded B2 and spot 3 barcoded B3. In parallel, we used barcodes B4, B5 and B6 for the PCR tubes, corresponding to tubes 1, 2 and 3, respectively, as shown in Figure 17 C. The complete list of barcoded oligo-dT primers is shown in Table 8. The protocol for this experiment (2.10 Sample preparation and cDNA generation on the DMA platform) is based on the methods described in the Materials and Methods section. Following the outlined steps, including cell seeding, treatment and lysis, dscDNA was pooled from all spots on the DMA slide and from the PCR tubes. These pooled cDNA samples were then subjected to RNA sequencing.

The sequencing data was analyzed to compare the performance of the DMA platform with the conventional PCR tubes, with a focus on the number of genes detected. This comparison is critical. The DMA platform is designed to provide a more efficient and cost-effective alternative for high-throughput transcriptome analysis. The DMA platform has the potential to significantly improve the efficiency of RNA sequencing experiments, particularly in contexts where sample availability is limited or where large-scale screening is required, by miniaturizing the reaction volume and increasing the number of simultaneous assays.

3.3.2 Comparison of transcriptome profiling in SK-MEL-28 Cells: DMA vs. tube sample preparation
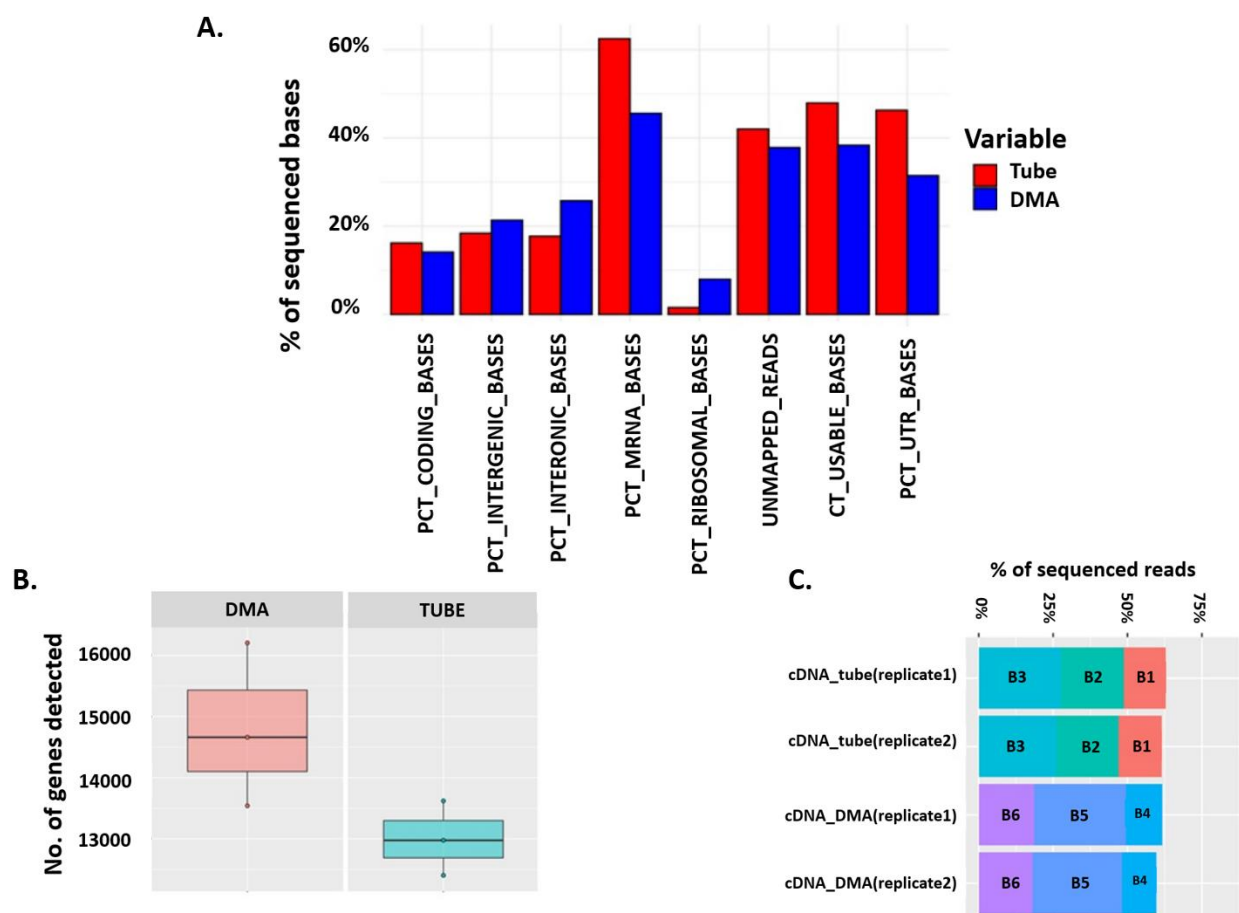

Figure 18. Comparison of SK-MEL-28 Transcriptome Data Between DMA and Tube Methods

(A) The percentage distribution of sequenced bases from SK-MEL-28 transcripts across various genic components, comparing barcoded cDNA synthesized in tube versus on DMA. The data is presented as mean ±SEM from three technical replicates. (B) The number of genes detected from the barcoded cDNA synthesized in tube versus on DMA, as show in box plots.

Following sample preparation on DMA and in tube, the process proceeded through tagmentation, library PCR, and indexing, as per the protocol instructions. After tagmentation, which facilitates the integration of sequencing adapters into the DNA fragments, library PCR was performed to amplify these fragments, followed by indexing to tag each library with unique identifiers. This sequencing preparation method ensures that multiple samples can be pooled and sequenced together while maintaining sample integrity and data accuracy. For 3'

enrichment, we utilized a specialized 3' Enrichment PCR Mix. This enrichment step is crucial as it enhances the representation of the 3' end of mRNA transcripts, thereby improving the accuracy and sensitivity of transcriptome analysis. Following this, library quantification was conducted to ensure that the concentration of the prepared libraries met the necessary criteria. Successful libraries typically exhibited concentrations exceeding 3-5 ng/µl, which is indicative of well-prepared and sufficiently amplified libraries. Sequencing was then carried out on a compatible Illumina sequencer. Prior to sequencing, the libraries were diluted to the recommended molarity of 2 nM, in accordance with Illumina's guidelines. Proper dilution is critical to achieve optimal sequencing performance and data quality. The primary data processing utilized the zUMIs pipeline, a comprehensive tool designed for single-cell RNA sequencing analysis. This pipeline integrates several steps, including alignment of reads to a reference genome, counting of UMIs, and generation of gene expression matrices, which are crucial for accurate quantification of gene expression and effective handling of large-scale sequencing data. The detailed protocol, encompassing tagmentation, library PCR and indexing, 3' enrichment, and precise sequencing, ensures high-quality transcriptome data. By applying zUMIs for primary data processing, the reliability of the results is significantly enhanced, providing a robust framework for interpreting the transcriptomic landscape of the samples.

The sample preparation was conducted similarly in both tube and DMA formats using 100 cells from the SK-MEL-28 cell line. The results are illustrated in Figure 18 panel (A) of Figure 18 displays the percentage distribution of sequenced bases from SK-MEL-28 transcripts across various genic components, comparing barcoded cDNA synthesized in tube versus on DMA. The data are shown as mean ± SEM from three technical replicates. The results indicate that the percentage distribution of sequenced bases is nearly identical between the two platforms. Specifically, the average percentage of PCT_coding bases was 19% for the tube method and 18% for the DMA method. This close similarity suggests that both methods are comparable in their ability to capture coding sequences from the SK-MEL-28 transcriptome. However, the DMA method exhibited a distinct advantage in terms of specificity and accuracy for other genic components. For intergenic sequences, DMA detected 20% of the bases compared to 19% detected by the tube method, showing a slight but notable improvement in coverage. For intronic regions, a more significant improvement in coverage was seen with DMA

identifying 24% of the bases compared to 19% by the tube method. Most remarkably, the DMA was able to detect 9% of the ribosomal RNA bases, compared to only 1% with the tube method. This significant difference highlights DMA's ability to quantify ribosomal RNA, which is critical for accurate transcriptome analysis. Therefore, DMA's enhanced specificity likely reduces the background noise and non-specific signals, leading to a more accurate assessment of these less abundant and more challenging regions. Figure 18 A further supports our hypothesis by showing that the number of genes detected by the DMA slide was greater than that detected by the PCR tube. Specifically, DMA detected an average of 14,500 genes, whereas the tube method detected approximately 13,000 genes. This increased gene detection with DMA can be attributed to its superior performance in capturing and processing transcripts, likely due to increased efficiency in enrichment and reduced losses during sample preparation. In addition, a wider range of gene expression may be detected with DMA due to its higher resolution and sensitivity. As shown in Figure 18 C, the sequencing data reveal the percentage of sequenced reads from two technical replicates, both in tubes and on the DMA platform. The technical repeats for cDNA in tubes 1 and 2 showed consistent barcode detection percentages for B1, B2, and B3, while the DMA platform showed similar consistency for barcodes B4, B5, and B6 (Figure 17 C). This consistency across both platforms highlights the reproducibility of our sample preparation methods. Furthermore, the experiment confirmed that the barcodes were accurately detected on both platforms, with identical percentage values for each barcode. (Figure 18 C). This result not only underscores the efficiency of the DMA platform but also its reliability in preventing cross-contamination and maintaining sample integrity across different spots. Additionally, the protocol has been successfully optimized to detect barcodes from samples prepared on a miniaturized, wall-less DMA platform, demonstrating its versatility and applicability in different experimental setups.

3.3.3 DMA Platform for accurate cDNA barcoding: workflow and barcode detection efficiency for human and non-human transcripts
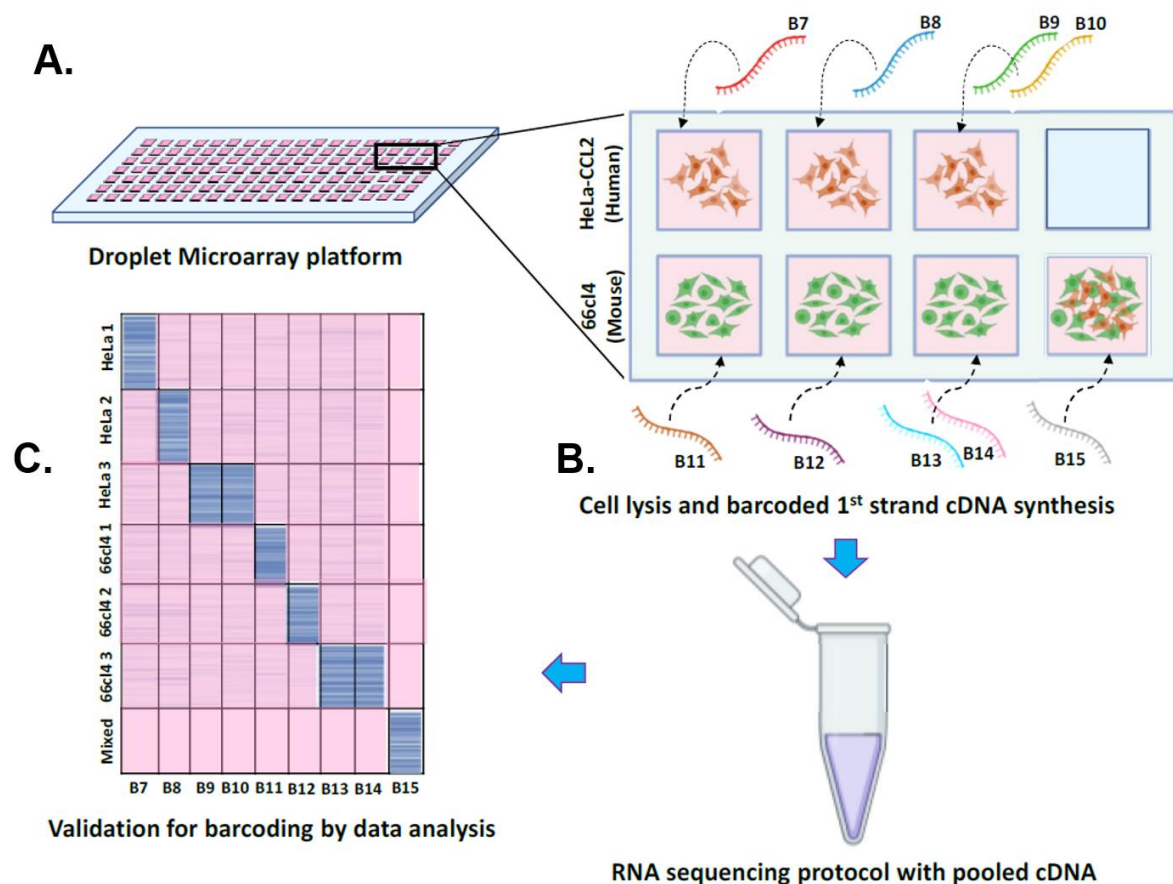

Figure 19. Workflow and Barcode Detection Efficiency from cDNA Barcoded per Spot on DMA from Human and Mouse Transcript Identification

(A) Schematic showing the workflow for identifying human and mouse transcripts through cDNA barcoding on DMA, (B) followed by RNA sequencing of pooled cDNA and subsequent bioinformatics analysis. (C) Percentage of sequenced reads containing cell barcodes in the first read, showing barcode detection results from two technical replicates using DMA and tube methods.

To evaluate the efficiency of our DMA platform and to ensure that there is no cross-contamination between neighboring spots during cDNA synthesis, we designed an experimental workflow as shown in Figure 19 A. On a single DMA slide, we used cell lines of different species in adjacent spots to generate cDNA for RNA sequencing. Specifically, HeLa CCL2 cells, which map to the human genome, were printed in three consecutive spots (each

containing 100 cells) labelled as B7, B8 and a mixture of B9 and B10. Similarly, the mouse cell line 66cl4, which maps to the mouse genome, was printed in different spots - B11, B12 and a mixture of B13 and B14. In addition, we prepared a mixed sample by printing both HeLa and 66cl4 cells in a single spot, barcoded as B15, to demonstrate that our protocol is not biased towards any particular cell line. Details of all barcodes used are given in Table 8.

Although we are still in the early stages of this project and have not yet achieved all the promising results, our primary goal remains to test the non-cross-contamination of sample preparation on DMA using another cell line without any bias, and to perform sequencing by mapping to both human and non-human genomes. However, the results obtained so far, which are not included in this paper, have highlighted several issues that need to be addressed. Firstly, we found that the barcodes used had a difference of only one base pair, which could lead to mis-mapping due to sequence errors. To overcome this, we plan to use more variable barcodes. Second, there was a problem with overlapping genomes between mice and humans, as the organisms are too closely related. To further refine our approach, instead of focusing on the entire genomes where the overlap occurs, we plan to mine the data by targeting known highly abundant human genes and highly abundant mouse genes. By focusing on these specific regions, we will be able to detect the barcodes more accurately between them, ensuring more accurate and contamination-free analysis. To overcome this, we next plan to use a species that is more distant from humans, such as Drosophila, to avoid overlapping genomic regions. However, we encountered a lysis problem when working with different cell lines on the same DMA slide. Specifically, human genes were underrepresented, probably due to incomplete lysis of the HeLa cells compared to other species such as Drosophila. This discrepancy arose because HeLa cells require a longer lysis time, whereas Drosophila cells lyse more easily. Addressing this lysis inconsistency is crucial to ensure accurate representation of human genes in the analysis. We are actively working to resolve these issues and are continuing our experiments with the aim of publishing our findings.

Chapter 4. Summary and Outlook

4.1 Summary

4.1.1 Hydrogel-integrated droplet microarray for enhanced drug sensitivity screening using patient-derived Chronic Lymphocytic Leukemia cells

In this study, we addressed the challenge of investigating DSRT in patient-derived CLL cells. However, patient derived CLL cells are characterized by their tendency to undergo early apoptosis and their difficulty in maintaining viability in conventional in vitro cultures. CLL cells often show a preference for co-culture with supportive stromal cells or the presence of soluble factors, as these conditions can enhance their survival and mimic their natural microenvironment. Our initial experiments in conventional media conditions, lacking these supportive elements, showed significantly low cell viability. This has highlighted the limitations of conventional approaches to the handling of patient-derived CLL cells and the need for alternative methods that better mimic the tumor microenvironment and support the functionality of the cells. We further validated the DMA platform by comparison of DSRT results from the DMA platform with those from conventional MTPs. Despite some differences in drug responses between the two platforms, the DMA showed a convincing correlation with MTP results, confirming its reliability in capturing biological responses comparable to traditional methods. As a result, the DMA platform offers several advantages, including reduced reagent volumes, increased throughput, and cost efficiency, making it particularly valuable for screening large numbers of drugs and patient samples. In order to overcome the limitation of low viability, we have for the first time used a hydrogel-integrated DMA platform for high throughput drug sensitivity screening. Through the integration of patient-derived CLL cells into a hydrogel matrix, we observed a significant improvement in cell viability in comparison to traditional medium conditions. We also investigated the effect of time on cell viability and proliferation. While CLL cell viability decreased over time, hydrogel conditions consistently provided a more favorable environment compared to traditional media. The hydrogel's ability to better mimic the ECM provided critical structural support and a more

stable environment, resulting in an average cell viability of 68% at 24 hours. This improvement is particularly notable given the inherent difficulty of culturing CLL cells and their tendency to thrive in conditions that more closely resemble their natural habitat. Although the exact mechanisms behind the improved viability under hydrogel conditions have not been fully investigated, it is believed that the supportive structure and stable environment of the hydrogel play a critical role in improving cell survival.

Overall, the hydrogel-integrated DMA platform represents a significant advance in functional personalized oncology. It offers a promising tool for high-throughput drug screening by providing a more physiologically relevant environment for patient-derived CLL cells. This approach addresses the limitations of traditional methods and enables more precise, individualized treatment strategies. Future research will focus on further optimizing the hydrogel conditions, investigating the reasons for the improved viability observed in the hydrogel and expanding the applications of the platform. These advances will be critical to improving the precision and efficacy of personalized cancer therapies, ultimately leading to better patient outcomes.

4.1.2 Drug-induced differential gene expression analysis on nanoliter droplet microarrays: enabling tool for functional precision oncology

In conclusion, our study presents a novel approach to drug-induced DGEA that addresses the challenges associated with high-throughput screening and limited cell availability, particularly in the context of patient-derived cancer cells. We have developed a streamlined protocol for DGEA that significantly reduces the amount of reagents required and enables the analysis of minute number of unique patient-derived cells on the DMA platform. We demonstrate the implementation of this protocol on both cell lines and primary patient-derived CLL cells, demonstrating its adaptability and relevance in clinical settings. Importantly, our results show comparative and correlative results between the DMA platform and conventional methods, highlighting the reliability and accuracy of our approach. Furthermore, we provide evidence for the efficacy of the platform by identifying upregulation of key genes, *SYK* and *GADD45β*,

following the treatment of CLL cells with the drug doxorubicin. These results highlight the utility of our optimized protocol in revealing molecular changes associated with drug response, thereby advancing our understanding of cancer biology and facilitating personalized therapeutic strategies in precision oncology. Thus, our research not only introduces a novel methodology for drug-induced DGEA in a miniaturized format, but also highlights its potential for broader applications in a high-throughput manner. The use of a 672-DMA drug library for precision oncology opens the horizon for high-throughput drug-induced DGEA in nanoliter formats from primary patient-derived cells, providing a method for in-depth analysis of molecular changes in unique patient-derived cells upon drug treatment. Following the comparison to the tube protocol, the DMA protocol shows a significant reduction in cell lysis volume from 2.25 µL to 0.2 µL, a reduction of approximately 91%. Similarly, for the reverse transcription mix (Table 10), the volume used per reaction is reduced from 5.1 µL to 0.15 µL (150 nL per spot), resulting in a reduction in reagent consumption across the platforms by approximately 97.06%. We have also significantly reduced the amount of drug required. In this study, doxorubicin was dispensed onto 672 DMA slides at a volume of 1.5 nL per spot, reducing drug consumption by approximately 99% compared to the 384-well plate where the same drug concentrations were prepared at volumes of 2.5 µL per well. In addition, we have significantly reduced the number of cells used. While the 384-well plate used 10,000 SU-DHL-4 cells per well in 22.5 µL of medium, the DMA chip used only 100 SU-DHL-4 cells in medium and 2,000 CLL cells in hydrogel per spot, each requiring only 150 nL of volume. Our results highlight the potential of the DMA chip to perform comprehensive DGEA analysis in a nanoliter format comparable to plates.

4.1.3 Seq-on-a-Chip: multiplexed sample preparation for global transcriptomic analysis in nanoliter reservoirs on droplet microarray

In conclusion, we highlight the development and optimization of a novel Seq-on-a-Chip protocol using the DMA platform for high-throughput global transcriptomic analysis. By miniaturizing the sample preparation process and integrating barcoded oligo-dT primers with UMIs, the DMA platform offers a significant improvement in the efficiency and precision of

RNA sequencing, particularly in scenarios where sample availability is limited or where large-scale screening is required. The study demonstrates that the DMA platform not only matches, but in some aspects surpasses the performance of conventional PCR tube methods in terms of detection, specificity and sensitivity. This is particularly true for the capture of complex transcriptomic features such as intronic and ribosomal RNA sequences. The detailed comparison between DMA slide and PCR tube cDNA synthesis showed that the DMA platform provides comparable, if not superior, transcriptome coverage with the added benefit of reduced reagent consumption and increased throughput. In addition, robust testing of barcode detection efficiency on the DMA platform confirmed the accuracy and reliability of this miniaturized approach, making it a reliable tool for transcriptomic studies. While research is ongoing and some challenges have yet to be fully addressed, such as species-specific lysis issues and cross-mapping between two different species, the results to date are promising. The DMA platform represents a significant advance in high-throughput transcriptome analysis with potential applications in several fields, including drug discovery, cell biology and personalized medicine. Future efforts will focus on addressing the identified challenges and further refining the protocol to fully utilize the potential of this innovative technology, paving the way for more comprehensive and cost-effective transcriptomic studies.

4.2 Outlook

While this work provides valuable insights into personalized oncology using CLL patient-derived cells, it is clear that there are significant avenues for further exploration. A notable advance in this research is the use of the DMA platform, which offers a powerful advantage by allowing experiments to be performed in a nanoliter format. This high-throughput approach not only conserves valuable patient-derived material, but also allows the precise and efficient screening of many conditions simultaneously. Expanding the use of this platform could significantly improve the scalability and applicability of drug susceptibility testing, paving the way for more refined and personalized therapeutic strategies. In the first project, a panel of 33 FDA-approved drugs was screened to identify drug responses in CLL. However, there is considerable potential to broaden the scope of this research by expanding the drug panel to include novel compounds and combination therapies. Such expansion could increase the comprehensiveness of the DSRT and potentially uncover novel therapeutic strategies and more personalized treatment options for CLL patients. In addition to expanding the drug panel, the study highlighted the significant improvement in CLL cell viability when cultured in a hydrogel-based environment compared to traditional medium. This observation raises important questions about the mechanisms underlying this improved survival. Future research should focus on investigating the factors contributing to this phenomenon, including the role of the extracellular matrix, cell-matrix interactions, and potential differences in nutrient diffusion, signaling pathways or mechanical properties within the hydrogel environment. A range of experimental approaches can be used to investigate these aspects, such as analyzing matrix composition, profiling gene expression, investigating key signaling pathways, studying cell-matrix interactions, and assessing nutrient and metabolite profiles. At the same time, our current research efforts are focused on evaluating drug solubility in hydrogel conditions using DMA platform. Understanding how the hydrogel environment influences drug solubility and distribution is critical to optimizing DSRT in this three-dimensional (3D) context. Upon completion of this solubility investigation, DSRT can be extended to patient derived CLL cells cultured in hydrogels, providing a more physiologically relevant model for assessing drug efficacy and resistance. This approach has the potential to reveal differences in drug response that are not apparent in traditional 2D cultures, thereby providing more predictive data for clinical outcomes. Therefore, by expanding the drug panel,

investigating the mechanisms driving hydrogel-specific survival and optimizing DSRT under 3D conditions, this research has the potential to significantly advance personalized medicine approaches for CLL. Integrating these findings could lead to the development of better therapeutic strategies and ultimately improve outcomes for patients with this challenging disease. In the second project, we successfully optimized a protocol for DGEA using the SUDHL4 cell line and demonstrated its applicability to patient-derived CLL cells. By treating both SU and CLL cells with the chemotherapeutic agent DOX, we were able to identify DGEA by qPCR as a proof of concept. This achievement provides a strong foundation for expanding the use of this protocol on DMA's platform. In the future, we aim to extend the application by performing DGEA on a larger drug library, which will allow the identification of additional genes and biomarkers associated with drug response. Such expansion could provide deeper insights into the molecular mechanisms of drug action and resistance, paving the way for more personalized therapeutic strategies. Furthermore, the potential of this protocol extends beyond DGEA. By integrating next-generation sequencing, we can delve deeper into the molecular profiling of individual patients. This approach would allow us to gain a comprehensive view of the genetic landscape and transcriptional changes in response to drug treatments. The ability to correlate molecular profiles with drug sensitivity or resistance could lead to the identification of novel therapeutic targets and predictive biomarkers, thereby increasing the precision of CLL treatment. Another promising direction is to validate the protocol on other types of patient-derived cells. In particular, those that are available in very limited quantities. The miniaturized nature of the DMA platform makes it ideal for such applications, as it requires fewer cells than traditional plate-based methods while maintaining robust and reproducible results. Demonstrating the effectiveness of the DMA platform in these contexts could highlight its versatility and utility in personalized medicine, particularly for rare or difficult-to-obtain patient samples. In addition, exploring the use of this protocol in various other cancer types or even non-malignant diseases could further broaden its applicability. Similarly, application of the protocol to cells from solid tumors or non-cancer diseases with limited cell availability could demonstrate the potential of the platform in different research and clinical settings. Briefly, by expanding the drug library, incorporating sequencing for detailed molecular profiling, and testing the protocol on various patient-derived cells of limited availability, this project has the potential to significantly advance the

field of personalized medicine. The versatility and scalability of the DMA platform, coupled with its ability to generate meaningful data from minimal cell input, make it a powerful tool for translational research and precision oncology. In the third project, there remains significant potential for further refinement and development. Currently, we are in the process of validating our protocol for barcode detection from synthesized cDNA on the DMA platform versus traditional tube-based methods. This validation involves testing across various spots to precisely map each species to its corresponding genome, such as mapping Hela cells to the human genome. Additionally, we aim to extend this barcode detection protocol to patient-derived samples following drug treatment on the DMA platform. This would enable us to accurately track and analyze treatment responses at a molecular level. Furthermore, a key objective is to perform a pathway-based analysis of the differentially expressed genes (DEGs) from CLL patient-derived cells after drug incubation. This analysis will provide crucial insights into the cellular pathways affected by the treatment, thereby enhancing our understanding of drug action in a personalized oncology context. By integrating this approach with the Seq-on-a-Chip protocol on the DMA platform, we move closer to achieving personalized drug screening that is both high-throughput and highly specific.

The DMA platform may also open up a number of other exciting opportunities in the field of personalized oncology. For example, the miniaturization of organ-on-a-chip systems on the DMA platform could provide a more physiologically relevant environment for drug testing that better mimics in vivo conditions. In addition, the platform's versatility allows a wide range of biological questions beyond oncology, such as cellular interactions, to be explored. By taking advantage of these innovative applications, future research on the DMA platform holds great promise for advancing personalized medicine and contributing to broader biological discovery.

Chapter 5. Appendix

5.1 Hydrogel-integrated droplet microarray for enhanced drug sensitivity screening using patient-derived Chronic Lymphocytic Leukemia cells
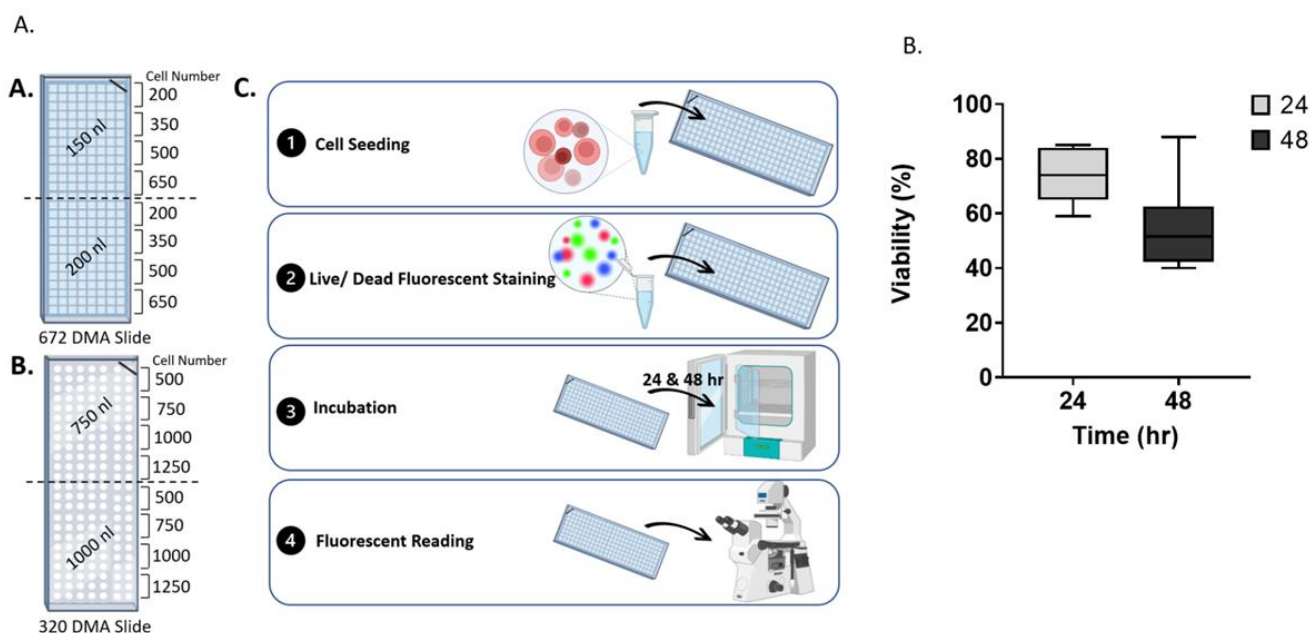

Figure A 1.: Differential CLL viability assessed using varying cell numbers across two volumes (150 and 200 nL) on the 672-DMA and 320-DMA platforms (750 and 1000 nL), as well as in a 384-well plate, following 24 and 48 hours of incubation.

(A) Cell numbers ranging from 200 to 650 cells per 150 and 200 nl volumes were dispensed onto a 672 DMA slide using a mechanical dispenser. (B) Cell numbers ranging from 500 to 1250 cells per 750 and 1000 nl volumes were seeded on a 320 DMA slide. (C) The following steps were carried out: (1) Cells were seeded onto the DMA slide. (2) Live/dead fluorescent dye (Hoechst, calceinAM, and PI) was applied for staining. (3) The seeded DMA slide was incubated for 24 and 48 hours. (4) Fluorescent images were captured using a Leica Microscope. (B.) Assessing the viability of 4,800 patient derived CLL cells after 24 and 48 hr of incubation in 384-well plates.
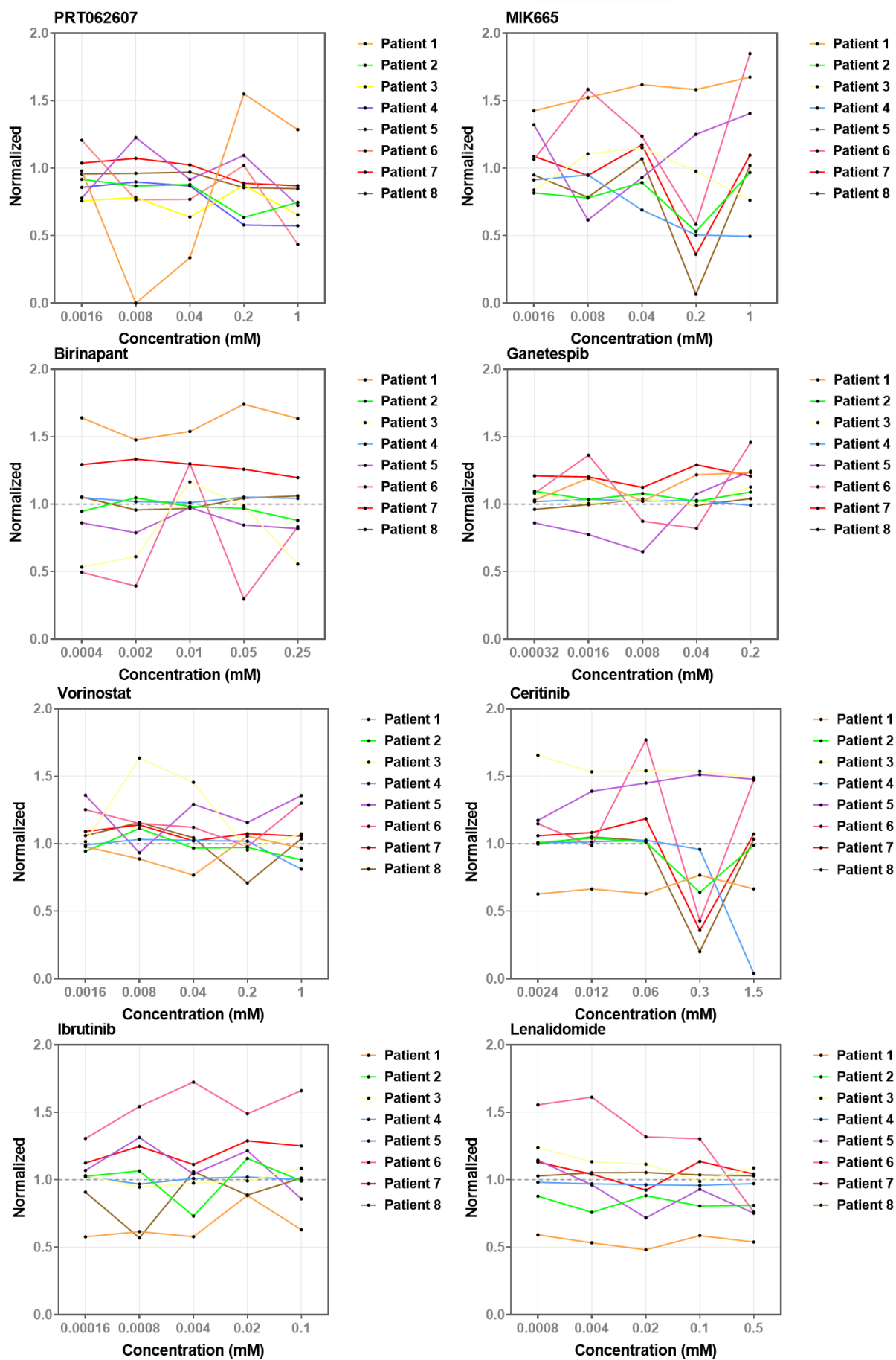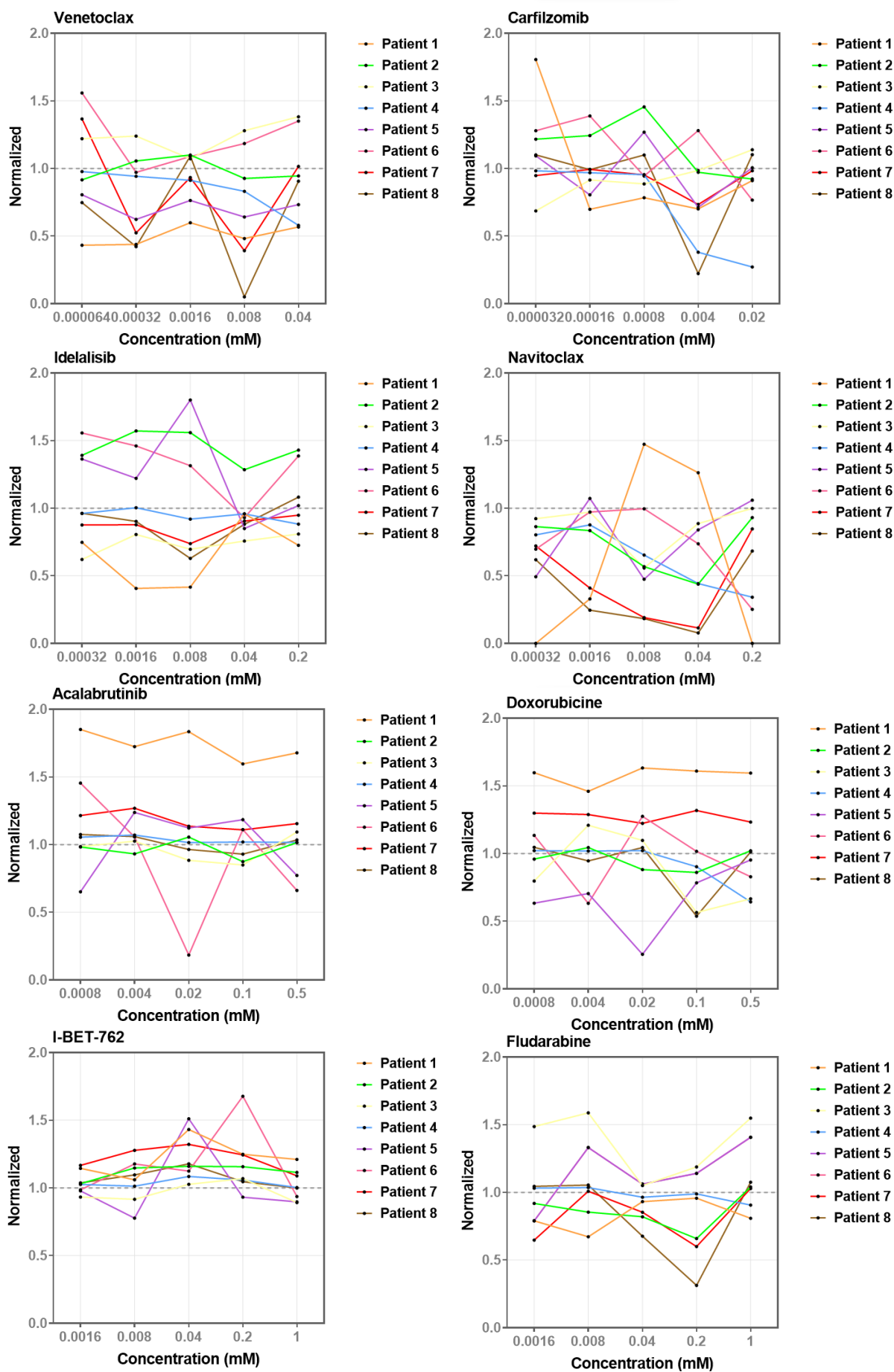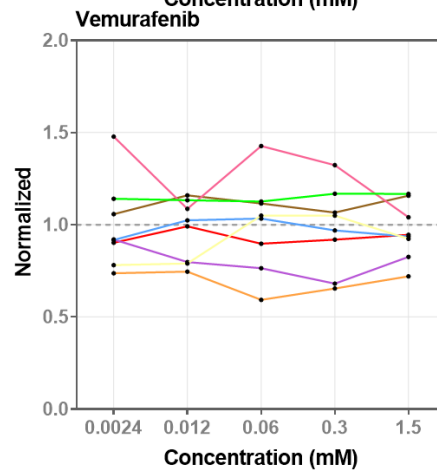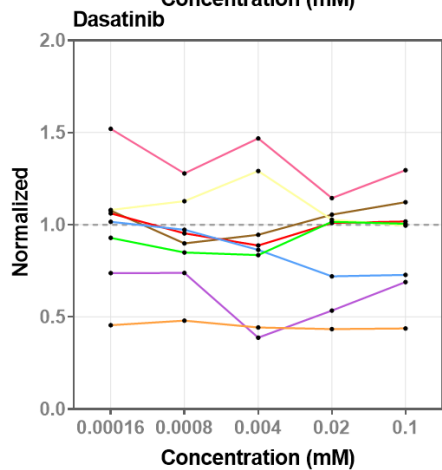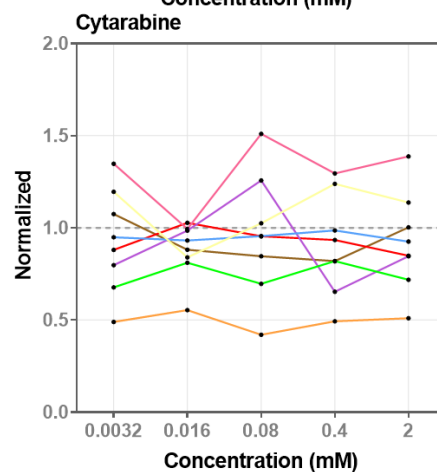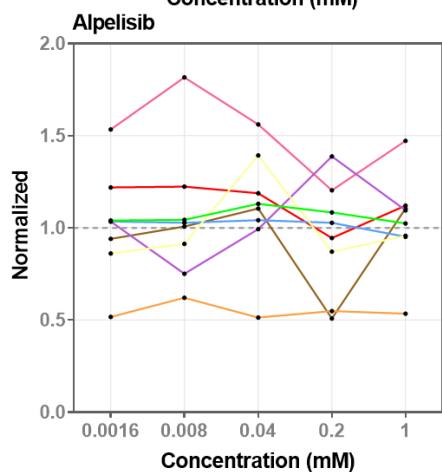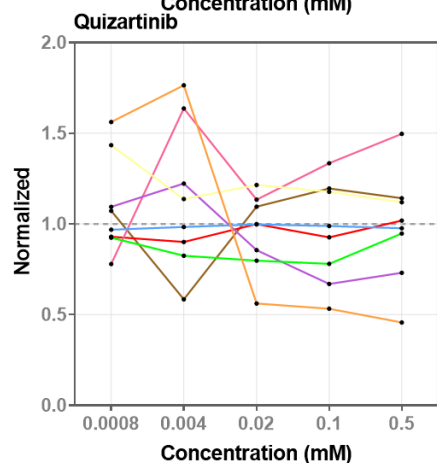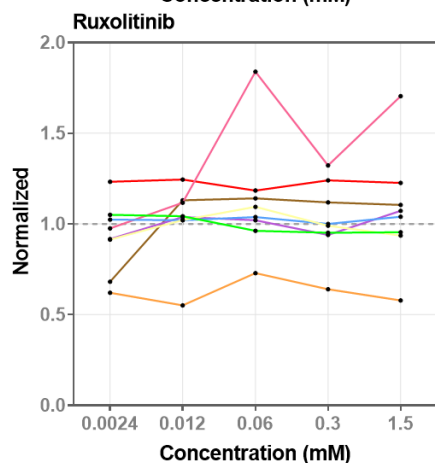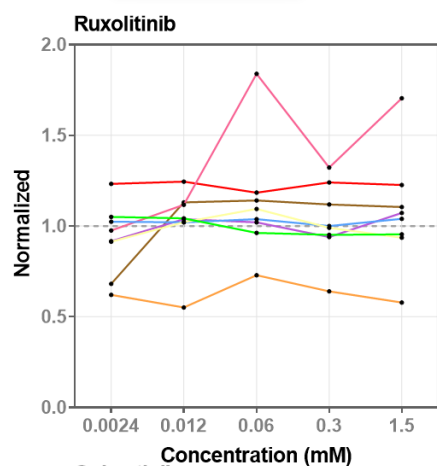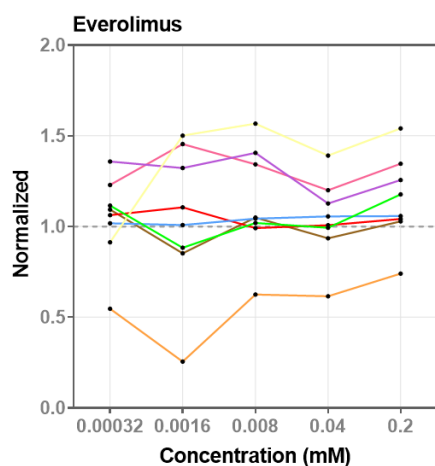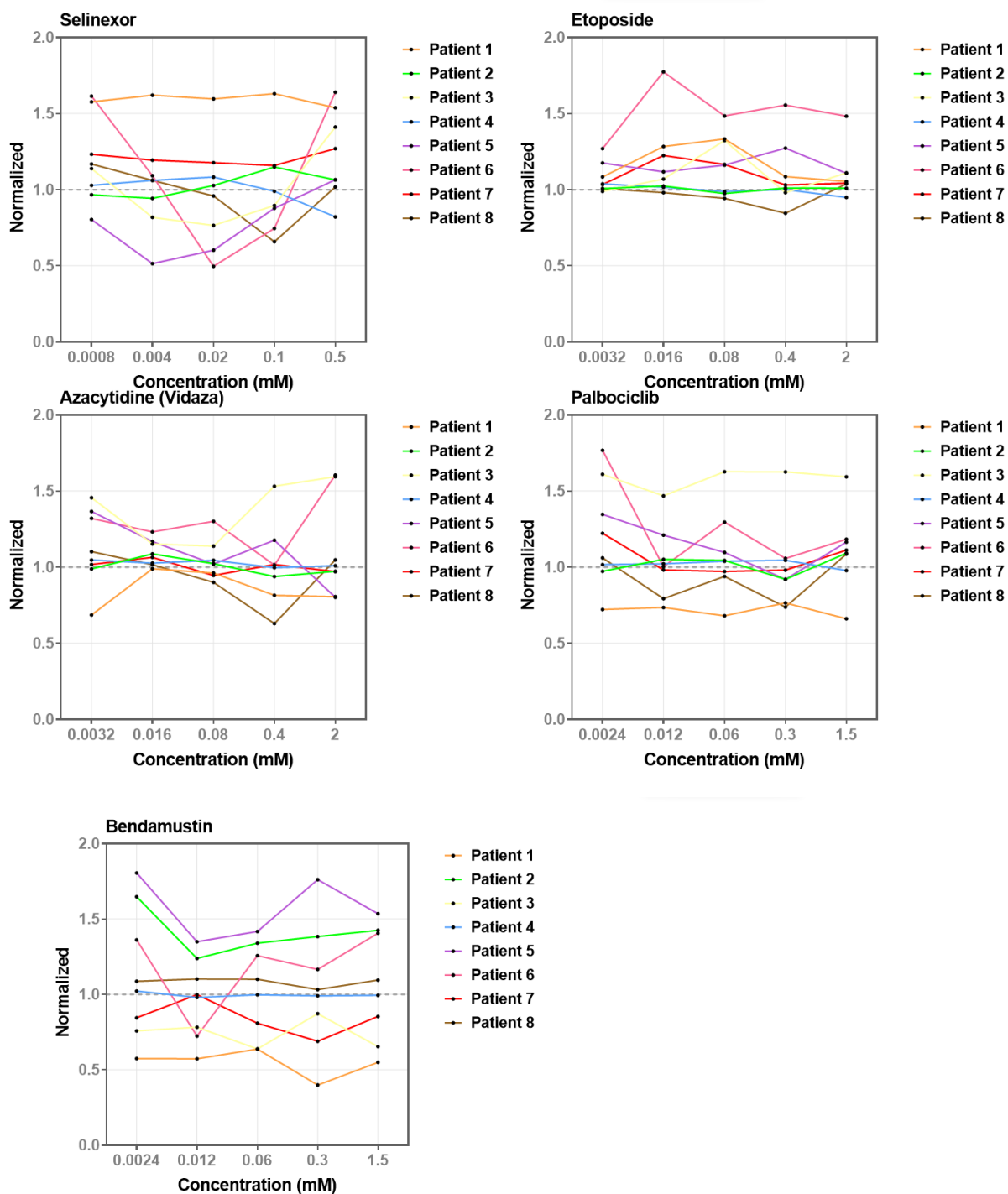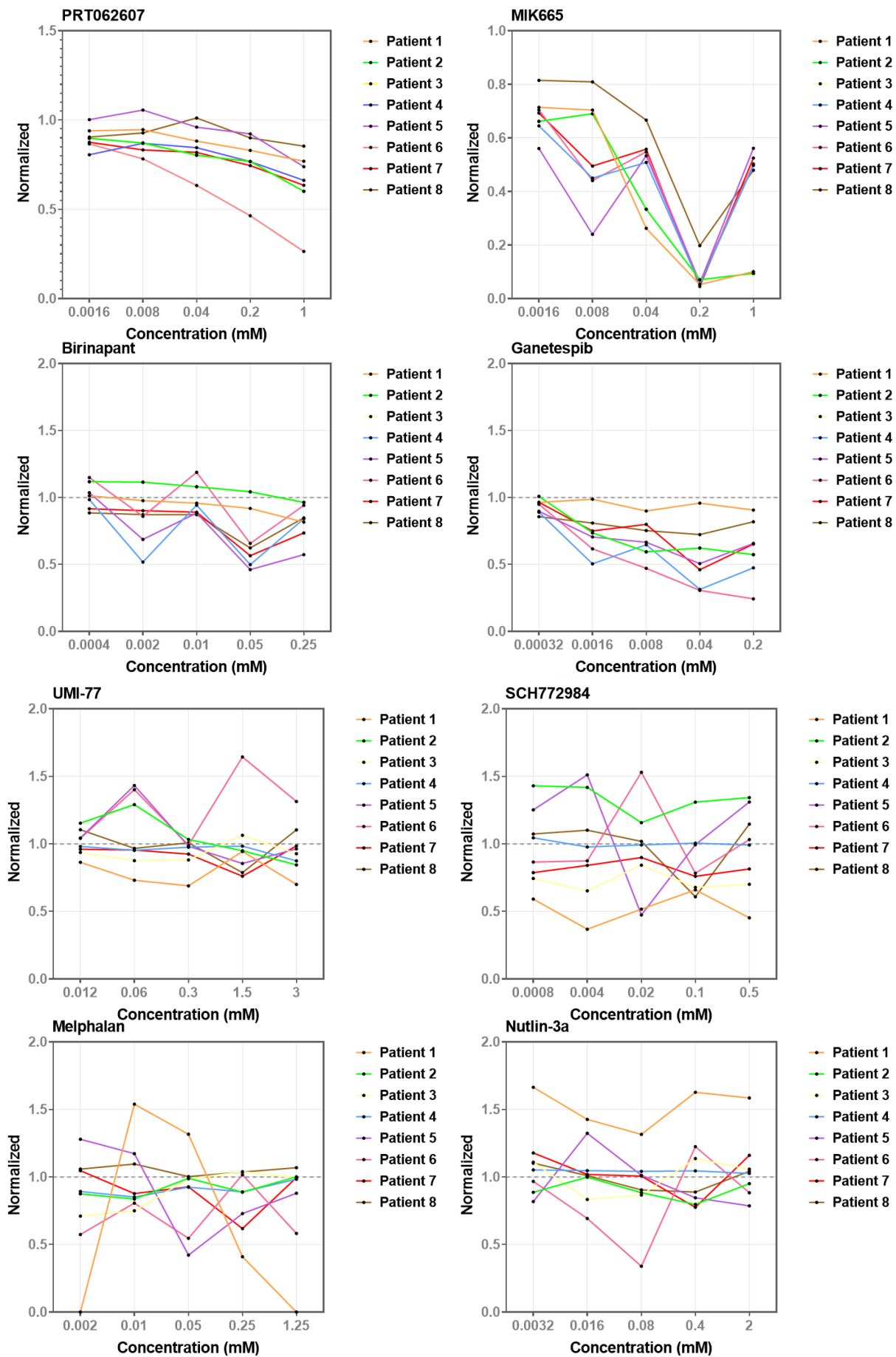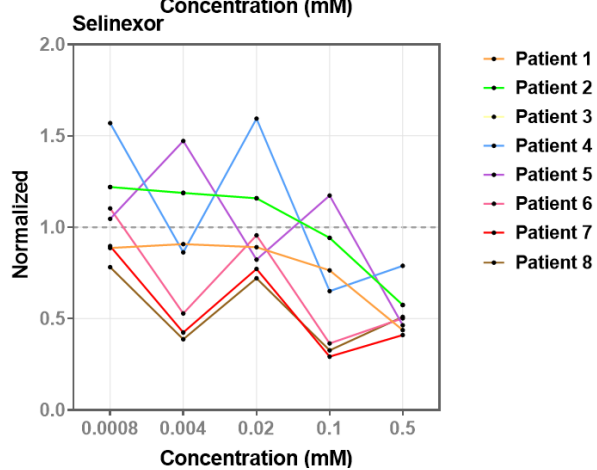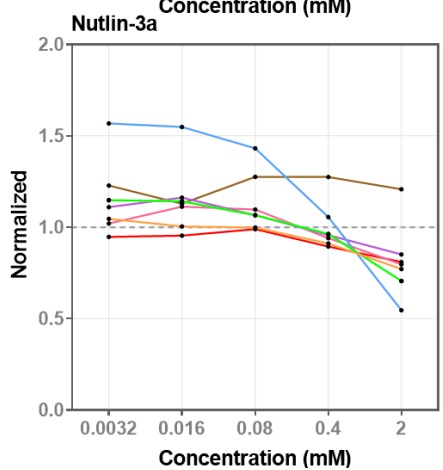
Figure A 2.: Normalized Viability of Patient-Derived CLL Cells on the 672-DMA Slide 33-Drug Library

The graphs illustrate the normalized viability results for a 33-drug library tested across different patient-derived CLL cells using the 672-DMA slide platform.
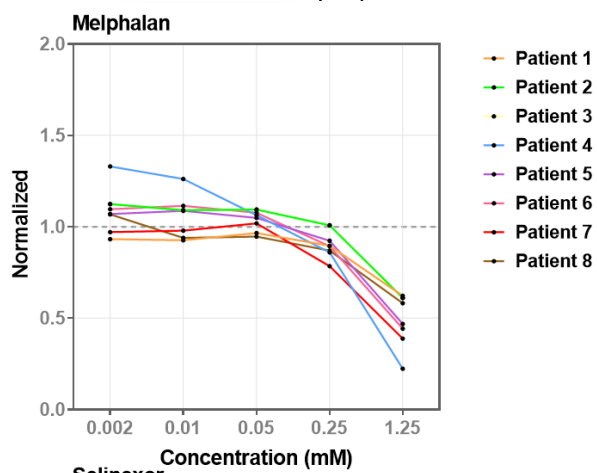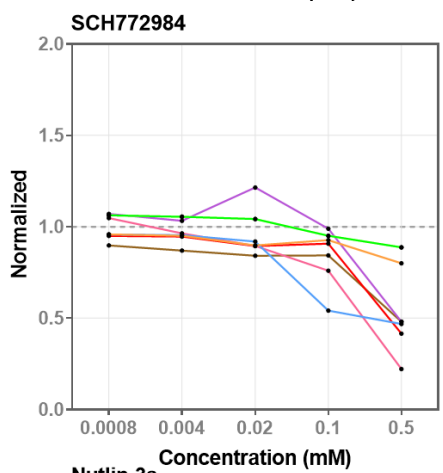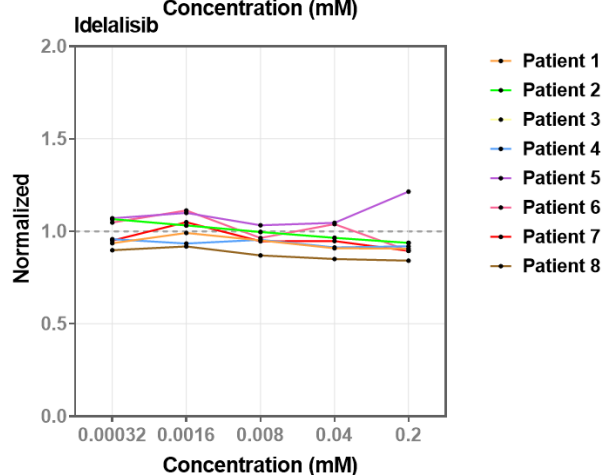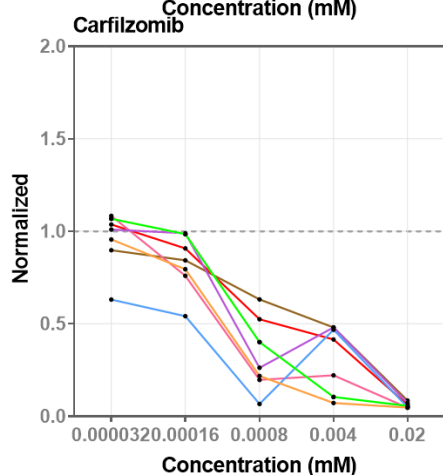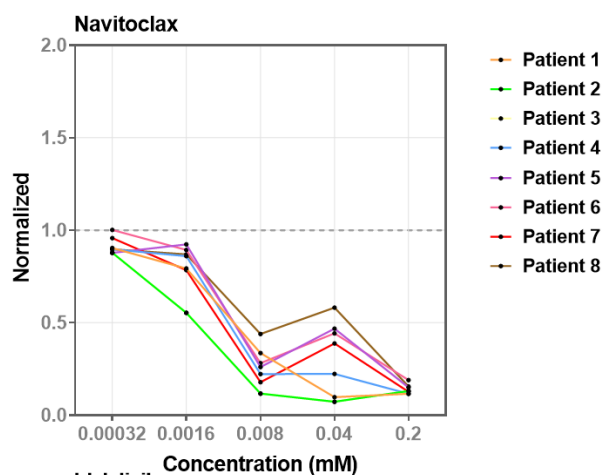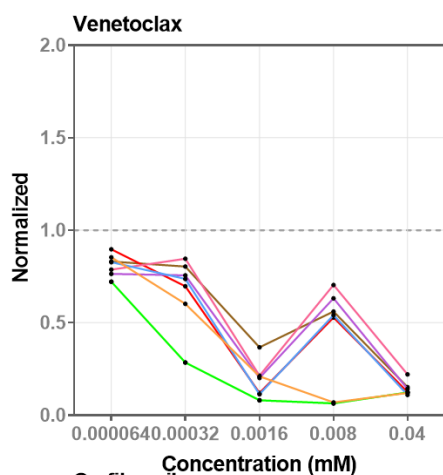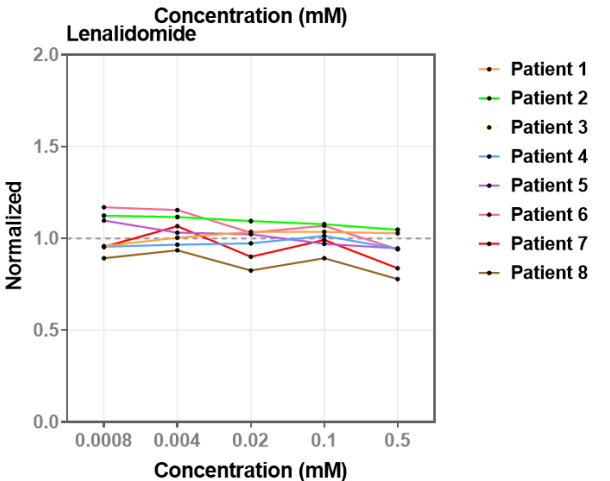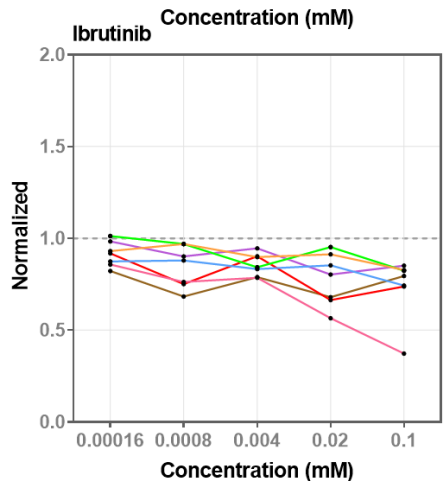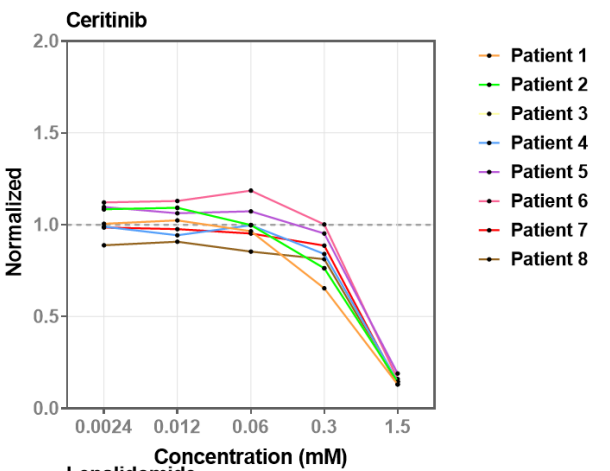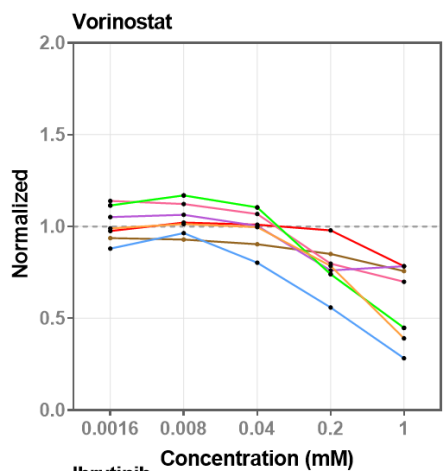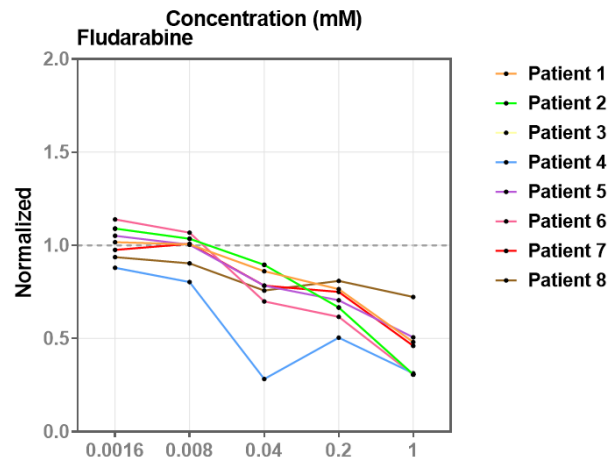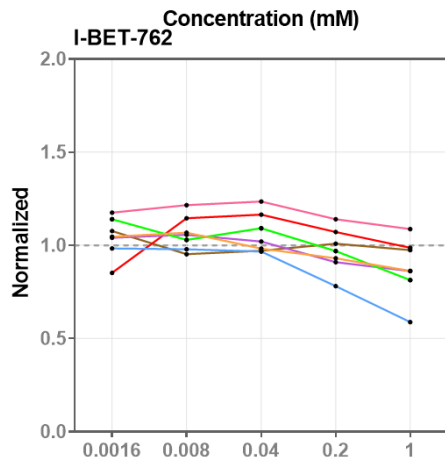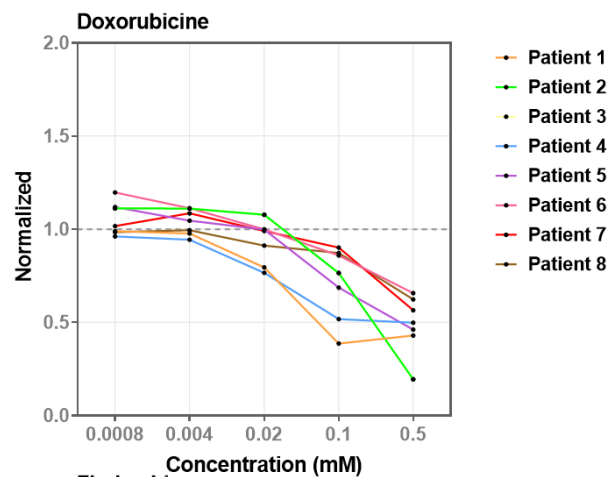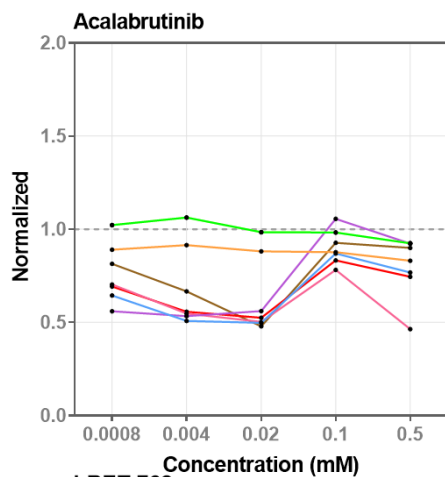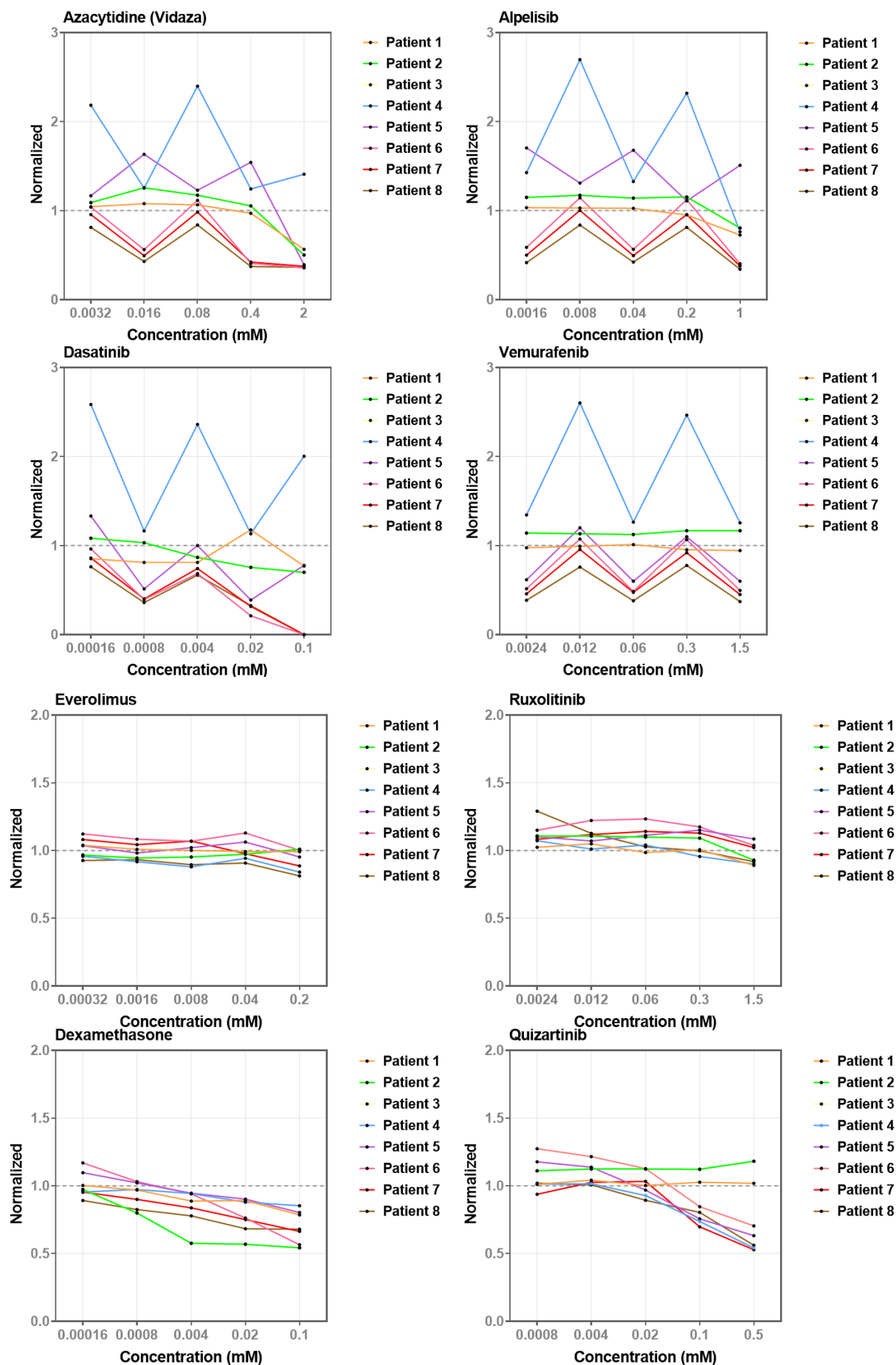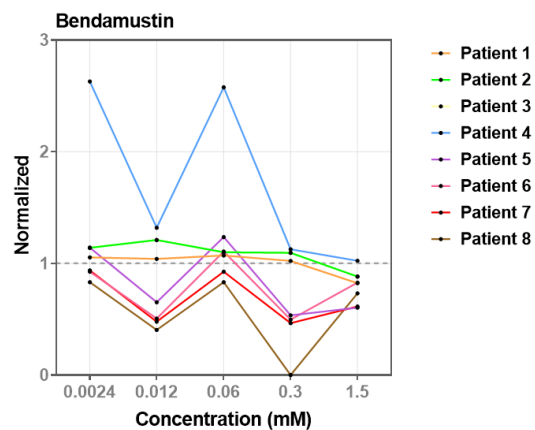
Figure A 3.: Normalized Viability of Patient-Derived CLL Cells in 384-well plate on the 33-Drug Library

The graphs illustrate the normalized viability results for a 33-drug library tested across different patient-derived CLL cells using the 672-DMA slide platform
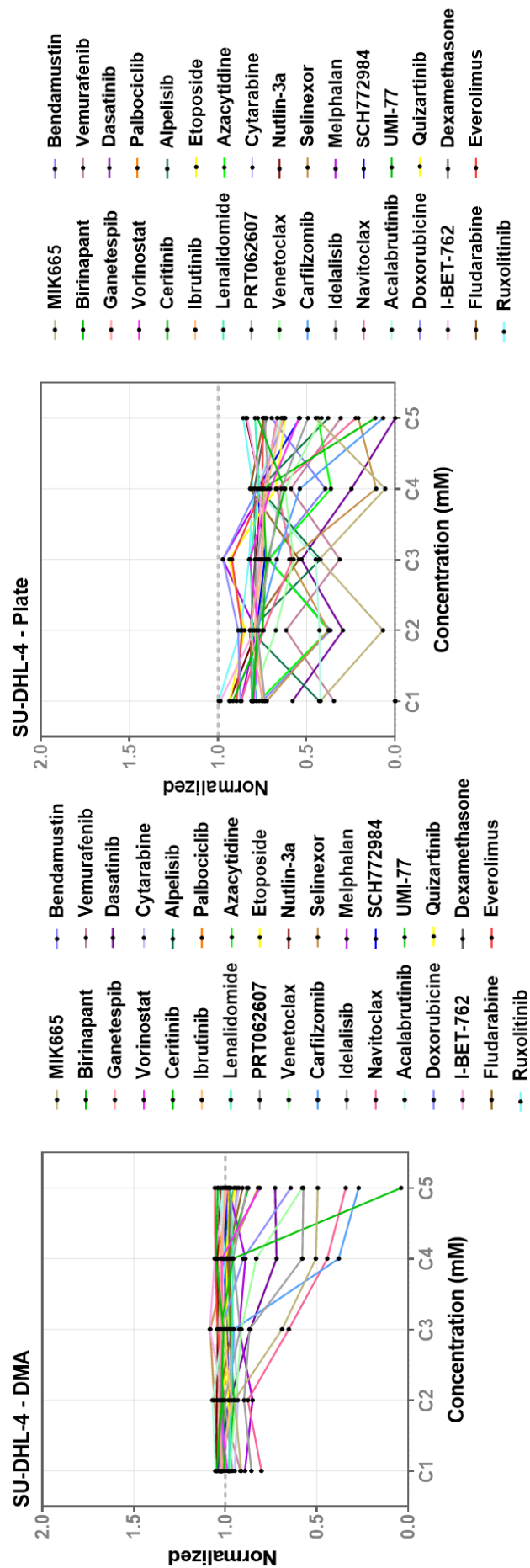
Figure A 4.: Normalized Drug screening Viability of SU-DHL-4 Cell Line in Both DMA and 384-well Plate tested 33-Drug Library

The graphs illustrate the normalized viability results for a 33-drug library tested using SU-DHL-4 cell line across 2 different platforms: 672-DMA slide vs. 384-well plate.
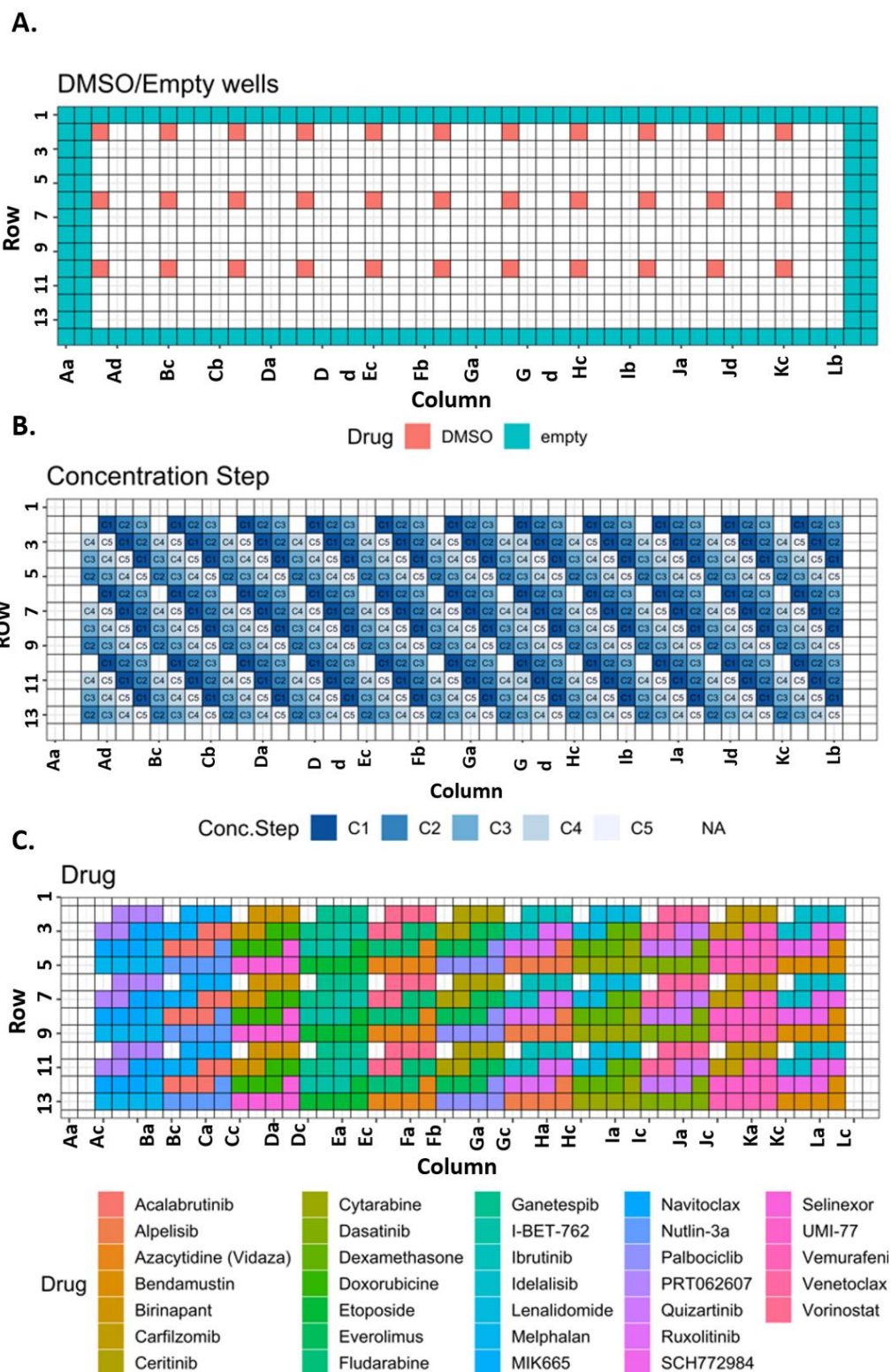
Figure A 5.: 672- DMA 33 drug library schematic

(A) Identification of the position of each drug on the DMA slide. (A) Placement of DMSO control on the DMA slide. (B) Organization of the 5 different concentrations for each drug on the 672 DMA slide. (C) 22 drugs randomly printed on DMA

135
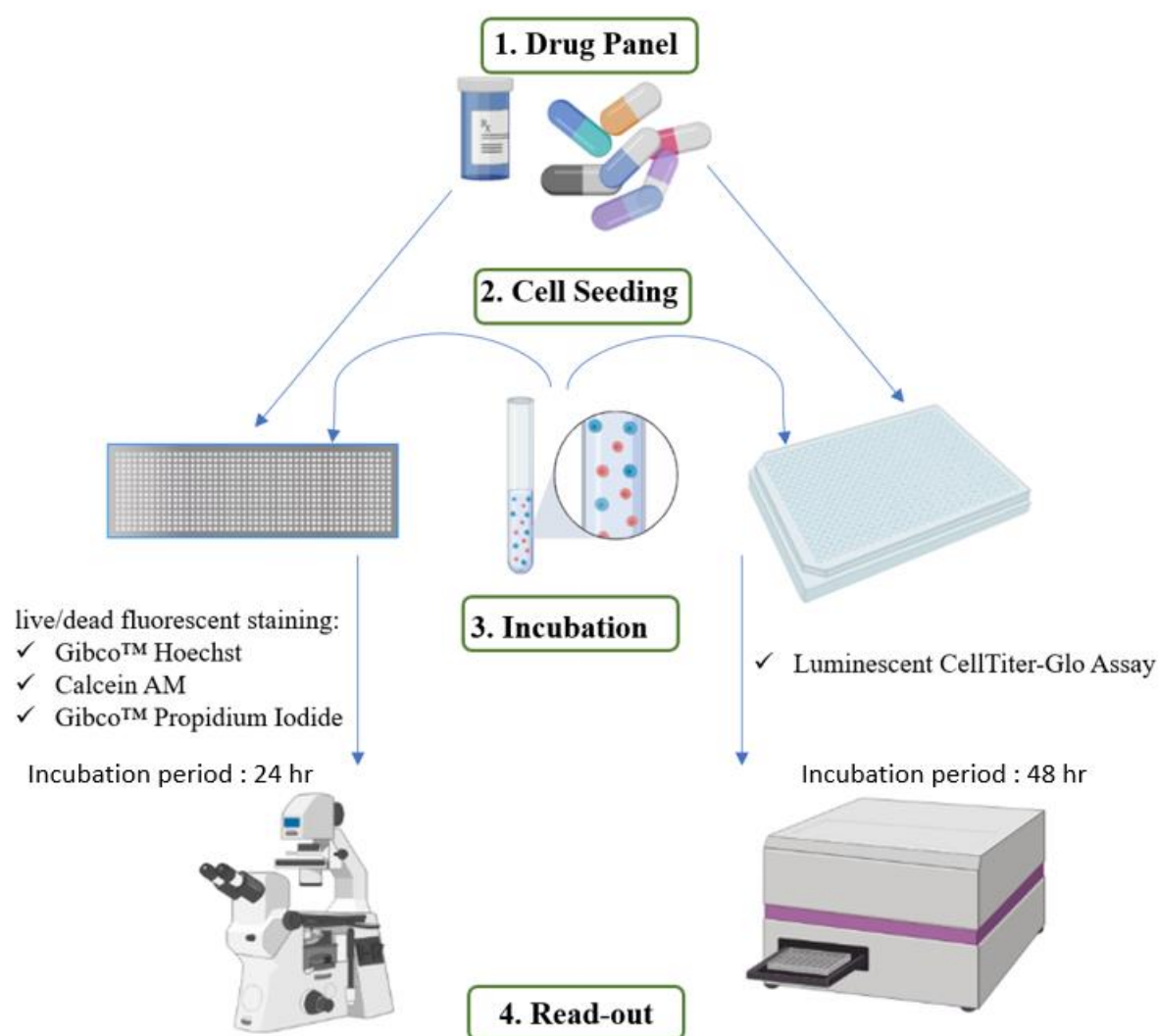
Figure A 6.: Screening of patient derived CLL cells on DMA and microtiter plates.

(A.) Experimental Workflow for Drug Screen: The drug library dispensing process takes place both on 672 DMA slides and in 384-well plates. On DMA slides, a total of 33 drugs are preprinted using an automated dispenser. In parallel, within wells, 33 drugs are dispensed using a pipette. Each drug condition is meticulously replicated three times. 500 CLL cells are dispensed per spot on DMA slide, and 10,000 CLL cells are pipetted per well in 384-well plate. Subsequent steps include a 24-hour incubation period for all conditions. Following this incubation, the DMA library undergoes fluorescent live/dead staining with Hoechst, Calcein, and PI. The staining procedure is accompanied by an additional 30-minute incubation period, with subsequent result read-out. Simultaneously, the Cell Titer-Glo assay is conducted within a 384-well plate, with each well containing the drug-treated samples. This assay is followed by an extra 20-minute incubation period before the final read-out.
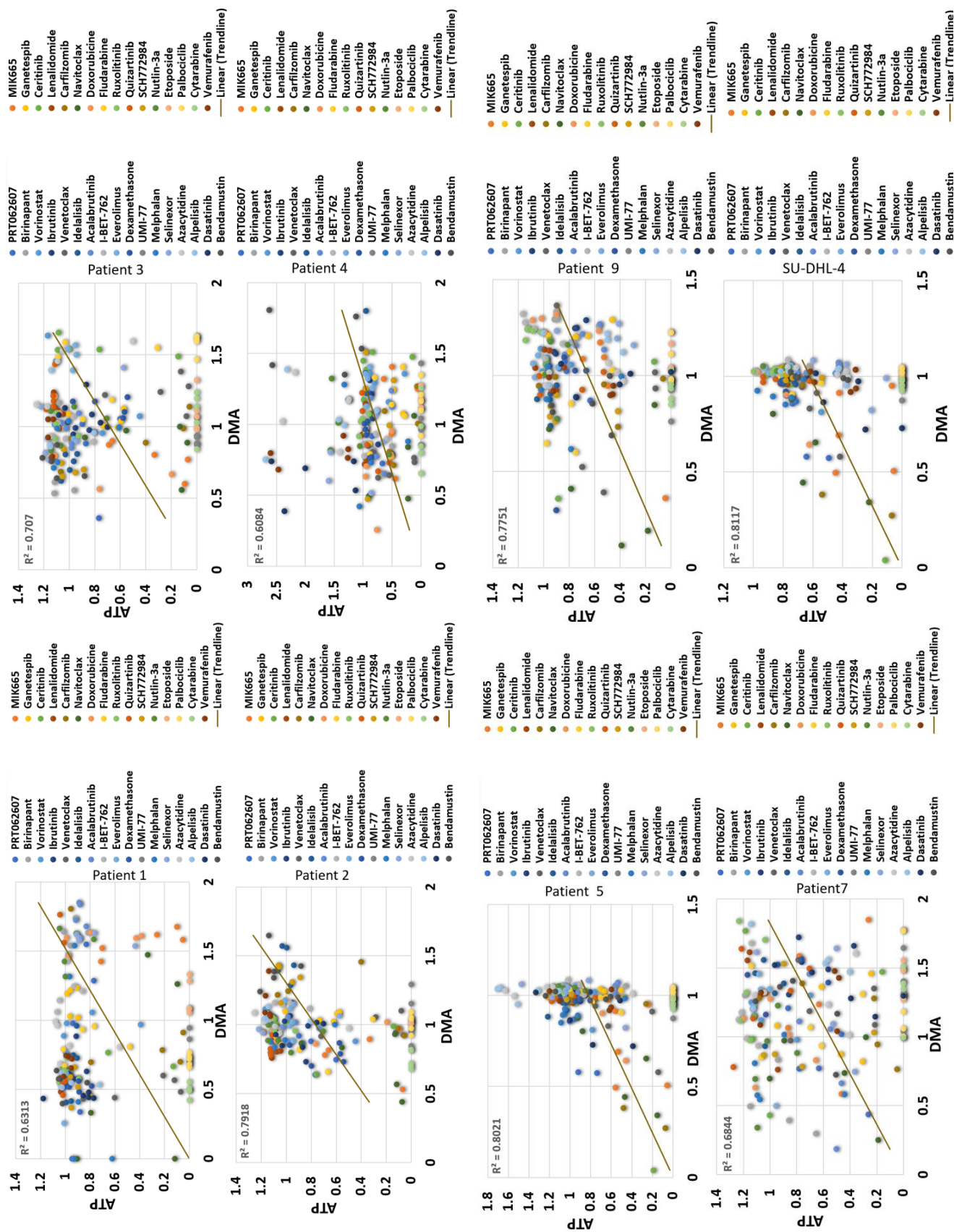
Figure A 7.: Correlation analysis of normalized viability between Microtiter Plates in ATP and the DMA slide across different CLL patients and their investigation of 33 distinct drugs. This work was conducted by Annika Strauß at Karlsruhe institute of technology, Germany.
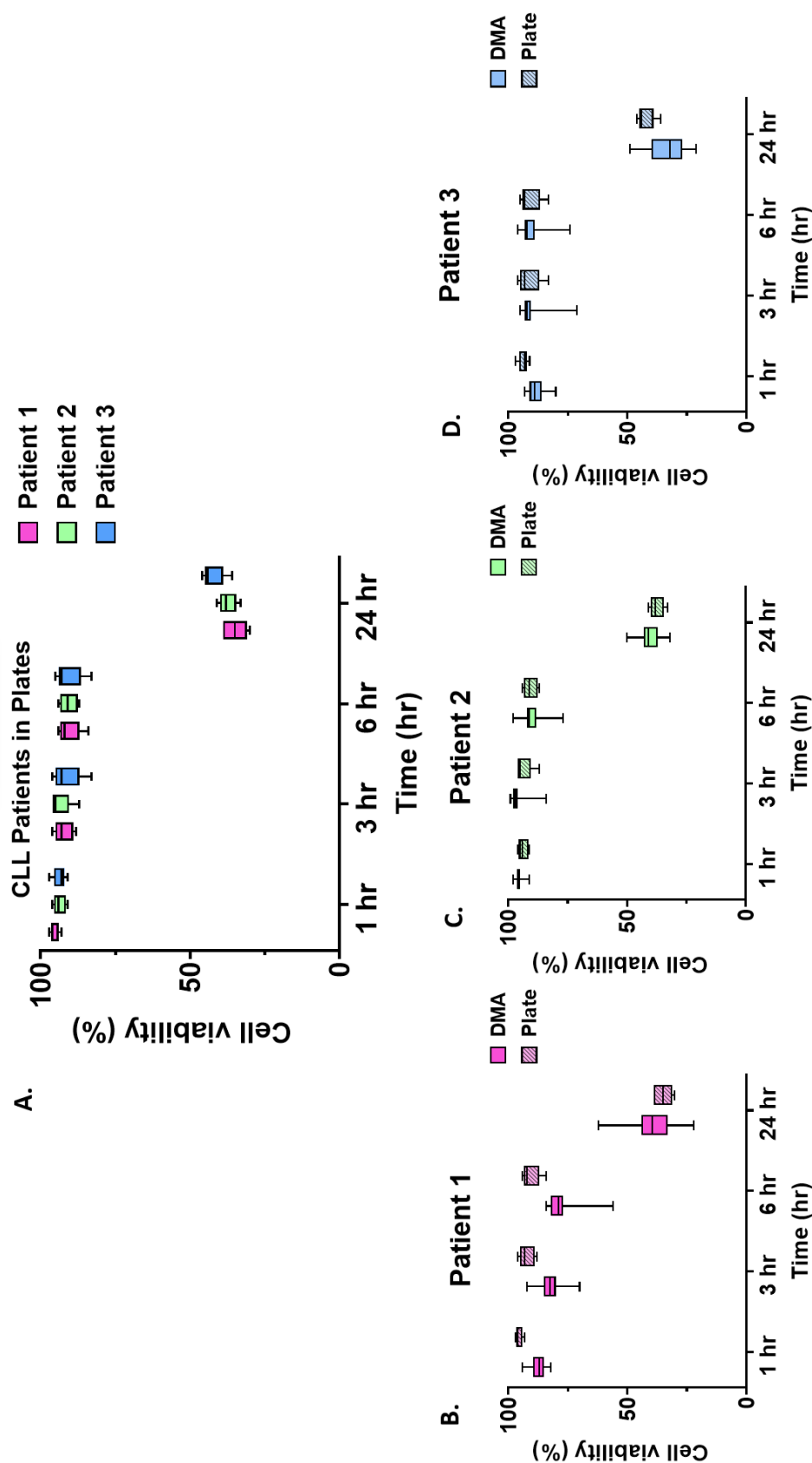
Figure A 8. Cell viability (%) from three CLL patient-derived cells cultured on 672-DMA vs. 384-well plates under various incubation times in standard medium conditions

(A) percentage viability estimated from 3 different CLL patients tested in 384-well plate (B) Comparative analysis for patient 1, (C) Patient 2 (D) Patient 3. showing similar trends across 1, 3, 6, and 24 hours of incubation on both DMA and plates.
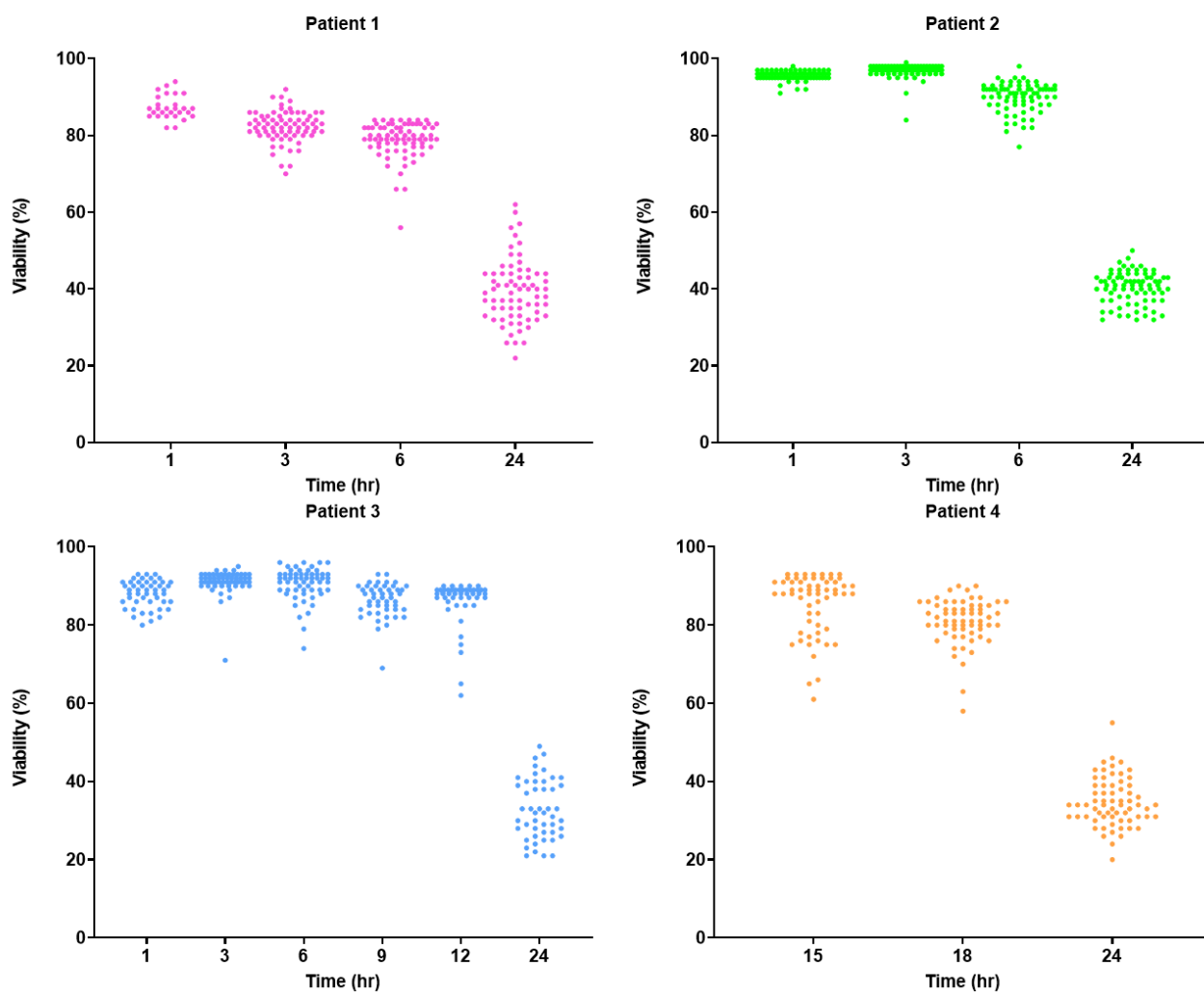
Figure A 9.: Cellular Viability of patient derived CLL cells from 4 different patients cultured in medium at varying incubation times (in hr) cultured on 672 DMA slide.
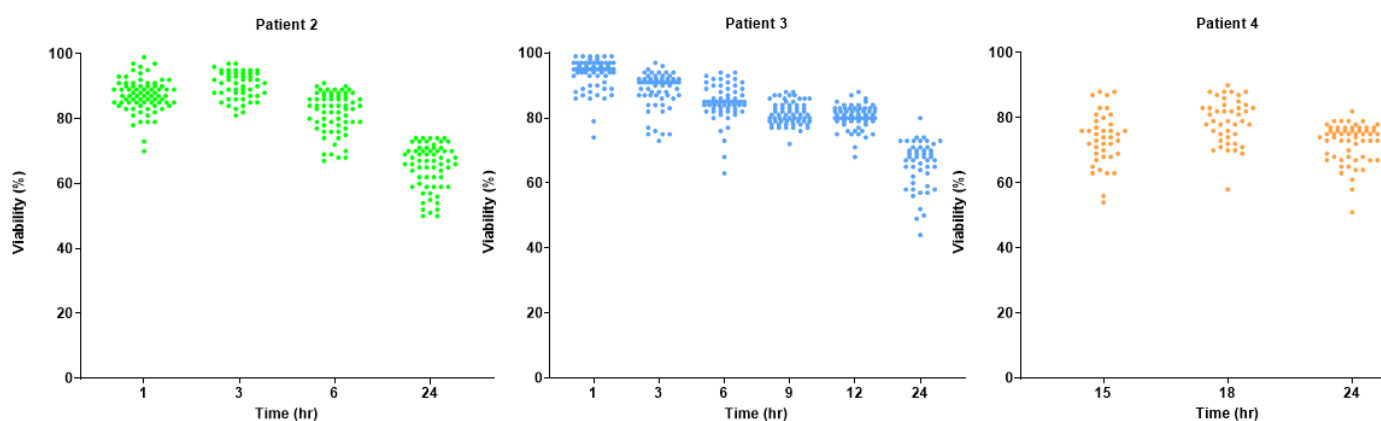
Figure A 10.: Cellular Viability of patient derived CLL cells from 3 different patients cultured in hydrogel at varying incubation times in hours cultured on 672 DMA slide.

Table A 1.: Cell counts and corresponding concentrations (cells/mL) for droplets with volumes of 150 nL, 200 nL, 750 nL, and 1000 nL.

Cells per 150nL droplet	Cell concentration per mL
200	$1,3x10^6$
350	$2,33x10^6$
500	$3,3x10^6$
650	$4,33x10^6$
Cells per 200 nl droplet	**Cell concentration per mL**
200	1x106
350	1,75x106
500	2,5x106
650	3,25x106

Cells per 750nL droplet	Cell concentration per mL
500	6,7x105
750	6,7x105
1000	6,7x105
1250	1,7x106
Cells per 1000nL droplet	**Cell concentration per mL**
500	5x105
750	7,5x105
1000	1x106
1*250*	1,25x106

5.2 Drug-induced differential gene expression analysis on nanoliter droplet microarrays: enabling tool for functional precision oncology

# Cells	Sample name	Lysis on DMA			Mean Cq	Cq SEM	Nucleic Acid(ng/uL)
		Proteinase K (50 °C)	heat inactivation (80°C)	RNAse inhibitor			
100 cells	Tube control	10 min	10 min	yes	15.12	0.0227	20.042
100 cells	DMA A	30 min	30 min	no	24.67	0.0348	32.858
100 cells	DMA B	23 min	22 min	no	20.31	0.0283	16.826
100 cells	DMA C	10 min	10 min	no	21.08	0.124	13.623
100 cells	DMA D	20 min	10 min	yes	30.21	0.0256	14.6935
100 cells	DMA E	30 min	10 min	yes	16.71	0.0573	28.49
100 cells	DMA F	40 min	10 min	yes	18.21	0.01846	16.721
100 cells	DMA G	15 min	12 min	no	31.96	0.153	12.6423333
200 cells	DMA H	15 min	12 min	no	30.15	0.1123	11.9873333
400 cells	DMA I	15 min	12 min	no	29.76	0.0924	12.4086667
400 cells	Tube I `	10 min	10 min	yes	9.46	0.0193	64.2196667
200 cells	Tube H '	10 min	10 min	yes	10.03	0.0248	55.3793333
100 cells	Tube G'	10 min	10 min	yes	11.17	0.0825	38.5525

Figure A 11.: Mean Cq Values Across Various Conditions: Optimizing Cell Lysis Protocol on DMA.

A bar graph illustrates the mean Cq value of the *GAPDH* housekeeping gene using different samples prepared on the DMA platform with varying conditions. Each sample is prepared in triplicate for technical repeats. Error bars represent the standard error of the mean (SEM).
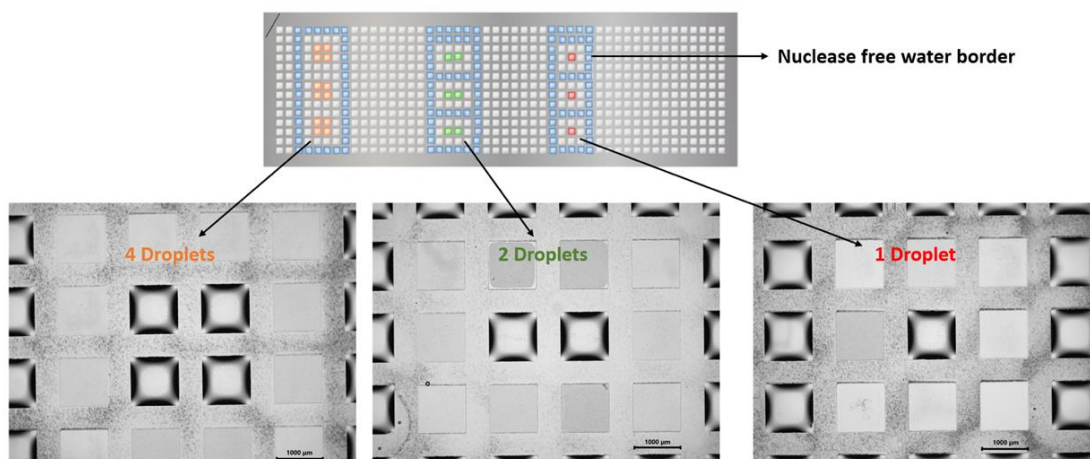
Figure A 12.: DMA slide layout for cell printing

Schematic representation of the pattern layout on a DMA slide, illustrating the arrangement of cells printed in droplets. Each spot contains a total of 100 cells, with 4 droplets equating to 400 cells, 2 droplets equating to 200 cells and 1 droplet equating to 100 cells. Nuclease-free water (NFW) is applied around the SU-DHL-4 cell spot to ensure adequate humidity.
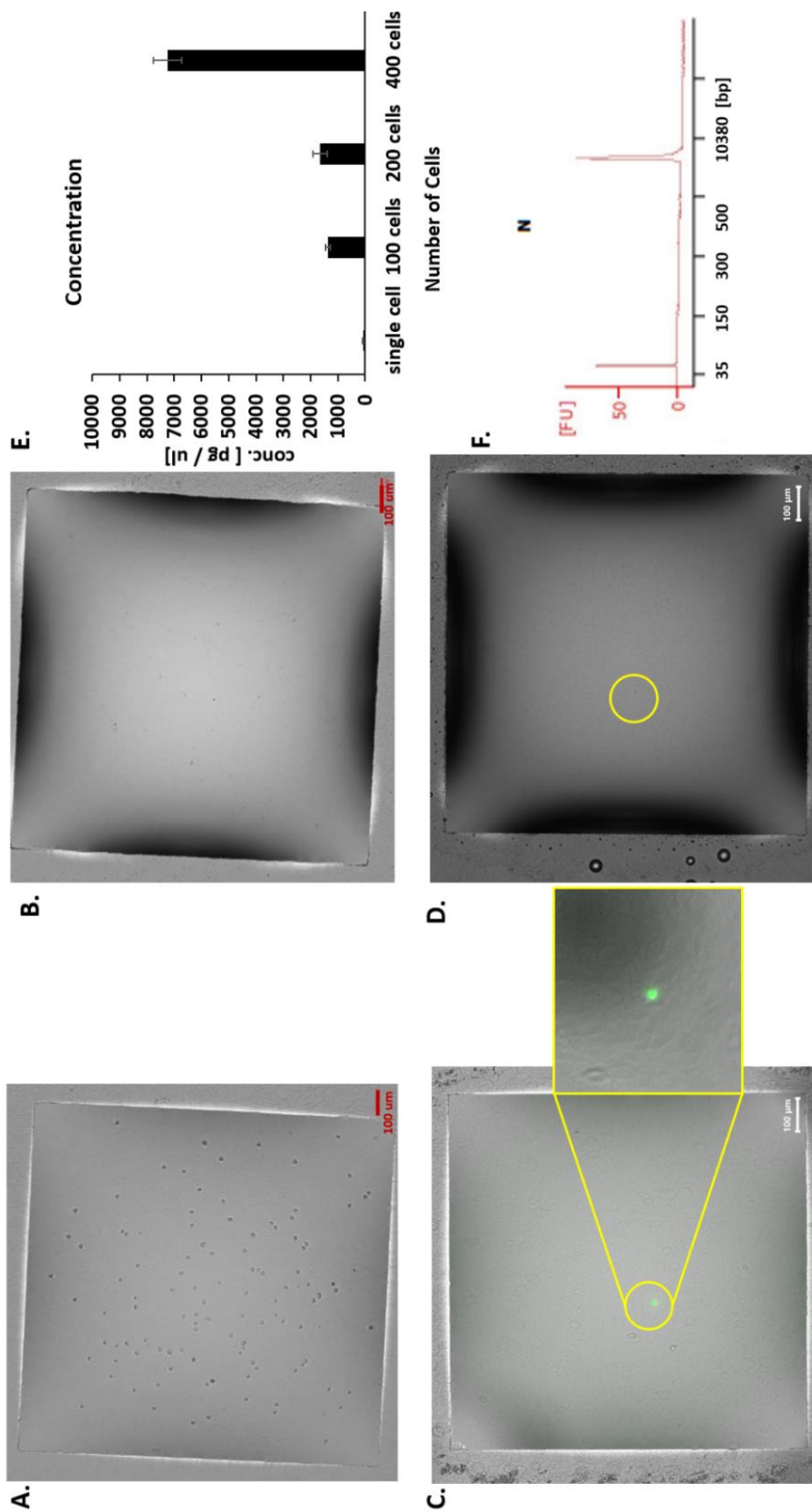
Figure A 13.: Cell printing, lysis and cDNA concentration analysis

(A) One hundred SU-DHL-4 cells were printed and checked using a Keyence-BZ-X810 microscope (x10 magnification) before the lysis step. (B) In the same spot, after the lysis step, the one hundred SU-DHL-4 cells were lysed. (C) A single cell, stained with Calcein AM dye, is shown within the center of a 1 mm × 1 mm droplet, as indicated by the yellow circle and magnified 20x. The cell exhibits a fluorescent signal due to the Calcein AM staining. (D) The single cell was then subjected to lysis, and a 10x image was taken post-lysis. (E) A bar graph illustrates the cDNA concentration (pg/μL) as the number of SU-DHL-4 cells used increases, from a single cell to 400 cells. Error bars represent the mean ± SEM with n = 3. (F) An electropherogram shows the Bioanalyzer results of a negative control. No template (no cells) was used during sample preparation.
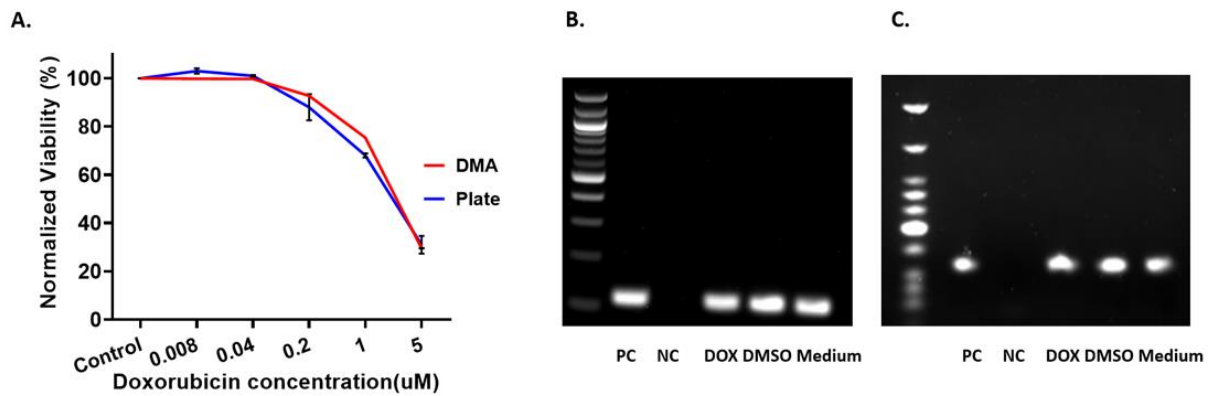
Figure A 14. Comparative analysis of SU-DHL-4 cell viability and *GAPDH* expression in response to DOX treatment.

(A.) Normalized viability (%) of SU-DHL-4 cells after treatment with DOX drug at different concentrations ranging from 5 uM to 0.008 uM. Comparison between DMA vs. plate. Error bars represent the mean ± SEM with n = 3. (B.- C.) Gel electrophoresis analysis of *GAPDH* expression in samples including positive control (PC), negative control (NC), DOX, DMSO and medium from plates and DMA respectively.
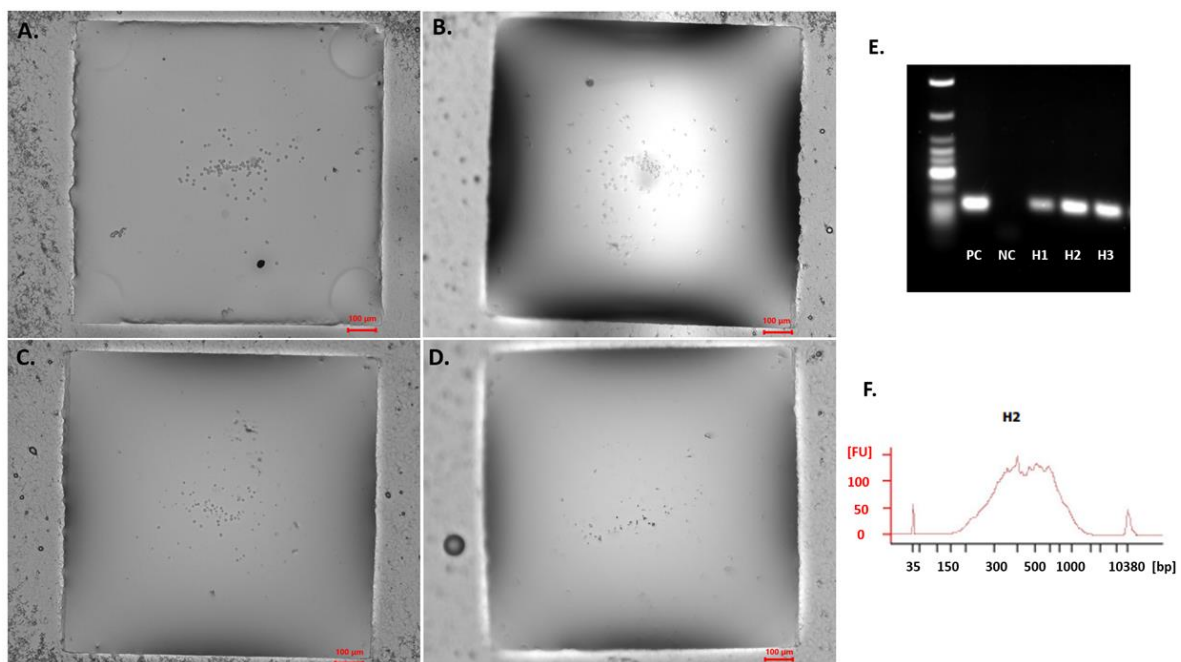
Figure A 15.: Sample preparation in hydrogel on a DMA slide

(A) Representation of 100 cells printed in the hydrogel mixture before solidification, observed under the Keyence-BZ-X810 microscope (x10 magnification). (B) The condition after solidification, followed by printing in RPMI medium for 24 hours incubation. (C) After the initial lysis step, the cell membrane integrity remains relatively rigid. (D) After an additional lysis step, the cells show complete lysis, indicating the loss of cell membrane integrity. (E) Gel electrophoresis results for cDNA synthesized in hydrogel in 3 technical replicates showing the *GAPDH* PCR product. The 'PC' lane represents the positive control, while the 'NC' lane is the negative control without template. Panels (H1), (H2) and (H3) show 3 technical replicates of samples prepared in hydrogel. Lane 1 corresponds to the 1 kb DNA ladder. (F) Qualitative assessment of the synthesized cDNA prepared on the DMA slide using the Agilent 2100 Bioanalyzer with High Sensitivity DNA Analysis Kit.
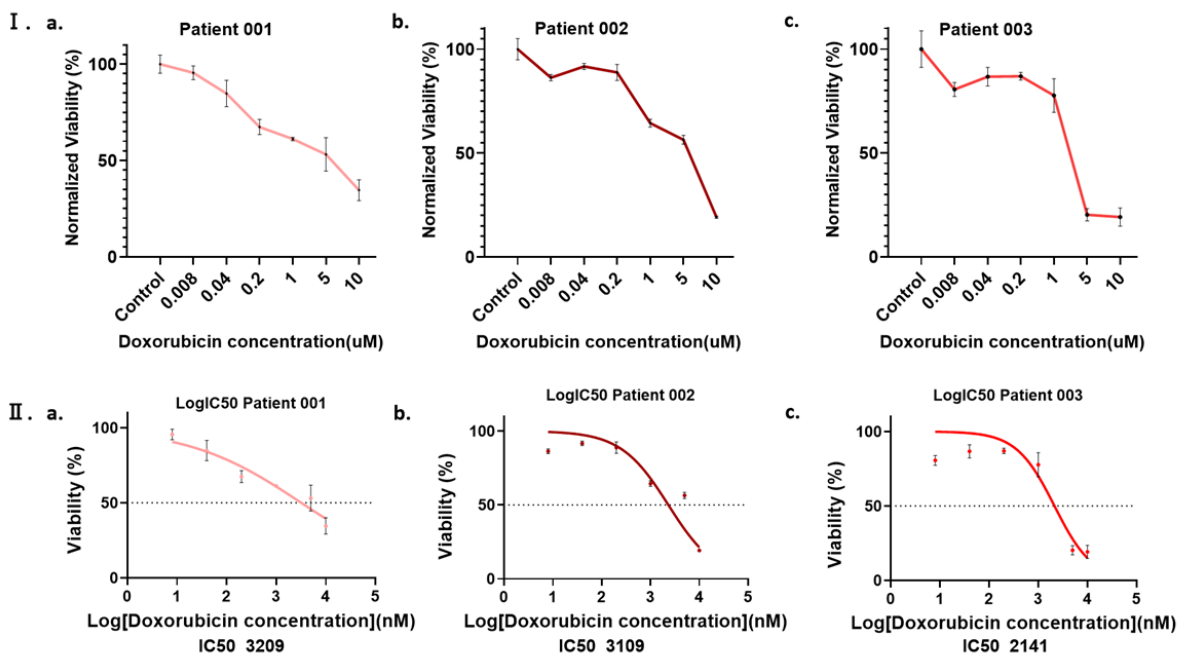
Figure A 16. Comparative Evaluation of DOX Drug Sensitivity for 3 Patient-Derived CLL Cells on DMA slide

(I) Normalized viability evaluation for 3 different patient-derived CLL cells (2,000 cells per spot) treated on the DMA slide with different drug concentrations ranging from 10 uM to 0.008 uM. Panels (a), (b) and (c) represent responses from 3 different CLL patients. (II) IC50 plots for the same three patients, illustrating the concentration at which 50% inhibition of cell viability occurs upon DOX treatment. Subpanels (a), (b) and (c) correspond to individual patient responses and provide insight into the variation in drug sensitivity between CLL patients. Error bars represent the mean ± SEM with n = 3.
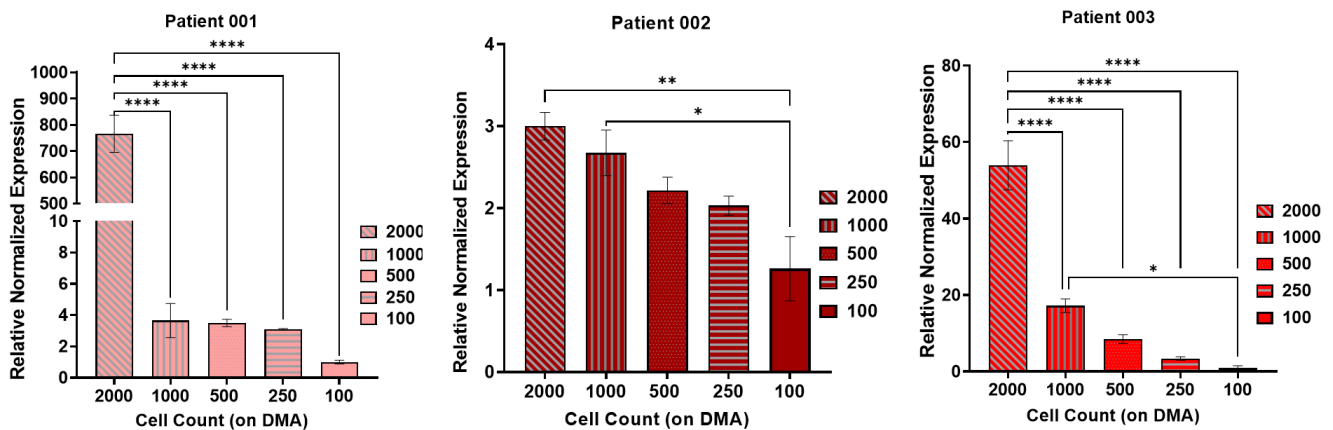
Figure A 17. Evaluation of the Relative Gene Expression of the Housekeeping Gene *GAPDH* in Different Cell Counts of CLL Patient-Derived Cell

The plots illustrate the expression levels across different cell counts (2000 cells down to 100 cells) in Tube and similarly on DMA prepared from three different CLL patients. The data provide insight into the effect of cell count and sample preparation method on the relative expression of the housekeeping gene *GAPDH*. Statistical analysis

revealed significant differences (p < 0.05) between cell numbers and sample preparation methods. Error bars represent the mean ± SEM with n = 3.
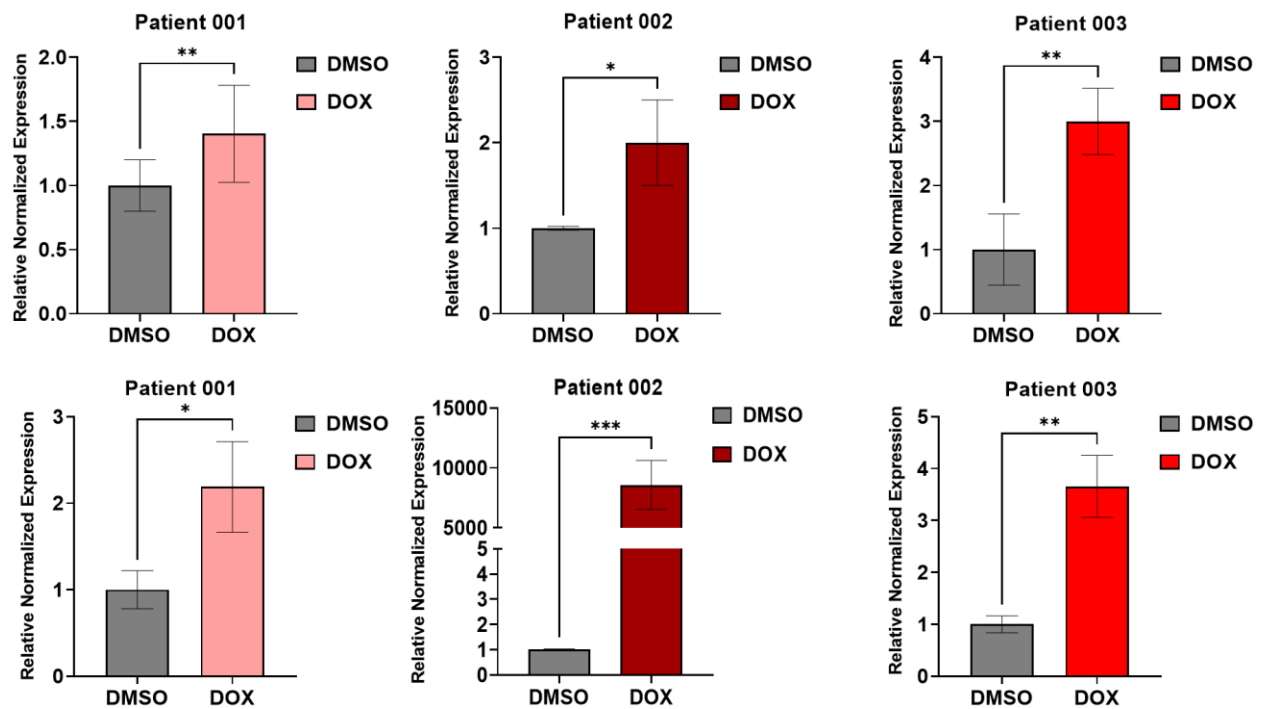
Figure A 18. Evaluation of Relative Gene Expression of *SYK* and *GADD45β* Genes using qPCR

The plots show the effect of 1 uM DOX drug treatment on the expression levels of SYK and GADD45β genes in CLL cells from three different patients, providing insight into the molecular response of CLL cells to DOX treatment and highlighting potential variations between individual patient samples. Statistical analysis revealed significant differences (p < 0.05) between cell counts and sample preparation methods. Error bars represent the mean ± SEM with n = 3.

References

1. Popova, A.A.S., S. M.; Demir, K.; Ueda, E.; Nesterov Mueller, A.; Levkin, P. A.;, Droplet-Array (DA) Sandwich Chip: A Versatile Platform for High-Throughput Cell Screening Based on Superhydrophobic-Superhydrophilic Micropatterning. Advanced Materials, 2015. 27(35): p. 5217-22.

2. Chakraborty, S., et al., "Cells-to-cDNA on Chip": Phenotypic Assessment and Gene Expression Analysis from Live Cells in Nanoliter Volumes Using Droplet Microarrays. Advanced Healthcare Materials, 2022. 11(12): p. e2102493.

3. Neto, A.I., et al., Fabrication of Hydrogel Particles of Defined Shapes Using Superhydrophobic-Hydrophilic Micropatterns. Advanced Materials, 2016. 28(35): p. 7613-9.

4. Bertram, J.S., The molecular biology of cancer. Molecular Aspects of Medicine, 2000. 21(6): p. 167-223.

5. The biology of cancer, Part 2. Seminars in Oncology, 1989. 16(3): p. 169-262.

6. Siegel, R.L., A.N. Giaquinto, and A. Jemal, Cancer statistics, 2024. CA: A Cancer Journal for Clinicians, 2024. 74(1): p. 12-49.

7. Seyfried, T.N. and L.C. Huysentruyt, On the origin of cancer metastasis. Critical Reviews in Oncogenesis, 2013. 18(1-2): p. 43-73.

8. Tachikawa, T. and M. Mori, Structural and molecular aspects of cancer invasion and metastasis. Medical Electron Microscopy, 1999. 32(1): p. 1.

9. Waldum, H.L., et al., Classification of tumours. Journal of Experimental & Clinical Cancer Research, 2008. 27(1): p. 70.

10. *, M.B.D., et al., Chapter 6 - Human Papillomavirus (HPV): Diagnosis and Treatment, ed. A.S. Ashish S. Verma. 15 November 2013, Animal Biotechnology. 95-120.

11. Hall, F., V. Villalobos, and B. Wilky, Future directions in soft tissue sarcoma treatment. Current Problems in Cancer, 2019. 43(4): p. 300-307.

12. Bispo, J.A.B., P.S. Pinheiro, and E.K. Kobetz, Epidemiology and Etiology of Leukemia and Lymphoma. Cold Spring Harbor Perspectives in Medicine, 2020. 10(6).

13. Union, S.O.o.t.E. Causes of death statistics 2023.

14. OECD. EU Country Cancer Profile: Germany 2023. EU Country Cancer Profiles 2023.

15. Global Cancer Observatory, International Agency for Research on Cancer. Cancer Today: Data Visualization Tools for Exploring the Global Cancer Burden [cited 2024 21/10/2024]; Available from: https://gco.iarc.fr/today/en/fact-sheets-populations#groups.

16. Delrose, N., Histological Type Cancer Classifications, in Biorender. 2019: National Cancer Institute. Cancer Classification / SEER Training.

17. Martin, T.Y., L. ; Sanders, AJ., Cancer Invasion and Metastasis: Molecular and Cellular Perspective., In: Madame Curie Bioscience Database

18. Hanahan, D. and R.A. Weinberg, Hallmarks of cancer: the next generation. Cell, 2011. 144(5): p. 646-74.

19. Hanahan, D. and R.A. Weinberg, The hallmarks of cancer. Cell, 2000. 100(1): p. 57-70.

20. Abreu Velez, A.M. and M.S. Howard, Tumor-suppressor Genes, Cell Cycle Regulatory Checkpoints, and the Skin. North American Journal of Medical Sciences, 2015. 7(5): p. 176-88.

21. Vogelstein, B.K., W., Cancer genes and the pathways they control. Nature Medicine, 2004. 10: p. 789-799.

22. Barnes, J.L., et al., Carcinogens and DNA damage. Biochemical Society Transactions, 2018. 46(5): p. 1213-1224.

23. Hecht, S.S., Tobacco smoke carcinogens and lung cancer. Journal of the National Cancer Institute, 1999. 91(14): p. 1194-210.

24. Bernstein, L. and R.K. Ross, Endogenous hormones and breast cancer risk. Epidemiologic Reviews, 1993. 15(1): p. 48-65.

25. Berza, N., et al., Understanding the high-risk human papillomavirus prevalence and associated factors in the European country with a high incidence of cervical cancer. European Journal of Public Health, 2024.

26. Burd, E.M., Human papillomavirus and cervical cancer. Clinical Microbiology Reviews, 2003. 16(1): p. 1-17.

27. Stamenkovic, I., Extracellular matrix remodelling: the role of matrix metalloproteinases. The Journal of Pathology, 2003. 200(4): p. 448-64.

28. Folkman, J., Angiogenesis: an organizing principle for drug discovery? Nature Reviews Drug Discovery, 2007. 6(4): p. 273-86.

29. Ardizzone, A., et al., Role of Basic Fibroblast Growth Factor in Cancer: Biological Activity, Targeted Therapies, and Prognostic Value. Cells, 2023. 12(7).

30. Petrie, K., A. Zelent, and S. Waxman, Differentiation therapy of acute myeloid leukemia: past, present and future. Current Opinion in Hematology, 2009. 16(2): p. 84-91.

31. Zhang, S., et al., Tumor initiation and early tumorigenesis: molecular mechanisms and interventional targets. Signal Transduct Target Ther, 2024. 9(1): p. 149.

32. Scaffidi, P. and T. Misteli, Cancer epigenetics: from disruption of differentiation programs to the emergence of cancer stem cells. Cold Spring Harb Symp Quant Biol, 2010. 75: p. 251-8.

33. Brown, J.M. and L.D. Attardi, The role of apoptosis in cancer development and treatment response. Nature Reviews Cancer, 2005. 5(3): p. 231-7.

34. Khezri, M.R., et al., The PI3K/AKT signaling pathway in cancer: Molecular mechanisms and possible therapeutic interventions. Experimental and Molecular Pathology, 2022. 127: p. 104787.

35. Czabotar, P.E., et al., Control of apoptosis by the BCL-2 protein family: implications for physiology and therapy. Nature Reviews Molecular Cell Biology, 2014. 15(1): p. 49-63.

36. Ghobrial, I.M., T.E. Witzig, and A.A. Adjei, Targeting apoptosis pathways in cancer therapy. CA: A Cancer Journal for Clinicians, 2005. 55(3): p. 178-94.

37. Hallek, M., T.D. Shanafelt, and B. Eichhorst, Chronic lymphocytic leukaemia. Lancet, 2018. 391(10129): p. 1524-1537.

38. Puente, X.S., et al., Whole-genome sequencing identifies recurrent mutations in chronic lymphocytic leukaemia. Nature, 2011. 475(7354): p. 101-5.

39. Hus, I.P., B.; Robak, T.;, PI3K Inhibitors for the Treatment of Chronic Lymphocytic Leukemia: Current Status and Future Perspectives. Cancers (Basel), 2022. 14(6).

40. Palma, M.M., T. A.; Osterborg, A.;, BTK Inhibitors in Chronic Lymphocytic Leukemia: Biological Activity and Immune Effects. Frontiers in Immunology, 2021. 12: p. 686768.

41. Cramer, P.H., M., Prognostic factors in chronic lymphocytic leukemia-what do we need to know? Nature Reviews Clinical Oncology, 2011. 8(1): p. 38-47.

42. Guarente, V. and P. Sportoletti, Lessons, Challenges and Future Therapeutic Opportunities for PI3K Inhibition in CLL. Cancers (Basel), 2021. 13(6).

43. Pui CH, R.L., Look AT, Acute lymphoblastic leukaemia. Lancet, 2008. 371(9617):1030-1043.

44. Papaemmanuil, E., et al., Genomic Classification and Prognosis in Acute Myeloid Leukemia. The New England Journal of Medicine, 2016. 374(23): p. 2209-2221.

45. Druker, B.J., et al., Efficacy and safety of a specific inhibitor of the BCR-ABL tyrosine kinase in chronic myeloid leukemia. The New England Journal of Medicine, 2001. 344(14): p. 1031-7.

46. Ansell, S.M., Non-Hodgkin Lymphoma: Diagnosis and Treatment. Mayo Clinic Proceedings, 2015. 90(8): p. 1152-63.

47. Ansell, S.M., Hodgkin Lymphoma: Diagnosis and Treatment. Mayo Clinic Proceedings, 2015. 90(11): p. 1574-83.

48. Rajkumar, S.V., Multiple myeloma: 2020 update on diagnosis, risk-stratification and management. American Journal of Hematology, 2020. 95(5): p. 548-567.

49. Society, T.L.L. The Leukemia & Lymphoma Society. 2015.

50. Terwilliger, T. and M. Abdul-Hay, Acute lymphoblastic leukemia: a comprehensive review and 2017 update. Blood Cancer Journal, 2017. 7(6): p. e577.

51. Commission, E. European Cancer Information System (ECIS). 2023; Available from: https://ecis.jrc.ec.europa.eu/.

52. Krebsgesellschaft, D. Deutsche Krebsgesellschaft – Aktuelle Krebsstatistiken. 2023 [cited September 17 2024; Available from: https://www.krebsgesellschaft.de.

53. Craig, F.E. and K.A. Foon, Flow cytometric immunophenotyping for hematologic neoplasms. Blood, 2008. 111(8): p. 3941-67.

54. Perez-Carretero, C.G.-G., Y. Marin I.; Rodriguez-Vicente, A. E.; Quijada-Alamo, M.; Hernandez-Rivas, J. A.; Hernandez-Sanchez, M.; Hernandez-Rivas, J. M., The Evolving Landscape of Chronic Lymphocytic Leukemia on Diagnosis, Prognosis and Treatment. Diagnostics (Basel), 2021. 11(5).

55. Madaci, L., et al., Impact of Next-Generation Sequencing in Diagnosis, Prognosis and Therapeutic Management of Acute Myeloid Leukemia/Myelodysplastic Neoplasms. Cancers (Basel), 2023. 15(13): p. 15(13):3280.

56. Hochhaus, A., et al., Long-Term Outcomes of Imatinib Treatment for Chronic Myeloid Leukemia. N Engl J Med, 2017. 376(10): p. 917-927.

57. Stagno, F., et al., Imatinib mesylate in chronic myeloid leukemia: frontline treatment and long-term outcomes. Expert Rev Anticancer Ther, 2016. 16(3): p. 273-8.

58. Kantarjian, H., et al., Blinatumomab versus Chemotherapy for Advanced Acute Lymphoblastic Leukemia. N Engl J Med, 2017. 376(9): p. 836-847.

59. Maude, S.L., et al., Tisagenlecleucel in Children and Young Adults with B-Cell Lymphoblastic Leukemia. N Engl J Med, 2018. 378(5): p. 439-448.

60. Jallouk, A.P., et al., Axicabtagene ciloleucel in relapsed or refractory large B-cell lymphoma patients in complete metabolic response. Haematologica, 2023. 108(4): p. 1163-1167.

61. Schuster, S.J., et al., Tisagenlecleucel in Adult Relapsed or Refractory Diffuse Large B-Cell Lymphoma. N Engl J Med, 2019. 380(1): p. 45-56.

62. Neelapu, S.S., et al., Axicabtagene Ciloleucel CAR T-Cell Therapy in Refractory Large B-Cell Lymphoma. N Engl J Med, 2017. 377(26): p. 2531-2544.

63. Hosen, N., Chimeric antigen receptor T-cell therapy for multiple myeloma. Rinsho Ketsueki, 2018. 59(10): p. 2189-2194.

64. Goetz, L.H. and N.J. Schork, Personalized medicine: motivation, challenges, and progress. Fertility and Sterility, 2018. 109(6): p. 952-963.

65. Rosenquist, R., et al., Novel precision medicine approaches and treatment strategies in hematological malignancies. Journal of Internal Medicine, 2023. 294(4): p. 413-436.

66. Tremblay, J. and P. Hamet, Role of genomics on the path to personalized medicine. Metabolism, 2013. 62 Suppl 1: p. S2-5.

67. Sager, M., et al., Transcriptomics in cancer diagnostics: developments in technology, clinical research and commercialization. Expert Review of Molecular Diagnostics, 2015. 15(12): p. 1589-603.

68. Jacob, M., et al., Metabolomics toward personalized medicine. Mass Spectrometry Reviews, 2019. 38(3): p. 221-238.

69. Parikh, V.N. and E.A. Ashley, Next-Generation Sequencing in Cardiovascular Disease: Present Clinical Applications and the Horizon of Precision Medicine. Circulation, 2017. 135(5): p. 406-409.

70. Nelson, A.C. and S.L. Yohe, Cancer Whole-Genome Sequencing: The Quest for Comprehensive Genomic Profiling in Routine Oncology Care. Journal of Molecular Diagnostics, 2021. 23(7): p. 784-787.

71. Kim, H.S.K., J.; Kim, Y., Recent advances in CRISPR-based functional genomics for the study of disease-associated genetic variants. Experimental and Molecular Medicine, 2024. 56(4): p. 861-869.

72. Yorio, J., et al., Association of Timely Comprehensive Genomic Profiling With Precision Oncology Treatment Use and Patient Outcomes in Advanced Non-Small-Cell Lung Cancer. Journal of Clinical Oncology: Precision Oncology, 2024. 8: p. e2300292.

73. Lander, E.S., et al., Initial sequencing and analysis of the human genome. Nature, 2001. 409(6822): p. 860-921.

74. Check Hayden, E., Is the $1,000 genome for real? Nature, 2014.

75. Kircher, M. and J. Kelso, High-throughput DNA sequencing--concepts and limitations. Bioessays, 2010. 32(6): p. 524-36.

76. Sanger, F., et al., Nucleotide sequence of bacteriophage phi X174 DNA. Nature, 1977. 265(5596): p. 687-95.

77. Margulies, M., et al., Genome sequencing in microfabricated high-density picolitre reactors. Nature, 2005. 437(7057): p. 376-80.

78. Valouev, A., et al., A high-resolution, nucleosome position map of C. elegans reveals a lack of universal sequence-dictated positioning. Genome Research, 2008. 18(7): p. 1051-63.

79. Zimmerman, E. 50 Smartest Companies: Illumina. MIT Technology Review 2014 01/08/2024].

80. Bentley, D.R., et al., Accurate whole human genome sequencing using reversible terminator chemistry. Nature, 2008. 456(7218): p. 53-9.

81. Turcatti, G., et al., A new class of cleavable fluorescent nucleotides: synthesis and optimization as reversible terminators for DNA sequencing by synthesis. Nucleic Acids Research, 2008. 36(4): p. e25.

82. Fedurco, M., et al., BTA, a novel reagent for DNA attachment on glass and efficient generation of solid-phase amplified DNA colonies. Nucleic Acids Res, 2006. 34(3): p. e22.

83. Illumina. Patterned Flow Cell Technology. 2015.

84. Genohub, Next Generation Sequencing Instrument Guide. 2017.

85. Goodwin, S., J.D. McPherson, and W.R. McCombie, Coming of age: ten years of next-generation sequencing technologies. Nature Reviews Genetics, 2016. 17(6): p. 333-51.

86. Eid, J., et al., Real-time DNA sequencing from single polymerase molecules. Science, 2009. 323(5910): p. 133-8.

87. Deamer, D., M. Akeson, and D. Branton, Three decades of nanopore sequencing. Nature Biotechnology, 2016. 34(5): p. 518-24.

88. Jain, M., et al., The Oxford Nanopore MinION: delivery of nanopore sequencing to the genomics community. Genome Biology, 2016. 17(1): p. 239.

89. Simpson, J.T., et al., Detecting DNA cytosine methylation using nanopore sequencing. Nature Methods, 2017. 14(4): p. 407-410.

90. Garalde, D.R., et al., Highly parallel direct RNA sequencing on an array of nanopores. Nature Methods, 2018. 15(3): p. 201-206.

91. Mimi Wan, J.W., Xiaobin Gao,Jeffery Sklar, RNA Sequencing and its Applications in Cancer Diagnosis and Targeted Therapy. 2014.

92.   Avery, O.T., C.M. Macleod, and M. McCarty, Studies on the Chemical Nature of the Substance Inducing Transformation of Pneumococcal Types : Induction of Transformation by a Desoxyribonucleic Acid Fraction Isolated from Pneumococcus Type Iii. The Journal of Experimental Medicine, 1944. 79(2): p. 137-58.

93.   Crick, F.H., On protein synthesis. Symposia of the Society for Experimental Biology, 1958. 12: p. 138-63.

94.   Vogel, C., Marcotte, E, Insights into the regulation of protein abundance from proteomic and transcriptomic analyses. Nature Reviews Cancer, 2012. 227–232.

95.   Edfors, F., et al., Gene-specific correlation of RNA and protein levels in human cells and tissues. Molecular Systems Biology, 2016. 12(10): p. 883.

96.   Voss, T.C. and G.L. Hager, Dynamic regulation of transcriptional states by chromatin and transcription factors. Nature Reviews Genetics, 2014. 15(2): p. 69-81.

97.   Jones, P.A., Functions of DNA methylation: islands, start sites, gene bodies and beyond. Nature Reviews Genetics, 2012. 13(7): p. 484-92.

98.   Vaquerizas, J.M., et al., A census of human transcription factors: function, expression and evolution. Nature Reviews Genetics, 2009. 10(4): p. 252-63.

99.   Madden, E. Central Dogma of Genetics. 2015-2024 06/08/2024].

100.   Alwine, J.C., D.J. Kemp, and G.R. Stark, Method for detection of specific RNAs in agarose gels by transfer to diazobenzyloxymethyl-paper and hybridization with DNA probes. Proceedings of the National Academy of Sciences of the United States of America, 1977. 74(12): p. 5350-4.

101.   Pachmann, K., In situ hybridization with fluorochrome-labeled cloned DNA for quantitative determination of the homologous mRNA in individual cells. Journal of Molecular and Cellular Immunology, 1987. 3(1): p. 13-9.

102.   Becker-Andre, M. and K. Hahlbrock, Absolute mRNA quantification using the polymerase chain reaction (PCR). A novel approach by a PCR aided transcript titration assay (PATTY). Nucleic Acids Research, 1989. 17(22): p. 9437-46.

103.   Weis, J.H., et al., Detection of rare mRNAs via quantitative RT-PCR. Trends in Genetics, 1992. 8(8): p. 263-4.

104.   Marra MA, H.L., Waterston RH, Expressed sequence tags--ESTablishing bridges between genomes. Trends in Genetics, 1998. 14(1):4-7.

105.   Adams, M.D., et al., Complementary DNA sequencing: expressed sequence tags and human genome project. Science, 1991. 252(5013): p. 1651-6.

106.   Miller, M.B. and Y.W. Tang, Basic concepts of microarrays and potential applications in clinical microbiology. Clinical Microbiology Reviews, 2009. 22(4): p. 611-33.

107.   Pozhitkov, A.E., D. Tautz, and P.A. Noble, Oligonucleotide microarrays: widely applied--poorly understood. Brief Funct Genomic Proteomic, 2007. 6(2): p. 141-8.

108.   Mortazavi, A., et al., Mapping and quantifying mammalian transcriptomes by RNA-Seq. Nat Methods, 2008. 5(7): p. 621-8.

109. Martínez-Pérez, A., O. Estévez, and Á. González-Fernández, Contribution and Future of High-Throughput Transcriptomics in Battling Tuberculosis. Frontiers in Microbiology, 2022. 13.

110. Lee, J., M. Yoo, and J. Choi, Recent advances in spatially resolved transcriptomics: challenges and opportunities. BMB Rep, 2022. 55(3): p. 113-124.

111. Pan, Y.F., et al., Role of long non-coding RNAs in gene regulation and oncogenesis. Chinese Medical Journal (English Edition), 2011. 124(15): p. 2378-83.

112. Nagalakshmi, U., et al., The transcriptional landscape of the yeast genome defined by RNA sequencing. Science, 2008. 320(5881): p. 1344-9.

113. Wilhelm, B.T., et al., Dynamic repertoire of a eukaryotic transcriptome surveyed at single-nucleotide resolution. Nature, 2008. 453(7199): p. 1239-43.

114. Marioni, J.C., et al., RNA-seq: an assessment of technical reproducibility and comparison with gene expression arrays. Genome Res, 2008. 18(9): p. 1509-17.

115. Levin, J.Z., et al., Comprehensive comparative analysis of strand-specific RNA sequencing methods. Nature Methods, 2010. 7(9): p. 709-15.

116. Choy, J.Y., et al., A resource of ribosomal RNA-depleted RNA-Seq data from different normal adult and fetal human tissues. Scientific Data, 2015. 2: p. 150063.

117. Mortazavi, A., et al., Mapping and quantifying mammalian transcriptomes by RNA-Seq. Nature Methods, 2008. 5(7): p. 621-8.

118. Head, S.R., et al., Library construction for next-generation sequencing: overviews and challenges. Biotechniques, 2014. 56(2): p. 61-4, 66, 68, passim.

119. Adey, A., et al., Rapid, low-input, low-bias construction of shotgun fragment libraries by high-density in vitro transposition. Genome Biology, 2010. 11(12): p. R119.

120. Picelli, S., et al., Tn5 transposase and tagmentation procedures for massively scaled sequencing projects. Genome Research, 2014. 24(12): p. 2033-40.

121. Meyer, M. and M. Kircher, Illumina sequencing library preparation for highly multiplexed target capture and sequencing. Cold Spring Harbor Protocols, 2010. 2010(6): p. pdb prot5448.

122. Kircher, M., S. Sawyer, and M. Meyer, Double indexing overcomes inaccuracies in multiplex sequencing on the Illumina platform. Nucleic Acids Res, 2012. 40(1): p. e3.

123. van Dijk, E.L., Y. Jaszczyszyn, and C. Thermes, Library preparation methods for next-generation sequencing: tone down the bias. Experimental Cell Research, 2014. 322(1): p. 12-20.

124. Wang, Z., M. Gerstein, and M. Snyder, RNA-Seq: a revolutionary tool for transcriptomics. Nature Reviews Genetics, 2009. 10(1): p. 57-63.

125. Conesa, A., et al., A survey of best practices for RNA-seq data analysis. Genome Biology, 2016. 17: p. 13.

126. Renaud, G., et al., deML: robust demultiplexing of Illumina sequences using a likelihood-based approach. Bioinformatics, 2015. 31(5): p. 770-2.

127. Hayer, K.E., et al., Benchmark analysis of algorithms for determining and quantifying full-length mRNA splice forms from RNA-seq data. Bioinformatics, 2015. 31(24): p. 3938-45.

128. Engstrom, P.G., et al., Systematic evaluation of spliced alignment programs for RNA-seq data. Nature Methods, 2013. 10(12): p. 1185-91.

129. Okonechnikov, K., A. Conesa, and F. Garcia-Alcalde, Qualimap 2: advanced multi-sample quality control for high-throughput sequencing data. Bioinformatics, 2016. 32(2): p. 292-4.

130. Liao, W.J., G.; Nham, P.; Phan, R. T.; Pelegrini, M.; Sharma, S.;, Gene expression and splicing alterations analyzed by high throughput RNA sequencing of chronic lymphocytic leukemia specimens. BMC Cancer, 2015. 15: p. 714.

131. Wang, L., et al., SF3B1 and other novel cancer genes in chronic lymphocytic leukemia. N Engl J Med, 2011. 365(26): p. 2497-506.

132. Del Gaizo Moore, V. and A. Letai, BH3 profiling--measuring integrated function of the mitochondrial apoptotic pathway to predict cell fate decisions. Cancer Lett, 2013. 332(2): p. 202-5.

133. Quesada, V., et al., Exome sequencing identifies recurrent mutations of the splicing factor SF3B1 gene in chronic lymphocytic leukemia. Nat Genet, 2011. 44(1): p. 47-52.

134. Burger, J.A. and A. Wiestner, Targeting B cell receptor signalling in cancer: preclinical and clinical advances. Nat Rev Cancer, 2018. 18(3): p. 148-167.

135. Byrd, J.C., et al., Targeting BTK with ibrutinib in relapsed chronic lymphocytic leukemia. N Engl J Med, 2013. 369(1): p. 32-42.

136. Beekman, R., et al., The reference epigenome and regulatory chromatin landscape of chronic lymphocytic leukemia. Nature Medicine, 2018. 24(6): p. 868-880.

137. Del Giudice, I., et al., Minimal Residual Disease in Chronic Lymphocytic Leukemia: A New Goal? Front Oncol, 2019. 9: p. 689.

138. Luo, M., et al., A comprehensive landscape of transcription profiles and data resources for human leukemia. Blood Advances, 2023. 7(14): p. 3435-3449.

139. Wang, S., et al., The Evolution of Single-Cell RNA Sequencing Technology and Application: Progress and Perspectives. International Journal of Molecular Sciences, 2023. 24(3).

140. Okada, H., U.I. Chung, and H. Hojo, Practical Compass of Single-Cell RNA-Seq Analysis. Current Osteoporosis Reports, 2023.

141. Deng, Q., et al., Single-cell RNA-seq reveals dynamic, random monoallelic gene expression in mammalian cells. Science, 2014. 343(6167): p. 193-6.

142. Kolodziejczyk, A.A., et al., Single Cell RNA-Sequencing of Pluripotent States Unlocks Modular Transcriptional Variation. Cell Stem Cell, 2015. 17(4): p. 471-85.

143. Martinez-Jimenez, C.P., et al., Aging increases cell-to-cell transcriptional variability upon immune stimulation. Science, 2017. 355(6332): p. 1433-1436.

144. Grun, D., et al., Single-cell messenger RNA sequencing reveals rare intestinal cell types. Nature, 2015. 525(7568): p. 251-5.

145.   Halpern, K.B., et al., Single-cell spatial reconstruction reveals global division of labour in the mammalian liver. Nature, 2017. 542(7641): p. 352-356.

146.   Muraro, M.J., et al., A Single-Cell Transcriptome Atlas of the Human Pancreas. Cell Systems, 2016. 3(4): p. 385-394 e3.

147.   Baron, M., et al., A Single-Cell Transcriptomic Map of the Human and Mouse Pancreas Reveals Inter- and Intra-cell Population Structure. Cell Systems, 2016. 3(4): p. 346-360 e4.

148.   Biase FH, C.X., Zhong S., Cell fate inclination within 2-cell and 4-cell mouse embryos revealed by single-cell RNA sequencing. Genome Research, 2014. 24(11):1787-1796.

149.   Nestorowa, S., et al., A single-cell resolution map of mouse hematopoietic stem and progenitor cell differentiation. Blood, 2016. 128(8): p. e20-31.

150.   Moignard, V., et al., Decoding the regulatory network of early blood development from single-cell gene expression measurements. Nature Biotechnology, 2015. 33(3): p. 269-276.

151.   La Manno, G., et al., Molecular Diversity of Midbrain Development in Mouse, Human, and Stem Cells. Cell, 2016. 167(2): p. 566-580 e19.

152.   Patel, A.P., et al., Single-cell RNA-seq highlights intratumoral heterogeneity in primary glioblastoma. Science, 2014. 344(6190): p. 1396-401.

153.   Tirosh, I., et al., Dissecting the multicellular ecosystem of metastatic melanoma by single-cell RNA-seq. Science, 2016. 352(6282): p. 189-96.

154.   Venteicher, A.S., et al., Decoupling genetics, lineages, and microenvironment in IDH-mutant gliomas by single-cell RNA-seq. Science, 2017. 355(6332): p. eaai8478.

155.   Song, Q. and L. Liu, Single-Cell RNA-Seq Technologies and Computational Analysis Tools: Application in Cancer Research. Methods Mol Biol, 2022. 2413: p. 245-255.

156.   Bhargava, V., et al., Technical variations in low-input RNA-seq methodologies. Scientific Reports, 2014. 4: p. 3678.

157.   Mullis, K., et al., Specific enzymatic amplification of DNA in vitro: the polymerase chain reaction. Cold Spring Harb Symp Quant Biol, 1986. 51 Pt 1: p. 263-73.

158.   Milligan, J.F., et al., Oligoribonucleotide synthesis using T7 RNA polymerase and synthetic DNA templates. Nucleic Acids Research, 1987. 15(21): p. 8783-98.

159.   Blanco, L., et al., Highly efficient DNA synthesis by the phage phi 29 DNA polymerase. Symmetrical mode of DNA replication. Journal of Biological Chemistry, 1989. 264(15): p. 8935-40.

160.   Tang, F., et al., mRNA-Seq whole-transcriptome analysis of a single cell. Nature Methods, 2009. 6(5): p. 377-82.

161.   Shapiro, E., T. Biezuner, and S. Linnarsson, Single-cell sequencing-based technologies will revolutionize whole-organism science. Nature Reviews Genetics, 2013. 14(9): p. 618-30.

162.   Sandberg, R., Entering the era of single-cell transcriptomics in biology and medicine. Nature Methods, 2014. 11(1): p. 22-4.

163. Wagner, A., A. Regev, and N. Yosef, Revealing the vectors of cellular identity with single-cell genomics. Nature Biotechnology, 2016. 34(11): p. 1145-1160.

164. Murphy, T.W., et al., Recent advances in the use of microfluidic technologies for single cell analysis. Analyst, 2017. 143(1): p. 60-80.

165. Wu, M. and A.K. Singh, Single-cell protein analysis. Current Opinion in Biotechnology, 2012. 23(1): p. 83-8.

166. Yixin Liu, Z.F., Liang Qiao, Baohong Liu, Advances in microfluidic strategies for single-cell research. TrAC Trends in Analytical Chemistry, 2022. 157.

167. Zhou, W.M., et al., Microfluidics applications for high-throughput single cell sequencing. J Nanobiotechnology, 2021. 19(1): p. 312.

168. Klein, A.M., et al., Droplet barcoding for single-cell transcriptomics applied to embryonic stem cells. Cell, 2015. 161(5): p. 1187-1201.

169. Zhenqi Jiang, H.S., Xiaoying Tang, Jieling Qin, Recent advances in droplet microfluidics for single-cell analysis. TrAC Trends in Analytical Chemistry, 2023. 159.

170. Whitesides, G.M., The origins and the future of microfluidics. Nature, 2006. 442(7101): p. 368-73.

171. Pollen, A.A., et al., Low-coverage single-cell mRNA sequencing reveals cellular heterogeneity and activated signaling pathways in developing cerebral cortex. Nature Biotechnology, 2014. 32(10): p. 1053-8.

172. Wu, A.R., et al., Quantitative assessment of single-cell RNA-sequencing methods. Nature Methods, 2014. 11(1): p. 41-6.

173. Macosko, E.Z., et al., Highly Parallel Genome-wide Expression Profiling of Individual Cells Using Nanoliter Droplets. Cell, 2015. 161(5): p. 1202-1214.

174. Zilionis, R., et al., Single-cell barcoding and sequencing using droplet microfluidics. Nature Protocols, 2017. 12(1): p. 44-73.

175. Zheng, G.X., et al., Massively parallel digital transcriptional profiling of single cells. Nature Communications, 2017. 8: p. 14049.

176. Svensson, V., R. Vento-Tormo, and S.A. Teichmann, Exponential scaling of single-cell RNA-seq in the past decade. Nat Protoc, 2018. 13(4): p. 599-604.

177. Magali Soumillon, D.C., Stefan Semrau, Alexander van Oudenaarden, Tarjei S. Mikkelsen, Characterization of directed differentiation by high-throughput single-cell RNA-Seq. bioRxiv, 2014.

178. Jaitin, D.A., Massively Parallel Single-Cell RNA-Seq for Marker-Free Decomposition of Tissues into Cell Types. Science. 343(6172).

179. Hashimshony, T., et al., CEL-Seq2: sensitive highly-multiplexed single-cell RNA-Seq. Genome Biology, 2016. 17: p. 77.

180. Hayashi Tetsutaro , N.S., Ryo Okumura, Tomomi Kudome, Osamu Nishimura, Hiroshi Tarui, Kiyokazu Agata, Single-cell gene profiling of planarian stem cells using fluorescent activated cell sorting and its "index sorting" function for stem cell research. Develop. Growth Differ, 2010. 52(1), pp.131–144.

181. Fan, X., et al., Single-cell RNA-seq transcriptome analysis of linear and circular RNAs in mouse preimplantation embryos. Genome Biology, 2015. 16(1): p. 148.

182. Gierahn, T.W., M.; Hughes, T. , Seq-Well: portable, low-cost RNA sequencing of single cells at high throughput. Nature Methods, 2017. 14, 395–398.

183. Hochgerner, H., et al., STRT-seq-2i: dual-index 5' single cell and nucleus RNA-seq on an addressable microwell array. Scientific Reports, 2017. 7(1): p. 16327.

184. Streets, A.M., et al., Microfluidic single-cell whole-transcriptome sequencing. Proc Natl Acad Sci U S A, 2014. 111(19): p. 7048-53.

185. Bose, S., et al., Scalable microfluidics for single-cell RNA printing and sequencing. Genome Biology, 2015. 16(1): p. 120.

186. Popova, A.A.T., T.; Demir, K.; Haitz, P.; Kuodyte, K.; Starkuviene, V.; Wajda, P.; Levkin, P. A., Facile One Step Formation and Screening of Tumor Spheroids Using Droplet-Microarray Platform. Small, 2019. 15(25): p. e1901299.

187. W. Feng, L.L., E. Ueda, J. Li, Dr. P. A. Levkin, Surface Patterning via Thiol-Yne Click Chemistry: An Extremely Fast and Versatile Approach to Superhydrophilic-Superhydrophobic Micropatterns. Advanced Materials, 2015. 27(8), 1344–1350.

188. Brehm, M., et al., Nanomolar Synthesis in Droplet Microarrays with UV-Triggered On-Chip Cell Screening. Small, 2020. 16(10): p. e1905971.

189. Geyer, F.L., et al., Superhydrophobic-superhydrophilic micropatterning: towards genome-on-a-chip cell microarrays. Angewandte Chemie International Edition, 2011. 50(36): p. 8424-8427.

190. Oudeng, G., et al., Droplet Microarray Based on Nanosensing Probe Patterns for Simultaneous Detection of Multiple HIV Retroviral Nucleic Acids. ACS Appl Mater Interfaces, 2020. 12(50): p. 55614-55623.

191. Gao, X. and L. Jiang, Biophysics: water-repellent legs of water striders. Nature, 2004. 432(7013): p. 36.

192. Law, K.Y., Definitions for Hydrophilicity, Hydrophobicity, and Superhydrophobicity: Getting the Basics Right. J Phys Chem Lett, 2014. 5(4): p. 686-8.

193. Schutzius, T.M., et al., Superhydrophobic-superhydrophilic binary micropatterns by localized thermal treatment of polyhedral oligomeric silsesquioxane (POSS)-silica films. Nanoscale, 2012. 4(17): p. 5378-85.

194. Brumbach, M., and N. Armstrong, Preparation of Monolayer Modified Electrodes. Modified Electrodes, 2007. 5-28.

195. M. Brehm, J.M.S., A. Welle, P. A. Levkin, Reversible Surface Wettability by Silanization. Advanced Materials Interfaces 2020. 7(12):1902134.

196. Young, T., An Essay on the Cohesion of Fluids. Philosophical Transactions of the Royal Society of London, 1805. 95, 65-87.

197. Lillington, J.M., D.J. Trafford, and H.L. Makin, A rapid and simple method for the esterification of fatty acids and steroid carboxylic acids prior to gas-liquid chromatography. Clinical Chimica Acta, 1981. 111(1): p. 91-8.

198. Rosenfeld, A., et al., Solid-phase combinatorial synthesis using microarrays of microcompartments with light-induced on-chip cell screening. Mater Today Bio, 2019. 3: p. 100022.

199. M. Bär, R.W., S. ; Levkin,P., Facile fabrication of robust superhydrophobic surfaces: comparative investigation. RSC Advances, 2016.

200. Chakraborty, S., et al., Droplet microarrays for cell culture: effect of surface properties and nanoliter culture volume on global transcriptomic landscape. Mater Today Bio, 2021. 11: p. 100112.

201. Popova, A.A.D., K.; Hartanto G. T.; Schmitta, E. and Levkin, P. , Droplet-microarray on superhydrophobic–superhydrophilic patterns for high-throughput live cell screenings. RSC Advances, 2016. 38263-38276.

202. Tronser, T.D., K.; Reischl, M.; Bastmeyer, M.; Levkin, P. A., Droplet microarray: miniaturized platform for rapid formation and high-throughput screening of embryoid bodies. Lab Chip, 2018. 18(15): p. 2257-2269.

203. Popova, A.A.M., D.; Peravali,R.; Wehl,I.; Schepers,U.; Levkin;P., Fish-Microarray: A Miniaturized Platform for Single-Embryo High-Throughput Screenings. Advanced Functional Materials, 2017.

204. Lei, W., Deckers, A., Luchena, C., Popova, A., Reischl, M., Jung, N., Bräse, S., Schwartz, T., Krimmelbein, I. K., Tietze, L. F., & Levkin, P. A., Droplet Microarray as a Powerful Platform for Seeking New Antibiotics Against Multidrug-Resistant Bacteria. Advanced biology, 2022. 6(12), e2200166.

205. Cui, H.T., T.; Wang,X.; Wesslowski,J.; Davidson,G.; Popova,A.A.; Levkin,P., High-throughput formation of miniaturized cocultures of 2D cell monolayers and 3D cell spheroids using droplet microarray. RESEARCH ARTICLE, 2022.

206. Rosenfeld, A., et al., Miniaturized high-throughput synthesis and screening of responsive hydrogels using nanoliter compartments. Mater Today Bio, 2020. 6: p. 100053.

207. Benz, M., et al., Marrying chemistry with biology by combining on-chip solution-based combinatorial synthesis and cellular screening. Nature Communications, 2019. 10(1): p. 2879.

208. Tian, Y., et al., High-Throughput Miniaturized Synthesis of PROTAC-Like Molecules. Small, 2024. 20(26): p. e2307215.

209. Iwohn, M.J.S., M.; Reiser,P.; Höpfner,J.; El Khaled El Faraj,R.; Heißler,S.; Popova,A.A.; Levkin,P., OligoHydrogelArray (OHA) for Parallelized Solid – Phase Extraction of Oligonucleotides. Advanced Materials Interfaces, 2023.

210. Schilling, M.P., El Khaled El Faraj, R., Urrutia Gómez, J.E. et al, Automated high-throughput image processing as part of the screening platform for personalized oncology. Sci Rep, 2023. 13, 5107.

211. Crouch, S.P., Kozlowski, R., Slater, K. J., & Fletcher, J., The use of ATP bioluminescence as a measure of cell proliferation and cytotoxicity. Journal of immunological methods, 1993. 160(1), 81–88

212.	Niles, A.L., R.A. Moravec, and T.L. Riss, Update on in vitro cytotoxicity assays for drug development. Expert Opinion on Drug Discovery, 2008. 3(6): p. 655-69.

213.	Urruticoechea, A., I.E. Smith, and M. Dowsett, Proliferation marker Ki-67 in early breast cancer. Journal of Clinical Oncology, 2005. 23(28): p. 7212-7220.

214.	Li, L.T., Jiang, G., Chen, Q., & Zheng, J. N, Ki67 is a promising molecular target in the diagnosis of cancer (review). Molecular Medicine Reports, 2015. 11(3), 1566-1572.

215.	Mullis, K.B. and F.A. Faloona, Specific synthesis of DNA in vitro via a polymerase-catalyzed chain reaction. Methods Enzymol, 1987. 155: p. 335-50.

216.	Green, M.R. and J. Sambrook, Analysis of DNA by Agarose Gel Electrophoresis. Cold Spring Harb Protoc, 2019. 2019(1).

217.	Heid, C.A., et al., Real time quantitative PCR. Genome Research, 1996. 6(10): p. 986-94.

218.	Livak, K.J. and T.D. Schmittgen, Analysis of relative gene expression data using real-time quantitative PCR and the 2(-Delta Delta C(T)) Method. Methods, 2001. 25(4): p. 402-8.

219.	Gallagher, S.R. and P.R. Desjardins, Quantitation of DNA and RNA with absorption and fluorescence spectroscopy. Current Protocols in Human Genetics, 2007. Appendix 3: p. Appendix 3D.

220.	Desjardins, P. and D. Conklin, NanoDrop microvolume quantitation of nucleic acids. Journal of visualized experiments, 2010(45): p. 45 2565.

221.	Odilo Mueller , S.L., Andreas Schroeder RNA Integrity Number (RIN) – Standardization of RNA Quality Control. Agilent Technologies, 2016.

222.	Mueller, O.H., K.; Dittmann, M.; Yee, H.; Dubrow, R.; Nagle, R.; Ilsley, D., A microfluidic system for high-speed reproducible DNA sizing and quantitation. Electrophoresis, 2000. 21(1): p. 128-34.

223.	Panaro, N.J.Y., P. K.; Sakazume, T.; Fortina, P.; Kricka, L. J.; Wilding, P., Evaluation of DNA fragment sizing and quantification by the agilent 2100 bioanalyzer. Clinical Chemistry, 2000. 46(11): p. 1851-3.

224.	Kim, T.K., Understanding one-way ANOVA using conceptual figures. Korean J Anesthesiol, 2017. 70(1): p. 22-26.

225.	Kao, L.G., C. , Analysis of Variance: Is There a Difference in Means and What Does It Mean? Journal of Surgical Research, 2008. 144(1):158-170.

226.	Napoli, G.C., W.D. Figg, and C.H. Chau, Functional Drug Screening in the Era of Precision Medicine. Frontiers in Medicine (Lausanne), 2022. 9: p. 912641.

227.	Rusert, J.M., et al., Functional Precision Medicine Identifies New Therapeutic Candidates for Medulloblastoma. Cancer Research, 2020. 80(23): p. 5393-5407.

228.	Popova, A.A., & Levkin, P. A, Precision Medicine in Oncology: In Vitro Drug Sensitivity and Resistance Test (DSRT) for Selection of Personalized Anticancer Therapy. Advanced Therapeutics, 2020.

229.	Giliberto, M., Raj, D. T. G. B., Cremaschi, A., Skanland, S. S., Gade, A., Tjonnfjord, G. E., Schjesvold, F., Munthe, L. A., & Tasken, K. , Ex vivo drug sensitivity screening in

multiple myeloma identifies drug combinations that act synergistically. Molecular Oncology, 2022. 16(6), 1241-1258.

230. Wang, D., Floisand, Y., Myklebust, C. V., Burgler, S., Parente-Ribes, A., Hofgaard, P. O., Bogen, B., Tasken, K., Tjonnfjord, G. E., Schjesvold, F., Dalgaard, J., Tveita, A., & Munthe, L. A., Autologous bone marrow Th cells can support multiple myeloma cell proliferation in vitro and in xenografted mice. Leukemia, 2017. 31(10), 2114-2121.

231. Hawkins, E.D., et al., Measuring lymphocyte proliferation, survival and differentiation using CFSE time-series data. Nat Protoc, 2007. 2(9): p. 2057-67.

232. Bose, S., H. Clevers, and X. Shen, Promises and Challenges of Organoid-Guided Precision Medicine. Med, 2021. 2(9): p. 1011-1026.

233. El Harane, S.Z., B.; El Harane, N.; Krause, K.-H.; Matthes, T.; Preynat-Seauve, O., Cancer Spheroids and Organoids as Novel Tools for Research and Therapy: State of the Art and Challenges to Guide Precision Medicine. Cells 2023. 12, 1001.

234. Li, Y., et al., Organoid based personalized medicine: from bench to bedside. Cell Regeneration, 2020. 9(1): p. 21.

235. Liu, Y. and Y.G. Chen, 2D- and 3D-Based Intestinal Stem Cell Cultures for Personalized Medicine. Cells, 2018. 7(12): p. 12 (225).

236. Darwiche, W.G., B.; Marolleau, J. P.; Ghamlouch, H.;, Chronic Lymphocytic Leukemia B-Cell Normal Cellular Counterpart: Clues From a Functional Perspective. Frontiers in Immunology, 2018. 9: p. 683.

237. Pascutti, M.J.M., : Tromp, JM., IL-21 and CD40L signals from autologous T cells can induce antigen-independent proliferation of CLL cells. Blood, 2013. 122:3010–3019.

238. Gstraunthaler, G.L., Toni. , Zellbiologische Grundlagen der Zell- und Gewebekultur. Vol. 51-52. 2013, ResearchGate.

239. Roden, D.M. and A.L. George, Jr., The genetic basis of variability in drug responses. Nature Reviews Drug Discovery, 2002. 1(1): p. 37-44.

240. Hafner, M., Niepel, M., Subramanian, K., & Sorger, P. K, Designing drug-response experiments and quantifying their results. Current Protocols in Chemical Biology, 2017. 9, 96–116.

241. Sahan, A.Z., M. Baday, and C.B. Patel, Biomimetic Hydrogels in the Study of Cancer Mechanobiology: Overview, Biomedical Applications, and Future Perspectives. Gels, 2022. 8(8).

242. Vitale, C., et al., Tumor Microenvironment and Hydrogel-Based 3D Cancer Models for In Vitro Testing Immunotherapies. Cancers (Basel), 2022. 14(4).

243. Popova, A.A., et al., Miniaturized Drug Sensitivity and Resistance Test on Patient-Derived Cells Using Droplet-Microarray. SLAS Technol, 2021. 26(3): p. 274-286.

244. Yuan, J. and P.A. Sims, An Automated Microwell Platform for Large-Scale Single Cell RNA-Seq. Scientific Reports, 2016. 6: p. 33883.

245. Dong, Z. and Y. Chen, Transcriptomics: advances and approaches. Science China Life Sciences, 2013. 56(10): p. 960-7.

246. Zhang, X., et al., Comparative Analysis of Droplet-Based Ultra-High-Throughput Single-Cell RNA-Seq Systems. Molecular Cell, 2019. 73(1): p. 130-142 e5.

247. Gomez, J.E.U., et al., ANDeS: An automated nanoliter droplet selection and collection device. SLAS Technology, 2024. 29(1): p. 100118.

248. Baudot, A., Jeandel, P., Mouska, X. et al., The tyrosine kinase Syk regulates the survival of chronic lymphocytic leukemia B cells through PKCδ and proteasome-dependent regulation of Mcl-1 expression. Oncogene 2009. 28, 3261–3273.

249. Humayun, A. and A.J. Fornace, Jr., GADD45 in Stress Signaling, Cell Cycle Control, and Apoptosis. Adv Exp Med Biol, 2022. 1360: p. 1-22.

250. Salvador, J.M., J.D. Brown-Clay, and A.J. Fornace, Jr., Gadd45 in stress signaling, cell cycle control, and apoptosis. Adv Exp Med Biol, 2013. 793: p. 1-19.

251. Guo, D., Zhao, Y., Wang, N., You, N., Zhu, W., Zhang, P., Ren, Q., Yin, J., Cheng, T., & Ma, X., GADD45g acts as a novel tumor suppressor, and its activation suggests new combination regimens for the treatment of AML. Blood, 2021. 138(6), 464–479.

252. Woyach JA, J.A., Byrd JC., The B-cell receptor signaling pathway as a therapeutic target in CLL. Blood, 2012. 120(6):1175-1184.

253. Dietrich, S., et al., Drug-perturbation-based stratification of blood cancer. J Clin Invest, 2018. 128(1): p. 427-445.

254. Althubiti, M., Spleen Tyrosine Kinase Inhibition Modulates p53 Activity. J Cell Death, 2017. 10: p. 1179066017731564.

255. DL., W., Gadd45 stress sensors in suppression of leukemia. Oncotarget, 2018. 9(76):34191-34192.

256. Popova, A.A.D., C.; Permana, K. M.; Trubitsyn, A.; Peravali, R.; Ordiano, J. A.; Reischl, M.; Levkin, P. A., Evaluation of the Droplet-Microarray Platform for High-Throughput Screening of Suspension Cells. SLAS Technology, 2017. 22(2): p. 163-175.

257. Tronser, T.P., A. A.; Jaggy, M.; Bastmeyer, M.; Levkin, P. A., Droplet Microarray Based on Patterned Superhydrophobic Surfaces Prevents Stem Cell Differentiation and Enables High-Throughput Stem Cell Screening. Advanced Healthcare Materials, 2017. 6(23): p. 6(23).

258. Bagnoli, J.W.Z., C.; Janjic, A.; Wange, L;. E. Vieth, B.; Parekh, S;. Geuder, J.; Hellmann, I.; Enard, W., Sensitive and powerful single-cell RNA sequencing using mcSCRB-seq. Nature Communications, 2018. 9(1): p. 2937.

259. El Khaled El Faraj, R.C., S.; Zhou, M.; Sobol, M.; Thiele, D.; Shatford Adams, L. M.; Correa Cassal, M.; Kaster, A. K.; Dietrich, S.; Levkin, P. A.; Popova, A. A.;, Drug-Induced Differential Gene Expression Analysis on Nanoliter Droplet Microarrays: Enabling Tool for Functional Precision Oncology. Advanced Healthcare Materials, 2025. 14(1): p. e2401820.

Curriculum vitae

Personal Data:

Name:	Razan El Khaled El Faraj
Data of birth:	15.09.1994
Place of Birth:	Tripoli, Lebanon
E-Mail:	Razan-faraj@hotmail.com
Phone	+4915750120762

Education:

2021 - 2024	**Karlsruhe Institut für Technologie – Karlsruhe (Germany)**
	Ph.D. Student in Faculty of Chemsitry and Biosciences
	Institute of Biological and Chemical Systems – Functional Molecular Systems (IBCS-FMS)
	BioInterfaces International Graduate School
	Dissertation topic: Personalized Drug Response Profiling for Patient-derived Chronic lymphocytic Leukaemia: Developing Miniaturized Gene Expression Analysis Protocol and Drug sensitivity testing on Droplet Microarray platform
2019 - 2021	**École des Mines de Saint-Étienne – Gardanne (France)**
	And
	Aix –Marseille University – Marseille (France)
	M.Sc in Nanoscience and Nanotechnology,Bio-Nanoelectronic
2016 - 2018	**Cyprus International University – Nicosia (Cyprus)**
	Obtained with Honor. CGPA: 4/4
	M.Sc. I, II in Bioengineering
	Published Paper: **Kavaz, D., Faraj, R.E. Investigation of composition, antioxidant, antimicrobial and cytotoxic characteristics from Juniperus sabina and Ferula communis extracts. Sci Rep 13, 7193 (2023). https://doi.org/10.1038/s41598-023-34281-x**
2012-2016	**Lebanese International University – Lebanon**
	Bachelor of Science in Biomedical Science
June,2012	**Rawdat Al Fayhaa High School – Lebanon**
	Baccalaureate " Life Science "

Work Experience

Oct– Nov 17 2020 **6 weeks**	**Laboratory Technician – Centaur Clinical Cro** **France – Gardanne** Continue internship project
April– Sept 2020 **6 months**	**Laboratory Internship "Research and development" –** **Centaur Clinical Cro (Private Company)** **France " Gardanne"** Developing and optimizing immunogenicity and pyrogenicity assays aimed at assessing the safety and efficacy of new medical devices, therapeutic antibodies, and biosimilars. This included validating the methodologies to ensure accurate detection and quantification of immune-related risks.
2018-2019	**Laboratory Trainee – Commerce Industry & Agriculture Laboratories** **Lebanon "Tripoli "** Practiced techniques food Quality and Control and Safety
2017-2018	**Graduation Project – Cyprus International University Laboratory**
2016-2017	**Biomedical Laboratory Intern. – Monla Hospital** **Lebanon "Tripoli "**
2015-2016	**Biomedical Laboratory Intern – Tripoli Medical Centre (Private Lab)** **Lebanon "Tripoli "**
2016-2017	**Biology, physics, chemistry teacher with NRC " Norwegian Refugee Council "**
2022-present	**Training Bachelor/ Master and Azubi students in acquiring new skills (Wet Lab)**

Additional Qualifications

Language

> English (fluent)
> Arabic (native)
> French(intermediate)
> German (beginer)

Software

> Office Software, Python, Graphpad prism, OriginLab, Endnote, ImageJ

Lab techniques

> Cell culture techniques / 3D Cell Culture
> Microbiology / bacteriology
> ELISA
> Cell Viability assays
> Fluorescence/Confocal/Light Microscopy
> Polymerase Chain Reaction (PCR)+gel electro

Real-Time Polymerase Chain Reaction (qPCR)
Spectrophotometer
Chromatography (e.g., GC-MS , HPLC)
RNA isolation and cDNA synthesis
Patch clamp
Ovo-Model technique
Wet lab skills

Scientific accomplishments

Publications

- **Razan El Khaled EL Faraj**, Shraddha Chakraborty, Meijun Zhou, Morgan Sobol, David Thiele, Lilly ShatfordAdams, Maximiano Correa Cassal, Anne-Kristin Kaster, Sascha Dietrich, Pavel A. Levkin and Anna A. Popova. (2024) Drug-Induced Differential Gene Expression Analysis on Nanoliter Droplet Microarrays: Enabling Tool for Functional Precision Oncology. Advanced Healthcare Materials e2401820. https://doi.org/10.1002/adhm.202401820

- Joaquín E. Urrutia Gómez, **Razan El Khaled El Faraj**, Moritz Braun, Pavel A. Levkin, Anna A. Popova: ANDeS: An automated nanoliter droplet selection and collection device. SLAS Technol, 2024. 29(1): p. 100118.

- Marcel P Schilling, **Razan El Khaled El Faraj,** Joaquín Eduardo Urrutia Gómez, Steffen J Sonnentag, Fei Wang, Britta Nestler, Véronique Orian-Rousseau , Anna A Popova 2, Pavel A Levkin 2, Markus Reischl 4 (2023). Automated high-throughput image processing as part of the screening platform for personalized oncology. Scientific reports, 13(1), 5107. https://doi.org/10.1038/s41598-023-32144-z

- Michelle J. Iwohn, Maximilian Seifermann, Patrick Reiser, Julius Höpfner, **Razan El Khaled El Faraj**, Stefan Heißler, Anna A. Popova, Pavel A. Levkin. OligoHydrogelArray (OHA) for Parallelized Solid-Phase Extraction of Oligonucleotides. Adv. Mater. Interfaces 2023, 10, 2300227. https://doi.org/10.1002/admi.202300227

- Doga Kavaz and **Razan El Faraj**. Investigation of composition, antioxidant, antimicrobial and cytotoxic characteristics from Juniperus sabina and Ferula communis extracts. Sci Rep 13, 7193 (2023). https://doi.org/10.1038/s41598-023-34281-x

Conferences

BioRN Annual Conference 2024	Pitch talk
	Heidelberg, Germany
EHA-SfPM Precision Medicine Meeting	Poster Presentation
	Copenhagen, Denmark
SLAS Europe 2024 conference and exhibition –	Poster Presentation
Revolutionizing life sciences innovation	Barcelona, Spain
	• Poster presentation winner award
SLAS Europe 2023 conference and exhibition - Science	Poster Presentation
Set in Motion	Brussels, Belgium
Personalized Health Technologies Conference	Poster Presentation
	ETH, Zurich, Switzerland

Awards and Honors

Conference grant, Biointerface international graduate school	2024
SLAS Student Poster Award	2024
BIF-IGS best talk award	2023
Honor Ms.c Student	2018